The implications of Sr and Nd isotope data on the genesis of the Platreef and associated BMS and PGE mineralisation, Bushveld Igneous Complex, South Africa

By

TSHIPENG MWENZE

[B.Sc., B.Sc.Hon., M.Sc.] In Applied Geology

A thesis submitted to the faculty of natural science (University of the Western Cape) in fulfilment of the requirements for the PhD degree in Applied Geology

UNIVERSITY *of the*
WESTERN CAPE

Declaration

I declare that "*The implications of Sr and Nd isotope data on the genesis of the Platreef and associated BMS and PGE mineralisation, Bushveld Igneous Complex, South Africa*" has not been accepted in substance for any degree, and is not concurrently been submitted for any degree other than that of doctor of philosophy in applied geology being studied at the University of the Western Cape. I also declare that this work is the result of my own research except where otherwise identified by references and that I have not plagiarized the work of others.

TSHIPENG MWENZE (PhD Candidate) …………….............……………………….……

Doctor ADBI-MOHAMOUD SIAD (1st Supervisor) ……………...……........….………

Professor CHARLES OKUJENI (2nd Supervisor) ……………….........……….…..….……

Professor DIRK FREI (3rd Supervisor) ………………….……......……........…………

July 2019

2
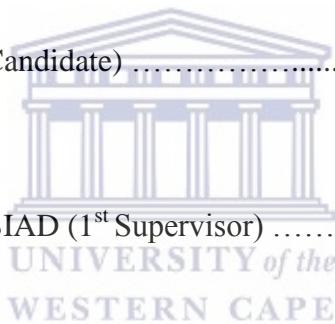
Keywords:

Platreef rocks

Whole-rock Sr–Nd isotopes

Crustal contamination

Magma source heterogeneity

Platinum group elements mineralisation

Northern Bushveld Igneous Complex

Abstract

The Platreef is a platinum group elements (PGE) deposit located in the Northern limb of the Bushveld Igneous Complex (BIC). It is a series of mafic and ultramafic sills that are overlain by rocks from the Main Zone (MZ) of the BIC. In comparison to PGE deposits (i.e., Merensky Reef and the UG-2 chromitite) occurring in the Critical Zone (CZ) of the Eastern and Western Limbs of the BIC, which are less than 1 m in thickness, the Platreef is 10 to 400 m in thickness and is comprised of a variety of rocks. PGE mineralisation in the Platreef is not confined to a specific rock type, and its distribution and styles also vary with depth and along strike. Despite the numerous researches that have been conducted, the genesis of Platreef is still poorly understood.

New major and trace elements in conjunction with Sr–Nd isotope data, generated from whole-rock analyses of different Platreef rocks, were collected from four drill cores along its strike. The data were examined to determine the source of the magmas and identify the processes involved in its genesis. The study also aimed at establishing whether a genetic link exists between the Platreef magmas and the magmas that formed the Lower Zone (LZ), CZ and MZ in the Rustenburg Layered Suite (RLS) of the BIC.

The petrography revealed that the Platreef in the four drill cores consists of harzburgite, olivine pyroxenite, pyroxenite, feldspathic pyroxenite and norite. Based on the textural and modal mineralogy variations, feldspathic pyroxenite was subdivided into five types (I, II, III, IV and V). The variation in the average contents of MgO, La_N/Yb_N and ΣREE for the Platreef rocks are consistent with the modal mineralogy from the least to the most differentiated rocks. However, the Sr–Nd isotope data of the Platreef rocks have revealed two distinct groups of samples with decreasing εNd_{2060}. Group 1 consists of pyroxenite and feldspathic pyroxenite II, III and V having εNd_{2060} values that range from −8.4 to −2.9, and $^{87}Sr/^{86}Sr_{2060}$ values from 0.707281 to 0.712106. The Platreef rocks of group 2 consist of olivine pyroxenite and feldspathic pyroxenite Type I with εNd_{2060} ranging from −12.6 to −10.8, and $^{87}Sr/^{86}Sr_{2060}$ ranging from 0.707545 to 0.710042.

4

In comparison to the LZ, CZ and MZ rocks, which have εNd values ranging from –8.5 to –5.1, and $^{87}Sr/^{86}Sr$ ranging from 0.704400 to 0.709671, Platreef pyroxenite of group 1 have lower negative $εNd_{2060}$ values (from –3.8 to –2.9) and higher $^{87}Sr/^{86}Sr_{2060}$ values from 0.709177 to 0.710492, whereas feldspathic pyroxenite of group 1 have overlapping $εNd_{2060}$ values (from –8.4 to –4.9) but also higher $^{87}Sr/^{86}Sr_{2060}$ values (from 0.707281 to 0.712106). Instead, the Platreef olivine pyroxenite and feldspathic pyroxenite in group 2 highly negative $εNd_{2060}$ values and overlapping $^{87}Sr/^{86}Sr_{2060}$ values.

It is therefore suggested that the Platreef magmas derived from the partial melting of an heterogeneous mantle source comprising depleted mantle melts and both metasomatized slightly unradiogenic Nd enriched melts and highly unradiogenic Nd enriched melts from the subcontinental lithospheric mantle. These magmas ascended via the continental crust using different paths and interacted with rocks of different Sr–Nd isotopic compositions which resulted in the formation the hybrid magmas. The study speculates that sulphide saturation in the Platreef magmas was reached in the staging chambers at depth, and the varying styles of the PGE mineralisation in the Platreef rocks are the result of the varying degree of partial melting of the heterogeneous source for their magmas.

In conlusion, this study suggests that the genesis of the Platreef is much more complex and should be considered very much independent from processes involved in the genesis of the RLS in the Eastern and Western Limbs of BIC in agreement with earlier studies.

5

Acknowledgements

Firstly, I would like to thank my supervisors Doctor Abdi Siad and Professors Charles Okujeni and Dirk Frei who have guided me throughout this academic journey. A special thank you also goes to Professors Maarten de Wit and Lorna Holtman and Doctor Russell Bailie who have supported me during the completion of my studies.

A very special mention goes out to my dear and lovely wife and children. Thank you so much for your unconditional understanding, love and support.

I would also like to express my sincere gratitude to my parents, sisters and brothers for the advice and support that they have given me throughout my studies.

To my dear colleagues and friends Marcelene Voigt (CGS, Bellville), Yafah Williams, Adjiba Makopo, Jose Calipa Salmao, Jabulile Majozi (De Beers, SA), Kaizer Magonono and Zama Mgaga, and to the departmental staff Wasielah Davids, Peter Meyer, Henok G. Solomon, Adrian Williams, Janine Becorney and Richard Harrison, your contributions are highly regarded and appreciated.

Lastly to The Almighty God, I surrender all.

"Leo Leo njo Leo, Leo Kivumbi na Jasu Leo"

6

Table of contents

List of figures

List of plates

List of tables

11

1 INTRODUCTION

The first part of this introduction chapter provides the readers, especially for those who are not familiar with the Bushveld Igneous Complex, a brief overview with regard to its host rock, magmas, outcrops, stratigraphy and rock types. This brief overview leads to the second part of this chapter which focuses on the Platreef, the main subject of this study. The latter section will present issues around ongoing debate about the genesis of the Platreef as well as some of the problems that have motivated this study.

1.1   A brief overview of the Bushveld Igneous Complex (BIC)

1.1.1   Host rock, magmas, outcrops and stratigraphy

The Bushveld Igneous Complex (BIC) was emplaced into the Kaapvaal Craton of South Africa ~2.06 Ga ago onto the Transvaal Supergroup sediments and Archaean granitoids of the Witwatersrand and Pietersburg blocks (Fig. 1; Walraven et al., 1990; Buick et al., 2001; Eglington and Armstrong, 2004; Yudovskaya et al., 2013b; Zeh et al., 2015). Its thickness reaches a maximum of up to 9 km, and its size covers an extent area of about 70,000 km^2 (Wilson, 2015). As such, the BIC is the largest igneous province on Earth (Van Tongeren et al., 2016).

The BIC is comprised of four major plutonic units, namely, the Rooiberg Group (at the base), followed by the Rustenburg Layered Suite (RLS), then the Lebowa Granite Suite and lastly the Rashoop Granophyre Suite (at the top) (SACS; 1980). Also, there are satellite bodies (e.g., the Molopo Farms Complex, Uitkomst intrusion, Losberg intrusion, Moloto intrusion, and the Rhenosterhoekspruit body) that are also considered to be part of the Bushveld magmatic episode (Eales and Cawthorn, 1996).

13
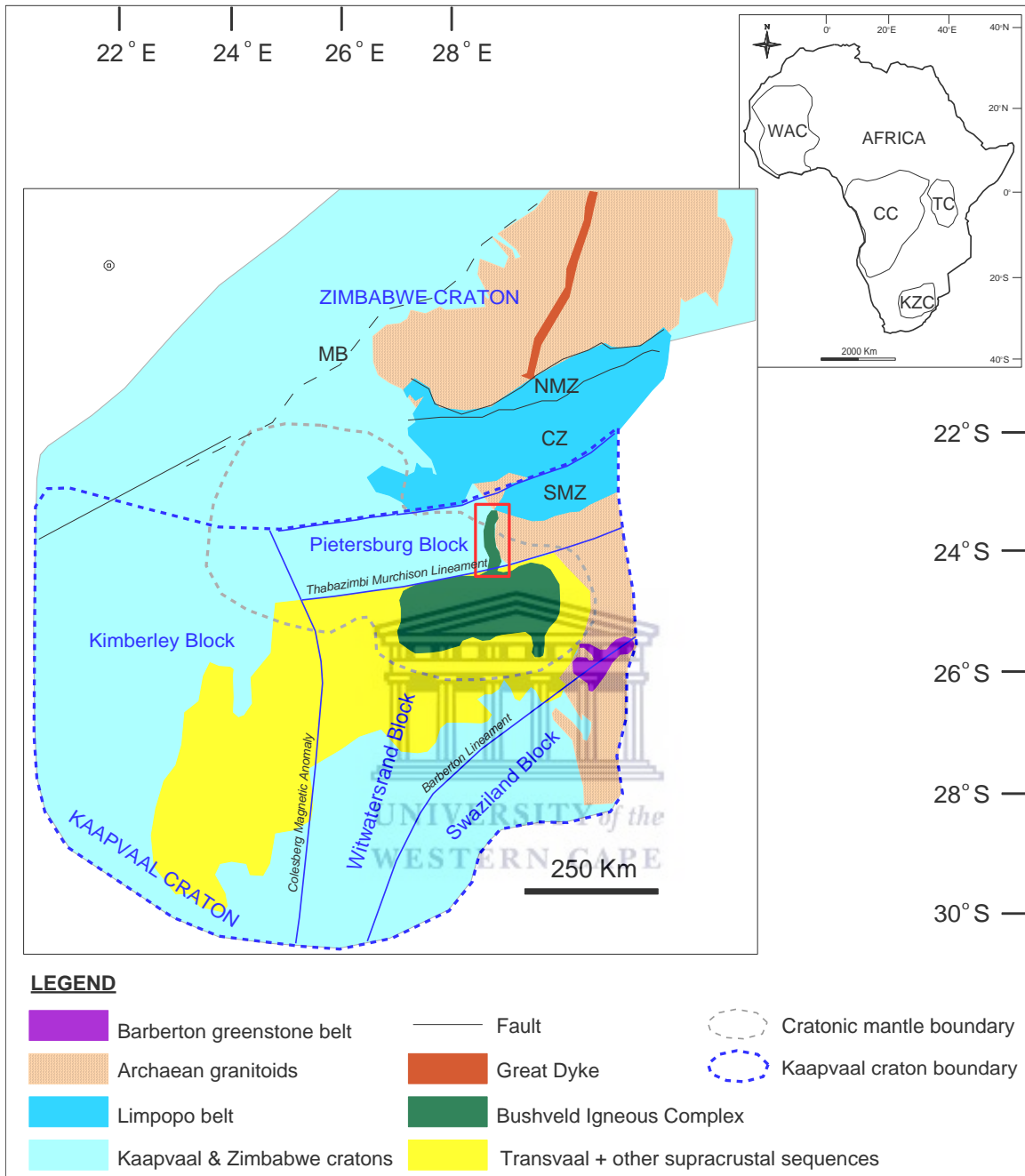
Figure 1: Sketch map of the Kaapvaal and Zimbabwe Cratons with surrounding Archaean and Proterozoic units modified after Eglington and Armstrong (2004); Richardson and Shirey (2008). Also on the map are the different blocks of the Kaapvaal Craton, and the Northern marginal zone (NMZ), central zone (CZ) and Southern marginal zone (SMZ) of the Limpopo belt. The inset map shows the West African Craton (WAC), Congo Craton (CC), Tanzania Craton (TC) and Kaapvaal and Zimbabwe Cratons (KZC) modified after Begg et al. (2009). The seismic boundary of the low Cratonic mantle is after James et al. (2001); Shirey et al. (2002). The red square shows the location of the Northern Limb of the Bushveld Igneous Complex.

14
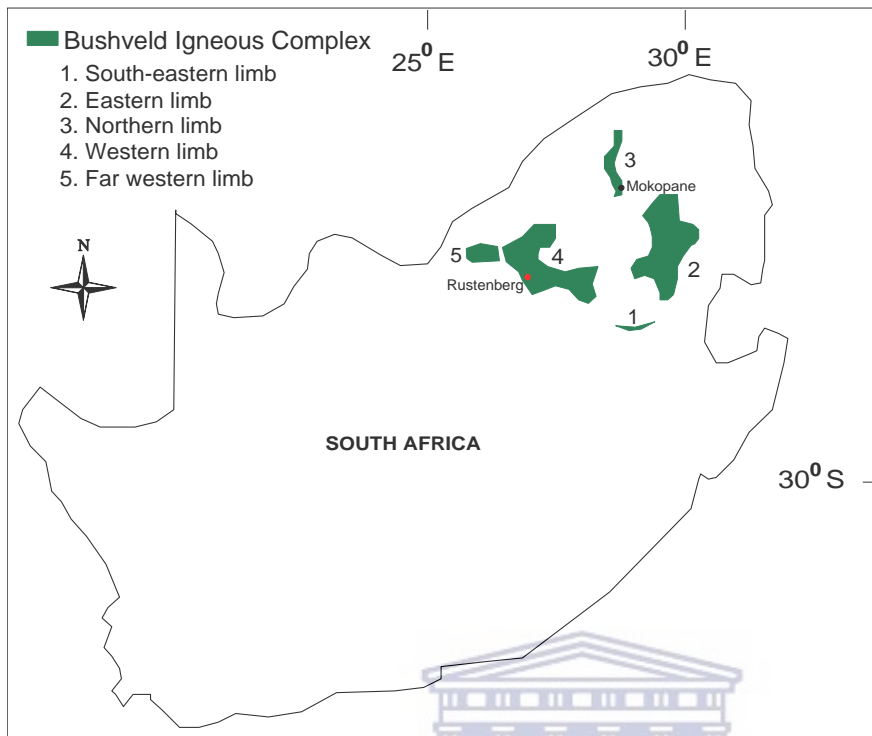
Figure 2: Location map of the five Limbs of the Bushveld Igneous Complex.

Amongst the four plutonic units of the BIC, the RLS has been the subject of numerous studies. Scientific interests vary from a wide range of issues related to 1) the RLS being the host for platinum group element (PGE), Cr, V and Ti deposits or the host of different PGE deposits (the Merensky reef, the Platreef and the UG-2 chromitite), 2) its size and mechanism of emplacement or 3) the lack of consistent stratigraphy for the RLS since its rocks outcrop in five major Limbs known as the Eastern, Western, Northern, far Western and South-eastern (Fig. 2; Eales et al., 1993; Cawthorn and Walraven, 1998).

From the base upwards, the stratigraphy of the RLS is made up of: 1) Basal Ultramafic Sequence (BUS) with dunites, harzburgites and pyroxenites 2) Marginal Zone (MaZ) with noritic and gabbroic rocks; 2) Lower Zone (LZ) having harzburgites and feldspathic pyroxenites; 3) Critical Zone (CZ) with chromitites, harzburgites, orthopyroxenites and feldspathic pyroxenites; 4) ain Zone (MZ) with gabbroic rocks; and 5) Upper Zone (UZ) having magnetitites and pigeonites in place of orthopyroxene (SACS, 1980, Eales et al., 1993; Kruger, 1994; Eales and Cawthorn, 1996; Wilson, 2012; 2015).

15
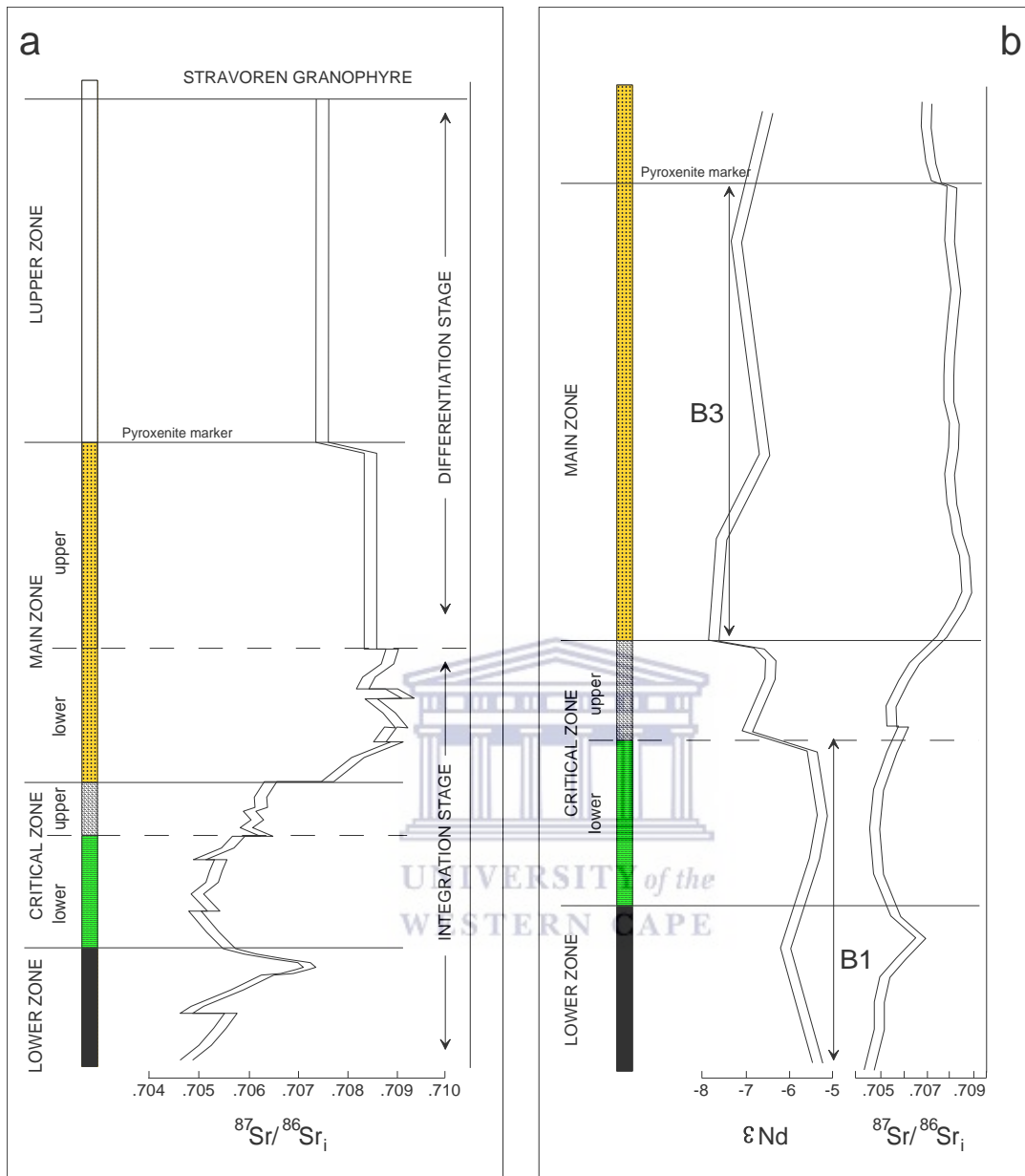
*Figure 3: $^{87}Sr/^{86}Sr$ and εNd variations for the Rustenburg Layered Suite of the BIC. The data plotted in profile (**a**) are from Kruger (1994) and those plotted in profile (**b**) are from Maier et al. (2000) and references therein.*

1.1.2   The Rustenburg Layered Suite (RLS)

Ever since the earlier studies by Sharpe (1981) and Harmer and Sharpe (1985), the RLS is viewed to consist of the product of three different magma types. The first magma (i.e., B1; MgO-rich) produced the LZ and the Lower CZ (C_LZ), while the second magma (B3;

Al_2O_3-rich) produced the MZ rocks (Fig. 3). The third RLS magma (B2), which produced the Upper CZ (C_UZ) rocks, was an intermediate between B1 and B3, and hosts the UG-2 chromitite and the Merensky reef.

Geochemical constraints on the emplacement and magmatic processes of the RLS in the Eastern and Western Limbs of the BIC have mainly emerged from Sr–Nd isotope studies (Hamilton, 1977; Sharpe, 1981; Harmer and Sharpe, 1985; Sharpe et al., 1986; Kruger, 1994; Eales et al., 1990; Maier et al., 2000). These studies have revealed breaks in the isotopic ratios with height which were interpreted as series of magmatic pulses, each having different isotopic signature. Kruger (1994) has suggested a two-phase process for the emplacement of the RLS magmas (Fig. 3a). The first phase, which he termed an "integration stage", is characterised by an irregular upward increase in $^{87}Sr/^{86}Sr$ with height from 0.7047 in the LZ to 0.7091 in the Lower MZ (M_LZ) (Fig. 3a). The second phase (i.e., differentiation stage; Kruger, 1994) is marked by constant $^{87}Sr/^{86}Sr$ (0.7085) with height in the Upper MZ (M_UZ) and constant $^{87}Sr/^{86}Sr$ (0.7073) with height in the UZ (Fig. 3a). Studies by Maier et al. (2000) show there is a general decrease in εNd and increase in $^{87}Sr/^{86}Sr$ with height from the LZ to the MZ in the BIC (Fig. 3b). The εNd ranges from –5.3 to –6.0 and the $^{87}Sr/^{86}Sr$ ranges from 0.705 to 0.707 in the LZ and CZ, whereas εNd ranges from –7.9 to –6.4 and $^{87}Sr/^{86}Sr$ ranges from 0.708 to 0.709 in the MZ (Fig. 3b; Maier et al., 2000).

In terms of stratigraphic correlations, not all the five zones of the RLS are present in each Limb of the BIC. The Eastern and Western Limbs of the BIC possess the five zones, and the stratigraphy and the rock types are quite similar (Eales et al., 1993). In the far Western Limb, there are only the LZ rocks, similar to those in the Western Limb (Cawthorn et al., 1998). The South-Eastern Limb of the BIC, which is inferred to be an extension of the Eastern Limb due to the fewer unique and anomalous marker horizons, only has a well-developed UZ rock sequence (Buchanan, 1975; Cawthorn et al., 1998). The Northern Limb of the BIC has also five zones. However, only the UZ and the MZ can be correlated to the Eastern and Western Limbs. The rocks that are generally assigned to the CZ are present in the Northern Limb as the Platreef, which is overlain by

17

the MZ. So, issues related to the genetic relationship between the magmas that formed the CZ in the Eastern and Western Limbs and the Platreef has since been the subject of debate. Besides, the Platreef overlies several country rocks below which the LZ is present (Yudovskaya et al., 2013a). However, studies have shown that the LZ in the Northern Limb has different signatures than the LZ in the Eastern and Western Limbs of the BIC (McDonald et al., 2009; Yudovskaya et al., 2013a). These have further triggered various studies to be conducted on the Platreef seeing that it is the main source of PGE in the Northern Limb and the BIC.

1.2   The Platreef

The Platreef is a PGE deposit that occurs along 30 km of strike in the Northern Limb (Fig. 4). It occurs as a series of mafic and ultramafic sills between the MZ and the country rock (also called floor rock) which consists of the Transvaal Supergroup sediments and the Archaean granite (Fig. 4; Ashwal et al., 2005; Van der Merwe, 2008). In contrast to the Merensky Reef and the UG-2 chromitite, which are less than 1 meter in thickness and occur at about the same stratigraphic position in the CZ of the Eastern and Western Limbs, the Platreef is 10 to 400 m in thickness and comprises pyroxenites, norites, gabbros, peridotites and dunites (Gain and Mostert, 1982; Harris and Chaumba, 2001; McDonald et al., 2005; Kinnaird et al., 2005; Mitchell and Scoon, 2012). Although the Platreef has been the focus of intense exploration; currently having seven open-pit operations of which three have been mined out, several issues are of significant concern and remain the subjects of research.

One of the issues related to the Platreef is the distribution and styles of the PGE mineralisation which vary with depth and along strike. The PGE mineralisation is mainly associated with the base metal sulphides (BMS), tellurides, bismuthides, antimonides and arsenides, and is hosted not only in different rock types but also at different depths along strike (Gain and Mostert, 1982; Armitage et al., 2002; Kinnaird et al., 2005; Hutchinson and Kinnaird, 2005; Holwell and McDonald, 2006; Hutchinson and McDonald, 2008; Mitchell and Scoon, 2012).
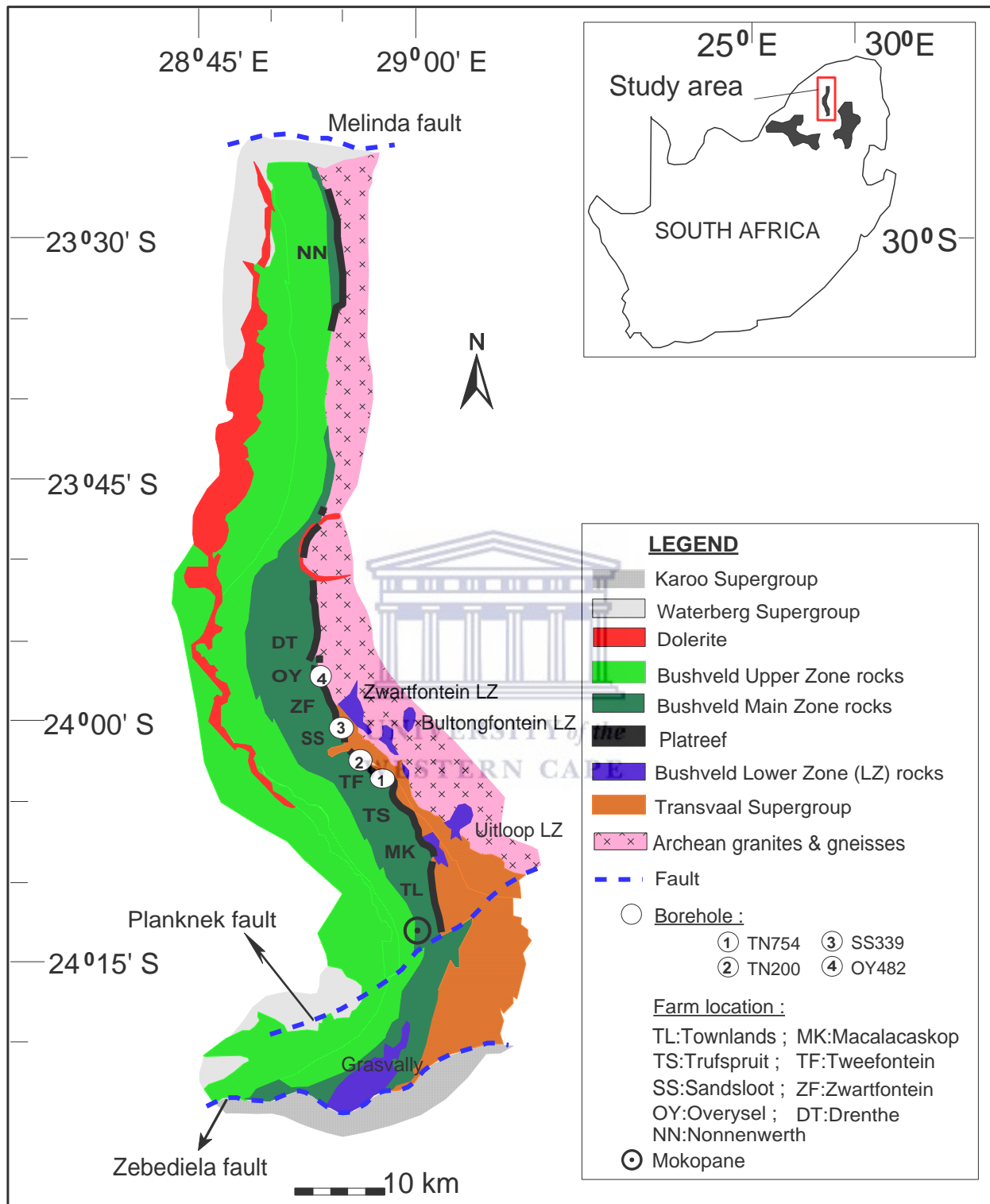
Figure 4: Simplified geological map of the Northern Limb of the Bushveld Igneous Complex after Kinnaird and McDonald (2005), modified from Van der Merwe (1978) and Ashwal et al. (2005). The inset map shows the location of the Northern Limb relative to the Eastern and Western Limbs of the BIC.

Although scientists agree that the PGE mineralisation is magmatic in origin, research has shown that its distribution and styles in the Platreef are still not fully understood since multiple magmatic injections influenced them (Kinnaird, 2005; Manyeruke et al., 2005; Yudovskaya and Kinnaird, 2010). Other processes that have contributed include crustal contamination (Sharman-Harris et al., 2005; Penniston-Dorland et al., 2008; Ihlenfeld and Keays, 2011; Sharman et al., 2013) and fluid-rock interaction (Holwell and McDonald, 2006). Further issues related to the timing of intrusion between the Platreef and the MZ magmas have also affected the distribution of the PGE (Holwell and Jordaan, 2006).

The lack of consistent stratigraphy for the Platreef, which has been largely evidenced from various drill cores extracted along strike, also poses a major challenge to locate areas of PGE mineralisation. Although the cause for this may be attributed to factors such as the floor rock topography which has affected the thickness of the Platreef (Armitage et al., 2002; Nex, 2005; Yudovskaya and Kinnaird, 2010) and the presence of xenoliths and MZ sills within the Platreef which has also complicated the rock sequence (Harris and Chaumba, 2001; Ihlenfeld and Keays, 2011; Yudovskaya et al., 2013a), the multiple magmatic injections (Kinnaird, 2005; Manyeruke et al., 2005; Yudovskaya and Kinnaird, 2010) have not produced a consistent stratigraphy and, consequently, it is responsible for the variation in the distribution of the PGE mineralisation with depth and along strike.

In terms of magma emplacement, Kinnaird (2005) suggested that the Platreef at the farm Turfspruit (Fig. 4) formed as inter-fingered intrusive sills, considering the compositional breaks in the major and trace elements data between pyroxenite sills which are marked by the changes in the mineral chemistry. Additionally, Kinnaird (2005) noted the occurrence of primitive pyroxenite sills towards the top part of the Platreef. At Townlands (Fig. 4), Manyeruke et al. (2005) suggested the sill-like intrusion model for the formation of the Platreef because of the compositional breaks in the trace elements and S isotope data between pyroxenite sills, also coupled with primitive rocks at the top part of the Platreef. Using drill cores from various farms along the Platreef, Yudovskaya and Kinnaird (2010) suggested a mixing model for the formation of chromitites as a result of the ultramafic magma influx that has interacted with a residual magma or another contaminant.

20

In a preliminary study at the Akanani prospect (Zwartfontein farm; Fig. 4), Mitchell and Scoon (2012) have proposed a three-stage emplacement for the Platreef magmas which consists of 1) an early injection of repeated gabbroic magmas that formed the PU1 sub-unit, followed by 2) injections of ultramafic magmas (PU2) into the partially crystalline early-formed gabbros and the M_LZ, and lastly by 3) partial melting and recrystallization of PU1 or MZ rocks which formed PU3 due to the intrusion of the ultramafic magmas.

On the basis of the models suggested, it can be said that the difference in geochemical attributes between the Platreef pyroxenite sills does not only indicate that these sills were emplaced from multiple magmatic injections (Kinnaird, 2005; Manyeruke et al., 2005) but, it may also indicate that their magmas have originated from different sources.

To this day, the genesis of the Platreef is a subject of debate. Some researchers suggested the Platreef and its hanging wall norite share a common parental magma (Pronost et al., 2008). Others (Kruger, 2005; Pronost et al., 2008; Reisberg et al., 2011) have suggested the Platreef shares a common origin with the Merensky reef in the Eastern and Western Limbs of the BIC. Contrary to the latter, some researchers (McDonald et al., 2005) have proposed that the Platreef is not genetically related to the Merensky reef, but it may represent a product of the interaction between the MZ and the LZ magmas of the BIC. There are also researchers who suggested the Platreef have similarities with the C_UZ and the MZ (Maier et al., 2008) or the CZ of the BIC (Yudovskaya and Kinnaird, 2010). More recently, others have suggested the Platreef is a more contaminated extension part of the CZ and LZ of the BIC (Yudovskaya et al., 2017a, 2017b; Gobler et al., 2018).

In this regard, Sr–Nd isotope data are of importance since they can be used to trace the source of magmas, understand processes involved in the genesis of mafic intrusions and are not affected by chemical fractionation associated with crystallisation (Stewart and DePaolo, 1990; Casquet et al., 2001; Maier et al., 2000; Chen et al., 2001; Zhou et al., 2004; Sun et al., 2013; Howarth and Prevec, 2013; Duan et al., 2016; Shu et al., 2018). The published Sr–Nd isotope data for the Platreef to date are from pyroxenite samples (Pronost et al., 2008). The fact that the Platreef consists of many rock types, previous

21

interpretations (Pronost et al., 2008) may not be representative for the Platreef as a whole. It is therefore important to expand the Sr–Nd isotope data and recognize the use of other rock types in order to understand how the Platreef formed.

1.3 The motivation for the study

This study uses whole-rock Sr–Nd isotope data to contribute towards our understanding on the processes involved in the genesis of the Platreef and will be undertaken in two steps.

The first step aims at determining the source of the Platreef magmas and identifying the processes involved in its genesis based on the major, trace and isotope data from the rock types (and the few MZ samples) collected from four drill cores, namely; two drill cores are from Tweefontein and the others two are from Sandsloot and Overysel (Fig. 4). This study, therefore, contributes new Sr–Nd isotope database for the Platreef rock types by adding data for olivine pyroxenite, pyroxenite and feldspathic pyroxenite (and also few MZ gabbronorite). The new data will complement the earlier published Platreef data obtained from pyroxenite taken at Overysel and Sandsloot (Pronost et al., 2008). No other studies have Sr–Nd isotope data for a variety of Platreef rock types and, in particular, for the Platreef at Tweefontein. Hence, the current Sr–Nd isotope data are unique.

The second step aims at comparing the new Sr–Nd isotope data for the Platreef rocks with published data from rock samples collected from the LZ, CZ, Platreef and MZ of the BIC (Maier et al., 2000; Pronost et al., 2008; Roelofse and Ashwal, 2012) to establish whether any genetic link exists between the Platreef magmas and the magmas of the RLS (i.e., B1 and B3) from the Eastern and Western Limbs of the BIC.

1.4 Study layout

Following this introductory chapter which focused on the BIC in general and the Platreef in particular, chapter two presents a summary of the geology of the Northern Limb of the BIC.

Chapter three describes the methods and protocols used for data generation in this study. Chapter four presents the petrography, while chapter five present the results from whole-rock geochemistry. The latter presents the results in sub-chapters which include: 1) major element geochemistry; 2) trace element geochemistry; 3) Sr–Nd isotope geochemistry and 5) BMS and PGE contents in the Platreef rocks. Chapter six contains our discussion which is then followed by our conclusions and recommendations in chapter seven.

2 SUMMARY OF THE GEOLOGY OF THE NORTHERN LIMB OF THE BUSHVELD COMPLEX

The Northern Limb of the BIC is located in the Limpopo Province of South Africa (Fig. 4). It is a sinuous outcrop (~120 km of length) and has a maximum width of ~15 km (Fig. 4) (Armitage et al., 2002; Van der Merwe, 2008). Along its N-S strike line, the Northern Limb stretches from the Melinda fault in the north to the Zebediela fault in the south (Fig. 4) (Van der Merwe, 2008), and is separated from the Eastern and Western Limbs of the Complex by the Thabazimbi-Murchison Lineament of which the Zebediela, Planknek and Welgevonden faults are part (Kinnaird et al., 2005; Kinnaird & McDonald, 2005).

The Platreef forms the base of the igneous unit of the Northern Bushveld and is ~30 km along strike from the farms Townlands in the south to Nonnenwerth further north (Fig. 4; Manyeruke et al., 2005; Maier et al., 2008; Van der Merwe, 2008). It is composed of a 10- to 400 m in thickness package of mainly pyroxenitic rocks with variable amounts of norites, gabbros, peridotite, serpentinite, rare dunites and xenoliths of metamorphosed sedimentary rocks (Armitage et al., 2002; Manyeruke et al., 2005; Hutchinson and Kinnaird, 2005; Holwell and McDonald, 2006; Pronost et al., 2008; Yudovskaya and Kinnaird, 2010; Ihlenfeld and Keays, 2011; Van der Merwe et al., 2012; Mitchell and Scoon, 2012).

From south to north, the Platreef overlies progressively different rocks of the Transvaal Supergroup. From the farm Macalacascop (south) to Sandsloot, the floor rock comprises quartzites of the Daspoort Formation, followed northwards by quartzite, shale and dolomite of the Timeball Hill Formation, the Penge banded iron Formation, dolomite of the Malmani Subgroup (Fig. 4; Harris and Chaumba, 2001; Armitage et al., 2002; Kinnaird et al., 2005; Nex, 2005; Holwell and Jordaan, 2006; Pronost et al., 2008; Ihlenfeld and Keays, 2011; Van der Merwe et al., 2012). From north of the farm Zwartfontein to Overysel and further north, the Platreef overlies Archaean granites as basement rock (Fig. 4; Holwell and McDonald, 2006; Maier et al., 2008; Yudovskaya and Kinnaird, 2010).

The Platreef is overlain by rocks of the MZ which are generally assigned to the BIC (Fig. 4; Harris and Chaumba, 2001; Armitage et al., 2002; McDonald et al., 2005; Kinnaird et al., 2005; Holwell and Jordaan, 2006; Van der Merwe et al., 2012).

The LZ rocks in Northern Limb of the BIC have been previously considered to occur as satellite bodies (Grasvally, Uitloop, Bultongfontein and Zwartfontein) that are adjacent to the Transvaal Supergroup (Fig. 4; Hulbert and Von Gruenewaldt, 1986; Maier et al., 2008; Van der Merwe, 2008; McDonald et al., 2009). A recent study (Yudovskaya et al., 2013a) has shown that the LZ is present underneath the floor rock to the Platreef at the farms Turfspruit and Sandsloot. Although the mineral composition of the LZ rocks differs from the LZ in the Eastern and Western Limbs (Yudovskaya et al., 2013a), its rock sequence is similar to that in the Eastern Limb of the BIC (Wilson, 2012). The LZ sequence reaches up to 800 m in thickness and consists of dunite, harzburgite, pyroxenite and feldspathic pyroxenite (Yudovskaya et al., 2013a).
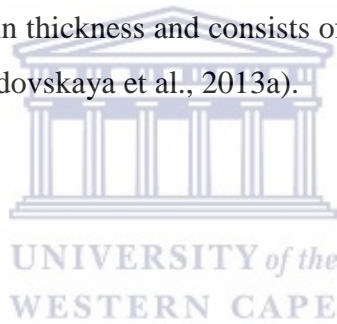
3 METHODOLOGY

3.1 Drill core selection, logging and sampling

Four borehole cores, drilled along the strike of the Platreef (TN754, TN200, SS339 and OY482; Fig. 4), were selected for this study. The drill cores, which comprises of rocks from the floor rock, Platreef and MZ, were made available by Anglo American Platinum at the Mogalakwena mine in metal trays. Core logging was done on the drill cores (from top to bottom depth) to identify the rock types, determine their thicknesses and assess the sampling procedure. It is worth mentioning that the sample depths and the thicknesses of the rock types used in this study should not be considered as true thicknesses since the cores were drilled at inclined angles.
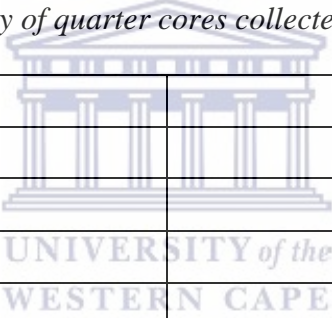
The detailed stratigraphic logs of the four drill cores are shown in Figures 5 − 8. Cores TN754 and TN200 were drilled at the farm Tweefontein (to the south) where the floor rock consists of BIF and Shale from the Transvaal Supergroup (Fig. 4). Drill core SS339 was taken at the farm Sandsloot (Centre) where the floor rock is dolomite from the Malmani Subgroup from the Transvaal Supergroup, whereas drill core OY482 is from the farm Overysel (to the North) where the floor rock is Archaean granite (Fig. 4). The age of these floor rocks increases from South to North; i.e., the BIF is the youngest and the Archaean granite is the oldest (Fig. 4).

These drill cores were mainly selected because they provide the opportunity to (1) access a variety of Platreef rock types (harzburgites, olivine-bearing pyroxenites, pyroxenites, feldspathic pyroxenites, norites and gabbronorites) and generate the Sr–Nd isotope data, (2) study their isotopic compositions and (3) also because they are PGE mineralised.

Drill cores TN200 and TN754 were selected, not only because they were extracted at the same farm and have the same footwall (i.e., hornfelsed BIF/Shale), but mostly because the two drill cores consist of Platreef rocks that can be correlated between them despite their stratigraphic differences (Figs. 5 − 6). The Platreef in drill core TN754 has two

26

feldspathic pyroxenite sills, one olivine-bearing pyroxenite sill and one harzburgite sill above the floor rock (Fig. 5); whereas drill core TN200 has four Platreef feldspathic pyroxenite sills separated from each other by norite, gabbronorite and leucogabbronorite cyclic units (Fig. 6). The Platreef in drill core SS339 consists of two feldspathic pyroxenite sills, four olivine-bearing pyroxenite sills and one harzburgite sill (Fig. 7), which can be correlated with the Platreef in drill cores TN200 and TN754 despite their difference in thicknesses and stratigraphic heights. Drill core OY482 consists of four Platreef feldspathic pyroxenite sills separated from each other by alternating fine- and medium-grained gabbronorite (Fig. 8). These Platreef feldspathic pyroxenite sills in drill core OY482, of which one is directly overlying the Archaean granite floor rock, can also be correlated with drill cores TN200, TN754 and SS339 (Figs. 5 – 8).

Table 1: Rock types and quantity of quarter cores collected for this study.

Rock type	N° of samples
BIF/Shale	5
Dolomite	2
Feldspathic pyroxenite	21
Gabbronorite/Gabbro	36
Granite	1
Harzburgite	2
Leucogabbronorite/Leucogabbro	2
Norite	11
Olivine-bearing pyroxenite	8
Pyroxenite	6
Total	**94**

A total of 94 quarter cores (~30 cm in length) were collected from the four drill cores (Table 1; Figs. 5 – 8). The sampling was done at irregular intervals due to the difference in thicknesses between the Platreef rock types. The MZ rocks were also collected since this study aims at comparing the new Sr–Nd isotope data with published data from rocks

27

collected from the LZ, CZ and MZ of the BIC. Floor rock samples (dolomite, granite and BIF/shale) were also collected.

3.2   Petrography

Thin sections were prepared from each core sample and studied for rock classification (mineral identification, textures and modal mineralogy) using transmitted and reflected light microscopes at the University of the Western Cape (UWC). The modal mineralogy was done by visual estimation of the surface area of a mineral grain relative to other mineral grains and the total surface area of the thin section. This method was favoured above the point counting method to avoid the complexity of the analysis that emerges between the mechanics of point counting (e.g. the choice of grid distance) and the rock properties (e.g. grain size, texture and distribution of the crystals). Although the proportions of the minerals in the thin sections are approximations, they agree well with the distribution of the minerals in the samples. In cases the rock samples had sulphide ores and/or few altered areas; the modal mineralogy was estimated using a combination of thin section and macroscopic studies.
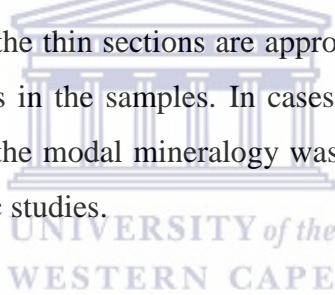
3.3   Geochemistry

3.3.1 Sample preparation

All quarter core samples were washed with double distilled-water and left to dry down at room temperature at UWC. Upon dryness, a portion of each quarter core (~50 g) was crushed and pulverised into homogenised powder for 3 minutes in a tungsten-carbide ring mill using the 5x3 inch Dickie & Stockler® T-S 250 mill. After milling, each sample was transferred from the ring mill into a clean paper sample bag between samples. A handful portion of medium-grained quartz was also pulverised in the ring mill to remove possible remaining powdered sample and avoid contamination of the next sample. The ring mill was washed with distilled water and cleaned to dryness after each round of milling. On completion of the milling, 9 g of the powdered sample were mixed with 2 g of EMU wax binder in plastic vial containers to homogeneity and pressed into pellet discs at 15 kilo

28

bars. Pellet discs and portions of the remaining powdered samples were used for further geochemical analyses.

Table 2: Accuracy and precision of the X-Ray Fluorescence (XRF) analysis.

Oxide	1	2	3	4
SiO_2	51.100	50.985	0.566	0.262
Al_2O_3	4.180	4.195	1.697	0.071
Fe_2O_3	12.700	12.620	0.356	0.045
MnO	0.220	0.220	0.000	0.000
MgO	25.330	23.881	0.313	0.075
CaO	2.660	2.753	0.242	0.007
Na_2O	0.370	0.441	0.907	0.004
K_2O	0.090	0.089	0.646	0.001
P_2O_5	P	0.029	3.936	0.001
TiO_2	0.200	0.210	0.726	0.002
SO_3	*	0.012	0.000	0.000

1. Published values for NIM-P CRM or SARM 5(SACCRM, 1984); 2. Average values obtained for the analysis of 3 separately prepared SARM 5 pellet discs; 3. Percentage coefficient of variations (%CV) for the analysis of the three separately prepared pellet discs of the SARM 5; 4. %RSD for instrumental precision as determined from the replicate analyses performed on the same SARM 5 pressed powder pellet.
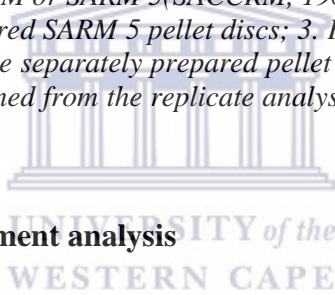
3.3.2 Whole-rock major element analysis

Ninety-four pressed pellet discs were made and analysed for major elements (i.e., SiO_2, Al_2O_3, Fe_2O_3, MnO, MgO, CaO, Na_2O, K_2O, P_2O_5, TiO_2 and SO_3) by X-ray fluorescence (XRF) in the Earth Sciences Department (UWC) using Phillips 1480® XRF spectrometer following the method described by Norrish and Hutton (1969). Loss on ignition (L.O.I.) was determined using 0.5 g of powdered sample. First, samples were placed in a crucible and heated at 60º C in an oven for 30 minutes to remove moisture. After that, L.O.I. was performed at 1000 ºC for 45 minutes using the Labcon® L-1200 furnace following the methods described by Potts (1987).

The accuracy and precision of XRF analysis were determined after analysis of pellet discs prepared from NIM-P (a pyroxenite from the CZ of the Bushveld Complex, also known as SARM 5) certified reference material (CRM). The precision of the analytical instrument was determined by repeated analysis of both, NIM-P CRM and randomly

selected-rock samples pellet discs as presented in Table 2. The precision (or %RSD) and repeatability for the major elements, expressed as percentage coefficient of variations (or %CV), are all less than 5% (Table 2).

3.3.3   Whole-rock trace element analysis

The samples used for trace element analysis were taken from the powdered samples left after preparation of pellet discs for XRF analysis.

Forty-nine samples were measured for trace element contents (i.e., Sc, V, Co, Ni, Cu, Zn, Rb, Sr, Y, Zr, Nb, Mo, Cs, Ba, Hf, Pb, Th, U and REEs) by Laser Ablation Inductively Coupled Plasma Mass Spectrometry (LA-ICP-MS) at the Central Analytical Facilities, University of Stellenbosch (South Africa), on fused glass bead disks. The glass beads, which were prepared using an automatic Claisse M4 Gas Fusion instrument and ultrapure Claisse Flux (using a ratio of 1:10 sample: flux), were coarsely crushed. A chip of sample was mounted along with up to 12 other samples in a 2.4 cm round resin disk. The mount was mapped, and then polished for analysis.
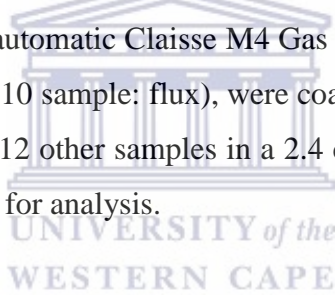
Table 3: Laser Ablation specifications.

Laser output	193 nm flat-top beam
Energy	3.6 J/cm^2
Pulse width	4ns nominal
Pulse rate	10 Hz
Spot size	100 μm
Scan pattern	3 lines of 450 μm per sample
Background counting time	15 sec
Data acquisition time	35 sec

Table 4: ICP-MS specifications.

RF Power	1350 kW
Plasma gas flow	15 L/min
Auxiliary gas flow	0.9 L/min
Carrier gas flow	0.9 L/min Ar; 0.35 L/min He; 0.4L/min N
Acquisition mode	Time Resolved Analysis
Integration time	0.01 sec / isotope
Optimized for oxide levels	< 0.6 %

30

A resolution 193 nm Excimer laser from ASI connected to an Agilent 7700 ICP-MS was used in the analysis of trace elements in bulk rock samples. The ablation was performed in Helium gas at a flow rate of 0.35 L/min then mixed with Argon gas (0.9 L/min) and Nitrogen (0.004 L/min) just before introduction into the ICP plasma. For traces in fusions, 2 spots of 100 μm were ablated on each sample using a frequency of 10 Hz with an energy capacity of 3.6 J/cm^2. Other parameters used for LA-ICP-MS are presented in Tables 3 and 4.

The SiO$_2$ values for each sample, pre-determined from the XRF analysis, were used as internal standards, and the instrument was calibrated using certified NIST 612 standard. The duplicate measurements were made on selected samples, and the calibration standard was run for every 5 samples. The certified reference standards BHVO both glass and powder (Jochum et al., 2005; 2016) were used for this purpose. The trace elements were analysed with analytical uncertainties of less than 5%.

3.3.4 Platinum group element analysis
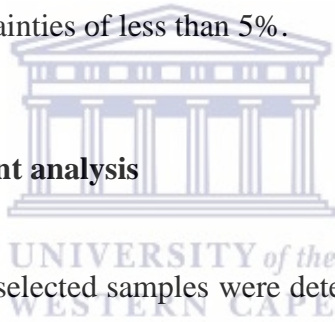
The Pt, Pd and Au contents in selected samples were determined by Inductively Coupled Plasma Optical Emission Spectrometry (ICP-OES). The analysis was done after their pre-concentration from 25 g of powdered sample on Pb beads by fire-assay at the Scientific Services Laboratories (Cape Town) using the method described by Hall et al. (1990). For this analysis, the accuracy within 5% or less was estimated using the reference standard ST 265 by fire-assay / ICP finish.

3.3.5 Whole-rock Sr–Nd isotope analysis

Twenty-four samples were used for Sr–Nd isotope analysis. The samples were taken from the same powdered samples prepared for major and trace elements (including PGE) analysis by XRF, LA-ICP-MS and ICP-OES. The sample preparation was done at the Department of Geological Science (University of Cape Town; UCT). Approximately 0.5 g of samples was placed into 7 ml clean Teflon beakers. The samples were digested in 4

ml mixture of concentrated acid (HF:HNO$_3$ at 4:1) placed onto the hotplate for 48 hours at 140° C. On complete digestion of the sample and drying down of the residue, 2 ml of concentrated HNO$_3$ (65%) was added into the sample and kept on the hotplate at 140° C. Once dried down, the residue was removed from the hotplate, cooled at room temperature and dissolved once again into 1.5 ml of 2M HNO$_3$ for the Sr–Nd separation chemistry. Two grams (recorded to 5 decimal places) of 2M HNO$_3$ was added to the samples in beakers. The latter were transferred into an ultrasonic bath for 20 minutes to allow for the complete dissolution of the sample into the acid.

The Sr–Nd separation chemistry was done by chromatographic techniques following the analytical procedures as described by Míková and Denková (2007), after those by Pin and Zalduegui (1997) and Pin et al. (1994). The starting process consists of the separation of Sr, by use of an Eichrome Sr resin bed, from the solutions. The Sr portions were dried down on a hot plate, cooled and diluted in 2 ml 0.2% HNO$_3$, ready for the determination of Sr isotope ratios using the multi-collector (MC) ICP-MS equipment. The remaining portions were dried down and converted to chloride salts by the addition of 2 ml of 6M HCl, followed by drying down of the samples. This process was done twice before dissolution of the residues in 1 ml of 0.5M HCl. The REEs were extracted using the AG50W cation resin (200 - 400#) columns. The REE portions were dried down and converted to nitrate by adding 2 ml of concentrated HNO$_3$ followed by drying down of the samples on a hotplate. After this process was done twice, the residues obtained were diluted in 1.75 ml of 0.05M HNO$_3$ and loaded onto Eichrome Ln resin columns for the collection of Nd. These portions were also dried down and diluted in 1.5 ml of 2% HNO$_3$, ready for the determination of Nd isotope ratios using the same MC ICP-MS equipment.

Considering the known Sr concentrations of the original samples, 3 ml of 200 ppb Sr solutions were prepared from the Sr portions using 0.2% HNO$_3$ and analysed using the NuPlasma HR MC ICP-MS at the Department of Geological Science (UCT). On-peak background compositions were measured for 2 minutes while aspirating 0.2% HNO$_3$, with the background measurements, including any Kr present in the Ar gas being subtracted from the measured signals. The Sr isotopes are analysed as 200 ppb 0.2%

32

HNO$_3$ solutions of the NIST SRM987 reference standard with the ^{87}Sr/^{86}Sr normalising value of 0.710255. The international rock standard JGb-1 was analysed and gave 0.705195±8, 0.705234±8 and 0.705247±8 relative to an average value of 0.705225 (0.705185 – 0.705247, literature Table 2; 0.705284±10 after Shibata et al., 2003). The Sr isotope data were corrected for Rb interference using the measured signal intensity for ^{85}Rb and the natural ^{85}Rb/^{87}Rb ratio. Instrumental mass fractionation was corrected using the exponential law and a fractionation factor based on correction of the measured ^{86}Sr/^{88}Sr ratio to the accepted value of 0.1194.

Taking into account the known Nd concentrations of the original samples, 1.5 ml of 50 ppb Nd solutions were prepared from the Nd portions using 2% HNO$_3$ and analysed on the same instrument used for Sr isotope ratios at UCT. Half a minute background measurement, which was performed before each analysis, was subtracted from the signals measured during subsequent analysis. The Nd isotopes are analysed as 50 ppb 2 % HNO$_3$ solutions of the JNdi-1, an isotope reference standard, with the ^{143}Nd/^{144}Nd normalising value of 0.512115 (Tanaka et al., 2000). The JGb-1 standard was analysed giving values of 0.512659±8 and 0.512668±8, relative to an average value of 0.512663±13 (0.512654 – 0.512672; Jochum et al., 2005). The Nd isotope data were corrected for Sm and Ce interference using the measured signal intensity for ^{147}Sm and ^{140}Ce, and the natural Sm and Ce isotope abundances. Instrumental mass fractionation was corrected using the exponential law and a fractionation factor based on the corrected observed ^{146}Nd/^{144}Nd ratio and the accepted value of 0.7219.

The initial ^{87}Sr/^{86}Sr and ^{143}Nd/^{144}Nd ratios were calculated using decay constant values of 1.42 x 10^{-11} y^{-1} for ^{87}Rb (Steiger & Jager, 1977) and 6.54 x 10^{-12} y^{-1} for ^{147}Sm (Lugmair & Marti, 1978; Begemann et al., 2001) considering the BIC published age at the nearest round-off of 2.06 Ga (Buick et al., 2001; Yudovskaya et al., 2013b; Zeh et al., 2015). The εNd was be calculated using λ^{147}Sm of 6.54x10^{-12} y^{-1}, (^{147}Sm/^{144}Nd)$_0$ value of 0.1967 for the chondritic uniform reservoir (CHUR), and (^{143}Nd/^{144}Nd)$_0$ CHUR of 0.512638. For age corrections, the Rb/Sr and Sm/Nd were obtained from the trace element analyses conducted separately. The geochemical data were processed using the *GCDKit* program after Janoušek et al. (2006).

33

4   PETROGRAPHY

4.1   Introduction

The rock nomenclature used for this study conforms to the Northern BIC nomenclature used in previous studies (Harris and Chaumba, 2001; Armitage et al., 2002; Kinnaird et al., 2005; Manyeruke et al., 2005; Holwell and McDonald, 2006; Roelofse and Ashwal, 2012). However, it should be noted that some rock types display a variety of textures and were subdivided into sub-types (e.g., feldspathic pyroxenites and norites). The Platreef rocks in the four drill cores consist of harzburgite, olivine-bearing pyroxenite (or simply olivine pyroxenite hereinafter), pyroxenite, feldspathic pyroxenite and norite (Figs. 5 – 8). The MZ consists of gabbronorites, leucogabbronorite and leucogabbro (Figs. 5 – 8). There are also granite sills that cut across the Platreef rocks in drill core TN754 (Fig. 5). Since these granite sills are different from the Archaean granite in drill core OY482 in colour and texture, they are considered late intrusions to the Platreef. Moreover, diopside-rich rocks occur in drill core SS339 (Fig. 7). Such rocks have been interpreted to be the products of the interaction between the intruding Platreef magmas and the country rock dolomite of the Malmani Subgroup (Harris and Chaumba, 2001; Armitage et al., 2002; McDonald et al., 2005). Furthermore, xenolith materials have also been noted in drill core OY482 (Fig. 8).

4.2   Drill core stratigraphy

4.2.1   Drill core TN754

Drill core TN754 is 140.84 m in length (210 – 350.84 m depth) and has the hornfelsed BIF/Shale as the floor rock (17.34 m in thickness) (Fig. 5). The latter is overlain by rocks from the Platreef and the Main Zone, having all together a maximum thickness of 123.50 meters (Fig. 5). Above the floor rock, the Platreef (~103 m in thickness) is subdivided into two units: The Lower and Upper Platreef (Fig. 5). The two units are separated from each other by gabbronorite Type III (~6 m in thickness) (Fig. 5). From the bottom to the top, the rock succession of Lower Platreef consists of olivine pyroxenite (~15 m in

34

thickness), harzburgite (~18 m), feldspathic pyroxenite Type II (~22 m) and feldspathic pyroxenite Type III (~8 m) (Fig. 5).
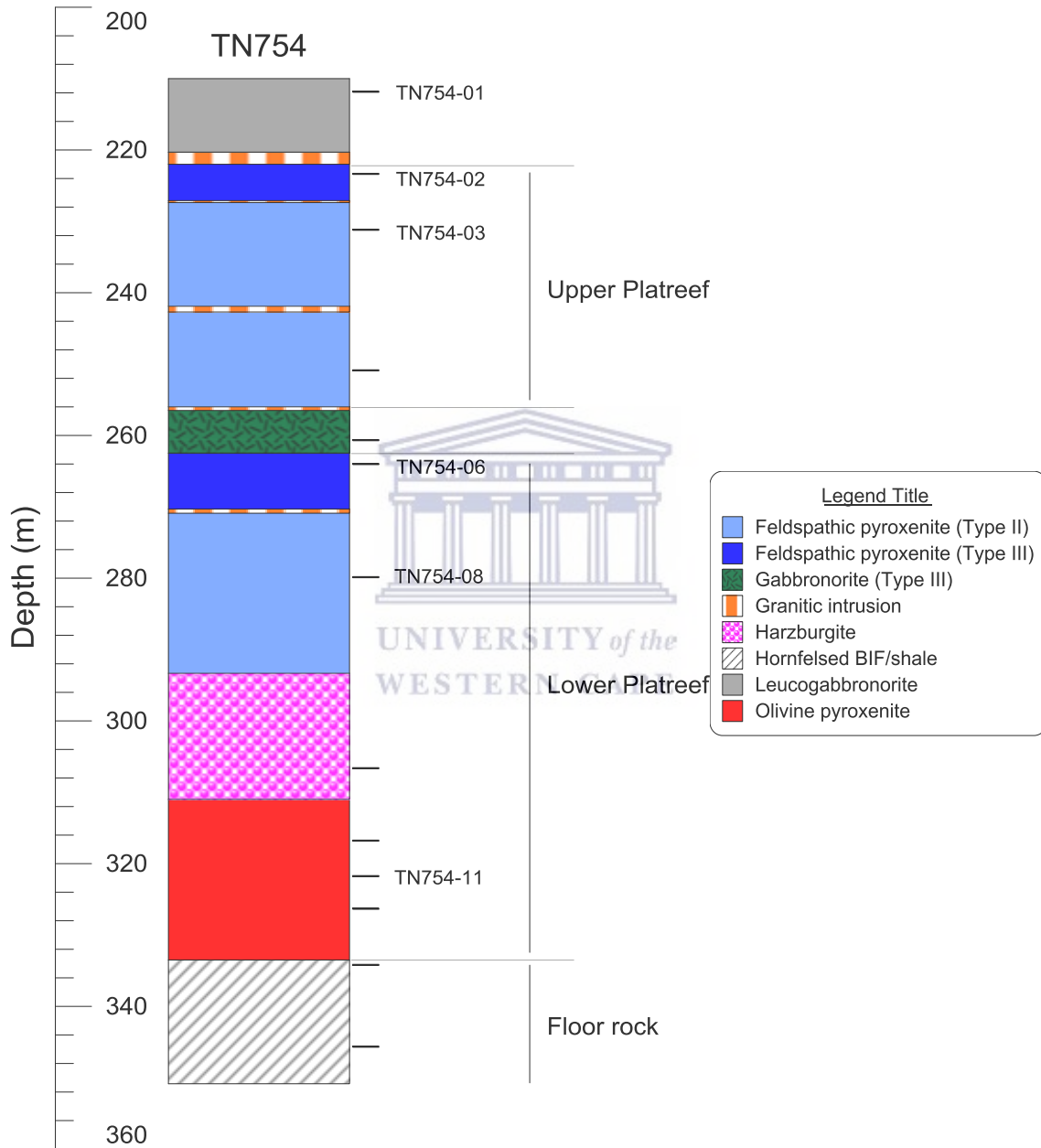
Figure 5: Stratigraphic log of drill core TN754: The "–"on the right side of the log is the location of quarter core samples used for major and trace elements. Samples used for Sr-Nd isotope analyses are annotated with their IDs also on the right side of the log.

35
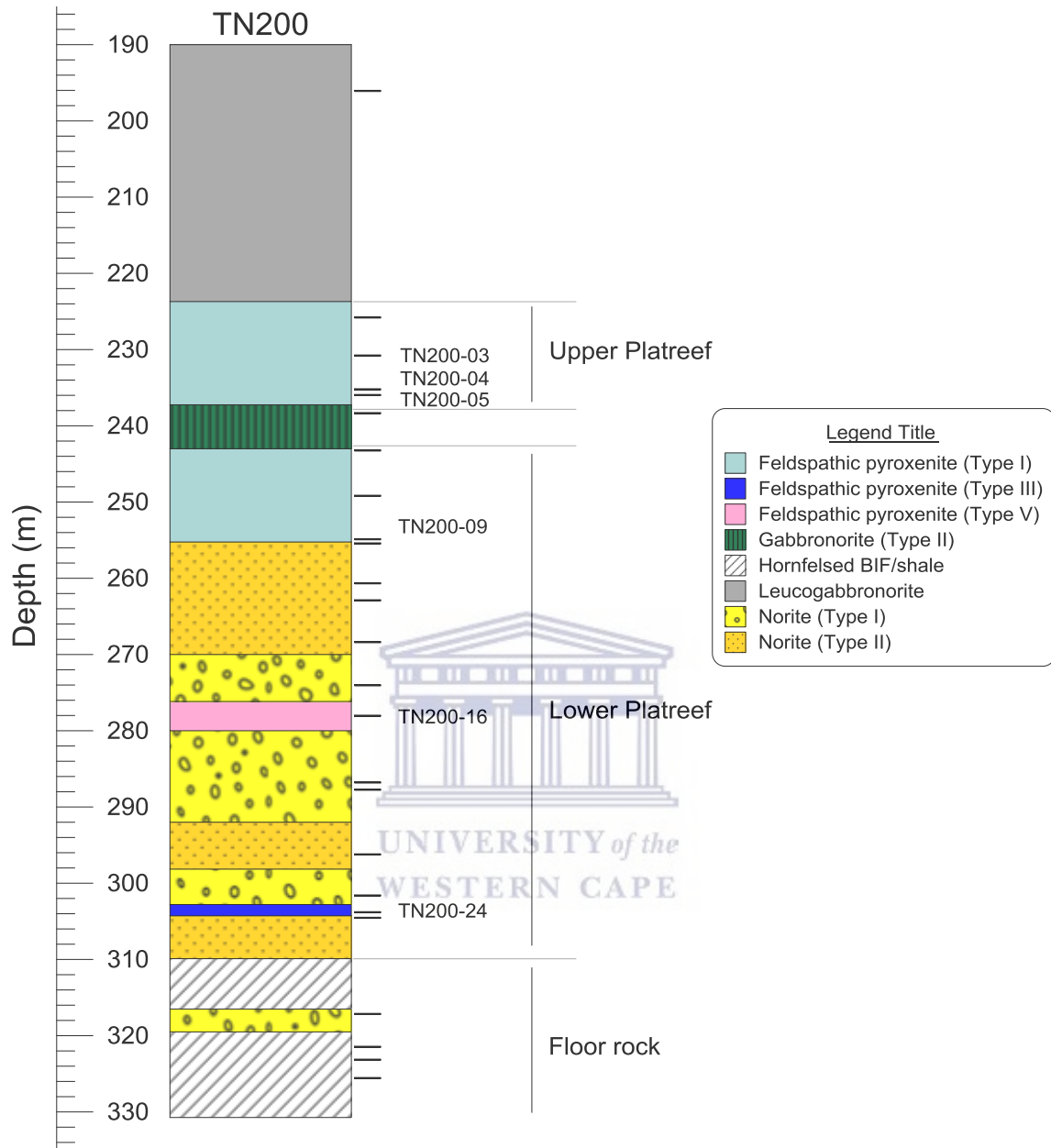
Figure 6: Stratigraphic log of drill core TN200: The "–"on the right side of the log is the location of quarter core samples used for major and trace elements. Samples used for Sr-Nd isotope analyses are annotated with their IDs also on the right side of the log.

On the other hand, the Upper Platreef consists of feldspathic pyroxenite Type II at the base (~28 m in thickness), followed by feldspathic pyroxenite Type III (~5 m) at the top (Fig. 5). There is a granite sill that cut across feldspathic pyroxenite Type II that is located in the Upper Platreef (Fig. 5).

36

In addition, the Upper Platreef has granite sills at the contact between 1) gabbronorite Type III and feldspathic pyroxenite Type II; 2) feldspathic pyroxenite Type II and Type III; and 3) feldspathic pyroxenite Type III and leucogabbronorite (Fig. 5). Moreover, there is a granite sill between feldspathic pyroxenite Type II and Type III in the Lower Platreef (Fig. 5). Leucogabbronorite, which is part of the Main Zone, is the uppermost lithology in drill core TN754 (Fig. 5).

4.2.2 Drill core TN200

Drill core TN200 is 140.73 m in length (from 190 – 330.73 m depth) and also has the hornfelsed BIF/Shale (~11 m thick) as the floor rock to the Platreef (Fig. 6). The latter is ~81 m in thickness and is also subdivided into two units: The Lower Platreef (~67 m in thickness) and the Upper Platreef (~14 m in thickness) (Fig. 6). These two units, as in drill core TN754, are also separated from each other by gabbronorite Type III (~6 m in thickness) (Fig. 6). From the bottom going up, the Lower Platreef consists of three medium-grained norite (or norite Type II) sills that are overlain by feldspathic pyroxenite Type I (~12 m in thickness) (Fig. 6).

The Lower norite Type II sill is separated from the Middle norite Type II sill by feldspathic pyroxenite Type III and norite Type I (Fig. 6). The Middle norite Type II sill is separated from the Upper norite Type II sill by norite Type I, feldspathic pyroxenite Type V and norite Type I (Fig. 6). The Upper Platreef, which consists of feldspathic pyroxenite Type I, is overlain by leucogabbronorite Type I (Fig. 6). There is also a norite Type I sill that cut across the hornfelsed BIF/Shale floor rock (Fig. 6).

4.2.3 Drill core SS339

Drill core SS339 is 180 m in length (from 2 – 182 m depth) and the floor rock dolomite has been partly metamorphosed into diopside-rich rocks (Fig. 7). In this drill core, the Platreef (~66 m in thickness) consists also of the Lower Platreef and the Upper Platreef (Fig. 7). These two Platreef units are separated from each other by gabbronorite Type III and diopside-rich rocks, all together having a maximum thickness of ~21 m (Fig. 7).
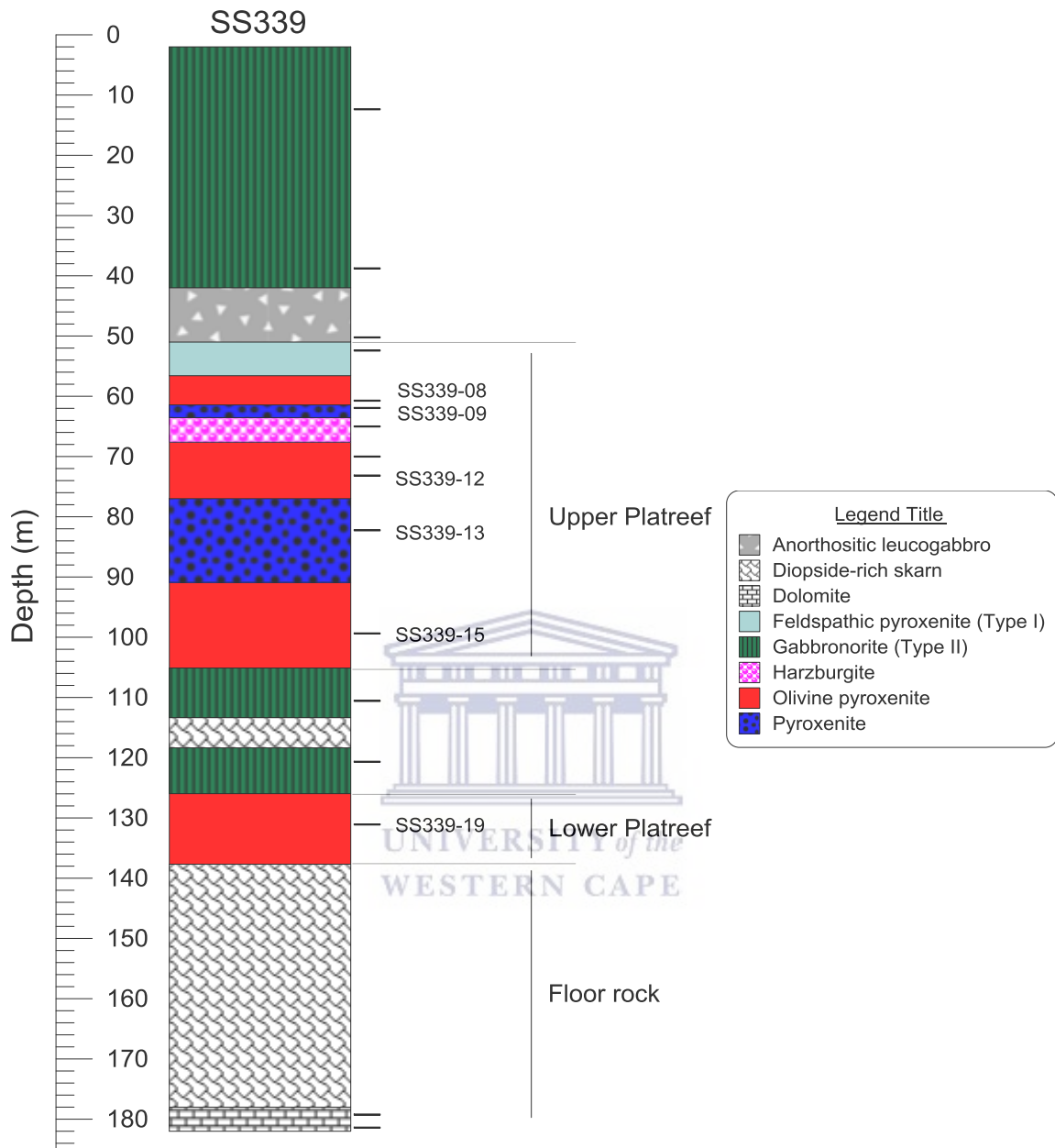
Figure 7: Stratigraphic log of drill core SS339: The "–"on the right side of the log is the location of quarter core samples used for major and trace elements. Samples used for Sr-Nd isotope analyses are annotated with their IDs also on the right side of the log.

The Lower Platreef (~12 m in thickness) consists of olivine pyroxenite (Fig. 7). From the base of the Upper Platreef (~54 m in thickness) going upward, the rocks consist of three olivine pyroxenite sills that are overlain by feldspathic pyroxenite Type I (Fig. 7).

38

The Lower olivine pyroxenite sill is separated from the Middle olivine pyroxenite sill by pyroxenite (Fig. 7). The Middle olivine pyroxenite sill is separated from the Upper olivine pyroxenite sill by harzburgite and pyroxenite (Fig. 7). The rocks, which occur above the Upper Platreef, consist of anorthositic leucogabbro and gabbronorite Type III (Fig. 7).
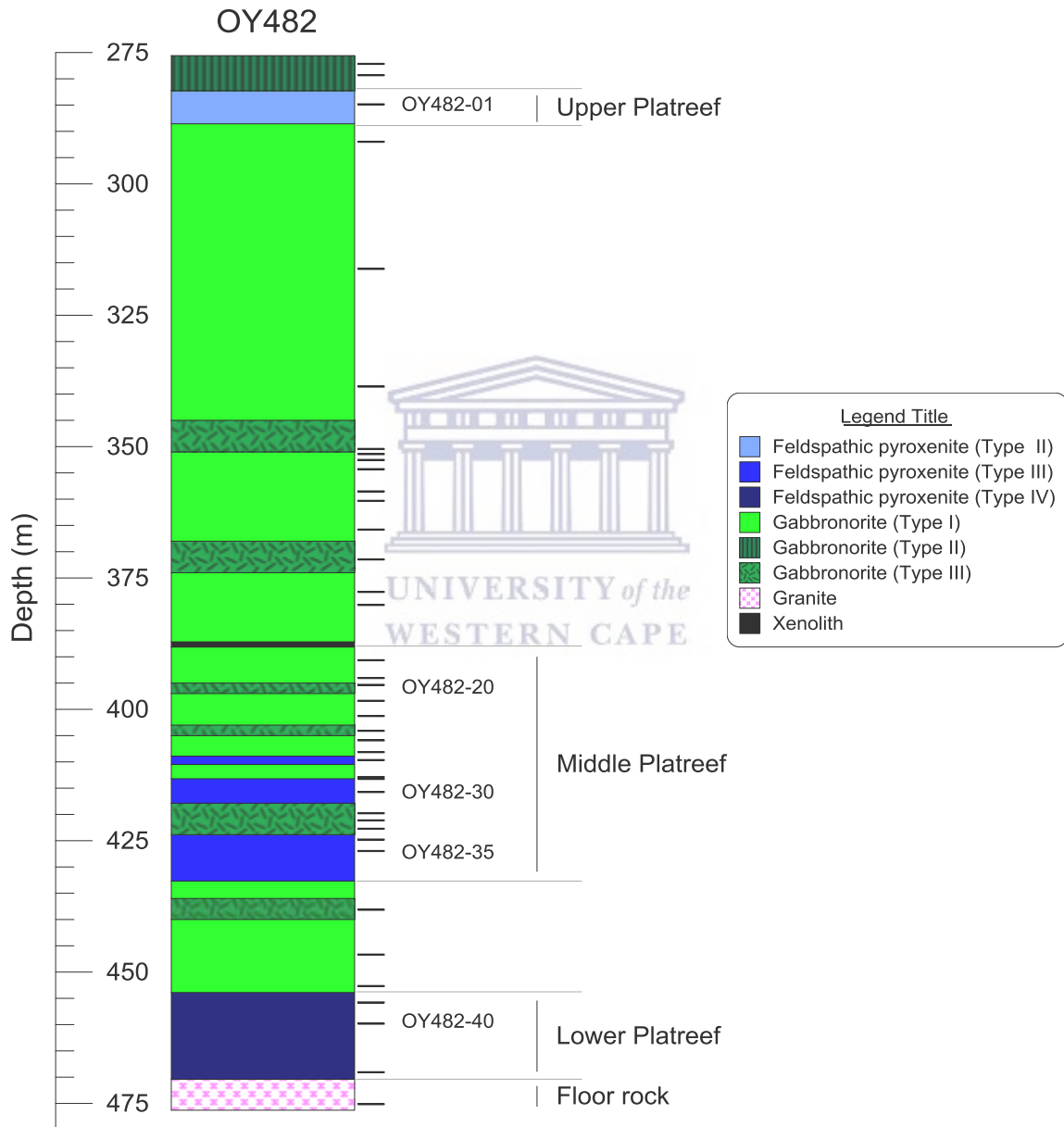
Figure 8: Stratigraphic log of drill core OY482: The "–"on the right side of the log is the location of quarter core samples used for major and trace elements. Samples used for Sr-Nd isotope analyses are annotated with their IDs also on the right side of the log.

4.2.4 Drill core OY482

Drill core OY482 is 200.7 m in length (from 275.59 – 476.29 m depth) and has Archaean granite (5.87 m in thickness) as the floor rock to the Platreef (Fig. 8). The latter (~67 m in thickness) consists of three units: The Lower Platreef, Middle Platreef and Upper Platreef (Fig. 8). The three Platreef units are separated from each other by gabbronorite Types I and III of varying thicknesses (Fig. 8). The Lower Platreef consists only of feldspathic pyroxenite type V (~17 m in thickness) (Fig. 8). The Middle Platreef consists of three feldspathic pyroxenite type III sills (of ~9, 5 and 2 m in thickness; from the lower to the upper sill) and the Upper Platreef consists of feldspathic pyroxenite Type II (~6 m in thickness) (Fig. 8). Above the Upper Platreef, the rock consists of gabbronorite Type III (Fig. 8). There is also a xenolith which occurs at ~387 m depth in this drill core OY482 (Fig. 8). Also, the contact between gabbronorite Types I and III is tectonised, and Type I appears eroded (Fig. 8). These features indicate that gabbronorite III was emplaced after gabbronorite I.

4.3   Macroscopic and thin section studies

The petrographic attributes obtained from the microscopic studies are presented in three sections:

- The first section presents the attributes of the Platreef rocks from the most primitive rock to the most evolved rock;
- The second section is attributed to the MZ rocks and;
- The last section provides a brief description of the floor rocks since these rocks are not of major interest for this study.

The terms used to describe the textures identified in the rocks (Table 5) are:

- Cumulate texture: Used to describe the occurrence of olivine or pyroxenes as the first minerals to crystallise and, in some cases, with plagioclase filling the remaining spaces in between them.
- Equigranular: Used when mineral grains are all approximately of the same size.

40

Table 5: A summary of the petrographic attributes of the Platreef and Main Zone rocks from the four drill cores.

Rock type	Sub-type	Textures & *alterations*	Modal mineralogy, and other specific attributes
Harzburgite (HZG)	–	- Cumulate. - *Serpentinisation & sericitisation.*	- Ol ~90 – 95 %; opx ~5 % ± plag 0 – 5 %. - *Rock variably mineralised in BMS*
Olivine pyroxenite (OB-Pyx)	–	- Poikilitic - *Serpentinisation & sericitisation.*	- Opx ~85 – 90 %; ol ~10 % ± cpx & plag 0 – 5 %. - *Rock variably mineralised in BMS.*
Pyroxenite (Pyx)	–	- Equigranular.	- Opx >95 %; cpx & plag <5 %. - *Rock variably mineralised in BMS.*
Feldspathic Pyroxenite (FPyx)	I	- Cumulate (Fine- to medium-grained rock). - *Sericitisation.*	- Opx ~60 – 80 %; plag ~10 – 30 %; cpx ~5 – 20 % - *Rock variably mineralised in BMS.*
	II	- Cumulate (Fine- to medium-grained rock). - *Sericitisation & uralitisation*	- Opx ~50 – 80 %; plag ~15 – 30 %; cpx ~10 – 20 % - *Rock variably mineralised in BMS.*
	III	- Cumulate (Fine- to medium-grained rock). - *Sericitisation & uralitisation*	- Opx ~50 – 80 %; cpx ~10 – 40 %; plag ~5 – 30 % - *Rock variably mineralised in BMS.*
	IV	- Cumulate (Fine-grained rock). - *Sericitisation & uralitisation*	- Opx ~50 – 80 %; cpx ~10 – 30 %; plag ~10 – 30 % - *Rock variably mineralised in BMS.*
	V	- Cumulate (Fine- to medium-grained rock). - *Sericitisation & uralitisation*	- Opx ~80 %; plag ~10 – 20 %; cpx ~5 – 10 % - *Mineralised in BMS.*
Norite (NRT)	I	- Inequigranular (Fine- to medium-grained rock). - *Sericitisation.*	- Opx ~50 %; plag ~50 %. - *Rocks are variably mineralised in BMS.*
	II	- Equigranular (Medium-grained rock) - *Sericitisation.*	- Opx ~50 %; plag ~50 %. - *Rocks are variably mineralised in BMS.*
Gabbronorite (GN)	I	- Equigranular (Fine-grained rock). - *Sericitisation.*	- Plag ~40 – 50 %; opx ~30 %; cpx ~30 %. - *Rocks are variably mineralised in BMS.*
	II	- Intergranular (Medium- to coarse-grained rock). - *Sericitisation.*	- Plag ~30 – 50 %; cpx ~30 – 50 %; opx 10 – 20 %. - *Most samples are barren rocks; except for few samples.*
	III	- Ophimottled (Fine- to medium-grained rock). - *Sericitisation.*	- Cpx+ opx ~50 – 60 %; plag ~ 40 – 50 %. - *Barren rocks.*
Leucogabbronorite/ Leucogabbro (LGN/ALG)	–	- Intergranular (Medium- to coarse- grained rock). - *Sericitisation.*	- Plag ~50 – 70 %; cpx ~20 – 40 %; opx ~0 – 10 %. - *Barren rocks.*

41

- Inequigranular: Used when mineral grains vary considerably in size.

- Intergranular texture: Used to describe the occurrence of mafic crystals filling the interstices in a random network of plagioclase laths.

- Ophimottled texture: Used to describe the occurrence of pyroxene crystals enclosing tiny plagioclase laths giving the rock a mottled or speckled appearance.

- Poikilitic texture: Used to describe the occurrence of large mafic crystals enclosing other smaller crystals.

For mineral grain sizes, the following terms were considered: 1) Fine-grained (average crystal diameter is less than 1 mm); 2) Medium-grained (average diameter is 1-5 mm); and 3) coarse-grained (average crystal diameter is greater than 5 mm).

4.3.1 Platreef rocks

4.3.1.1 Harzburgite (HZG)

Harzburgite sills occur in drill cores SS339 and TN754 (Figs. 5 and 7). Drill core SS339 has one sill of ~4 m in thickness, and drill core TN754 has also one sill of ~18 m in thickness (Figs. 5 and 7). Quarter core samples were collected from each sill from the two drill cores (Figs. 5 and 7).

In hand specimen, harzburgite samples are fine- to medium-grained rocks. The quarter core sample from SS339 contains more BMS (i.e., disseminated grains) than the quarter core sample from drill core TN754 indicating they are variably mineralised. Because of the harzburgite sill in S339 occurs at the top part of the Platreef and the sill in TN754 is located at the bottom part, we can conclude that BMS mineralisation is top-loaded in SS339, whereas it is bottom-loaded in TN754. In terms of alteration, the core samples from SS339 and TN754 were relatively fresh despite the presence of few millimetre-sized serpentine veins.

42
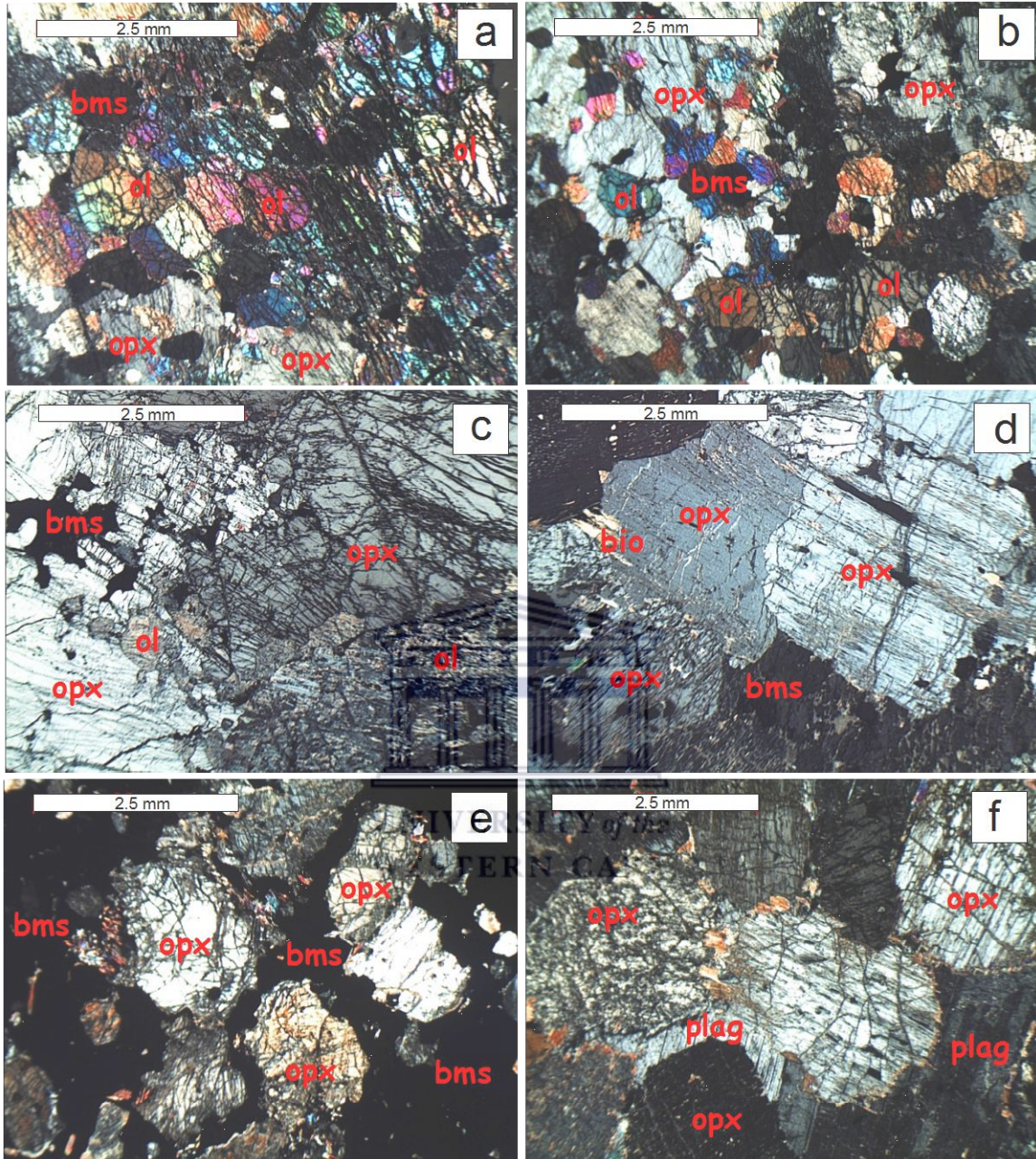
Plate 1: Photomicrographs of selected Platreef rocks. Scale bar is 2.5 mm and the field of view is 6.3 mm across for each photomicrograph. A) Harzburgite sample TN754-09: Tiny olivine inclusions in orthopyroxene at the bottom centre should be noted; B) Olivine pyroxenite sample TN754-11: The presence of aggregate grains of olivine associated with bms enclosed within orthopyroxene should be noted; C) Olivine pyroxenite sample SS339-15: The occurrence of irregularly-shaped bms within fractures of orthopyroxene should be noted; D) Pyroxenite sample SS339-13; E – F) Feldspathic pyroxenite Type I samples TN200-03 and TN200-05, respectively: The presence of bms surrounding orthopyroxene grains in sample TN200-03 should be noted. The reader is referred to text for more details on the feldspathic pyroxenite Types. Mineral abbreviations: bms: base metal sulphides; ol: olivine; opx: orthopyroxene; plag: plagioclase.

43

In thin sections, harzburgite samples have cumulate texture and are dominated by subhedral to euhedral fractured olivine primocrysts (~90 – 95 vol. %; 0.1 – 2 mm) (Plate 1a). The fractures in olivines are filled with Fe-rich oxide as veinlets and appear to have the same orientation (Plate 1a). In observed areas of the thin sections, olivine crystals have been replaced by serpentine indicating post–crystallisation fluid–rock interaction.

Orthopyroxenes occur as subhedral to anhedral crystals (~5 vol. %; 1 – 2 mm) and are mainly intergrown with olivine crystals (Plate 1a). There are also few very fine-grained olivine crystals which occur as inclusions within the orthopyroxenes (Plate 1a).

Plagioclase, whenever present (0 – 5 vol. %; <0.5 mm), is mainly interstitial to olivine crystals and is partly altered to sericite.

Base metal sulphides (i.e., pyrrhotite, pentlandite and chalcopyrite) occur (1) mainly as irregularly-shaped disseminated grains (0.25 – 1 mm) in contact with the silicates (Plate 1a), but (2) also as millimetre-sized veinlets within the fractures of olivines. The amount of olivine grains that have been altered to serpentine is less in sample TN754-09 than that in sample SS339-10.
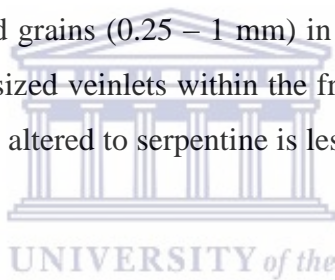
The harzburgite sample from SS339 has abundant olivine than the sample from TN754. This feature indicates that the magma from which harzburgite crystallised at Sandsloot was less fractionated than the magma at Tweefontein North.

4.3.1.2 Olivine-bearing pyroxenite (OB-Pyx)

Olivine pyroxenite sills occur in drill cores SS339 and TN754 (Figs. 5 and 7). Drill core SS339 has four sills of ~12, ~14, ~9 and ~5 m in thickness each, from the lower sill to the upper sill (Fig. 7). Drill core TN754 has only one sill of ~23 m in thickness just above the floor rock (Fig. 5). Quarter core samples were collected from each sill of the two drill cores (Figs. 5 and 7).

In hand specimen, olivine pyroxenites are fine- to coarse-grained rocks. There is a decrease in BMS contents (i.e., disseminated grains and blebs) from the upper olivine pyroxenite sill to the lower sill in SS339. In TN754, core samples at the top and bottom

44

part of the olivine pyroxenite sill have higher BMS contents (semi-massive) than the sample in the middle of the sill. These variations indicate that BMS mineralisation is top-loaded in SS339, whereas it is bottom-loaded in TN754. In terms of alteration, quarter core samples from SS339 have fewer millimetre-sized serpentine veins than those from TN754. This is an indication that samples from SS339 are less serpentinised than those from TN754.

Under the microscope, olivine pyroxenite samples have poikilitic texture and are mainly dominated by anhedral orthopyroxene oikocrysts with olivine chadacrysts (Plate 1b – e). Orthopyroxene crystals (~85 – 90 vol. %; 1.5 – 5 mm) are, in most cases, intergrown with each other (Plate 1b – d). The fractures in orthopyroxene crystals are very noticeable in samples from SS339 and those from TN754 (Plate 1b – d) indicating they were subjected to different physical conditions during or post emplacement. Subhedral orthopyroxene crystals were noticed during the thin section studies, but are rare in these rocks.

Olivines are subhedral to euhedral crystals (~10 vol. %; 0.1 – 2 mm), fractured and have different sizes (Plate 1b – d). Despite being mainly enclosed within orthopyroxene phenocrysts as single grains, olivine occurs also as aggregate of grains within or mainly intergrown with orthopyroxenes (Plate 1b). In some cases within a single thin section, olivine grains are completely altered to serpentine, whereas other grains are completely unaltered (Plate 1c). As observed in harzburgite samples, the fractures in olivine grains for olivine pyroxenites (Plate 1b – d) are also filled with Fe-rich oxide.

Clinopyroxene and plagioclase, whenever present (0 – 5 vol. %; <0.5 mm), occupy the interstitial spaces between orthopyroxene and olivine crystals. All plagioclase identified in the rocks are altered to sericite.

The ores in the rocks are blebs and/or disseminated grains of pyrrhotite, pentlandite and chalcopyrite (0.25 – 1.5 mm) with irregular shape in contact with and/ or enclosed within orthopyroxene (Plate 1b – d). They occur also as smaller veins that filled the fractures in orthopyroxene grains or as semi-massive surrounding the silicates.

In summary, the olivine pyroxenite sill from TN754 contains more abundant olivine than any of the sills in drill core SS339 indicating that the magma which emplaced the sill at Tweefontein North was less fractionated than the magmas which emplaced those at Sandsloot.

In addition, drill core SS339 has three olivine pyroxenite sills, of which one (i.e., Middle olivine pyroxenite) is in contact with the harzburgite sill (Fig. 7). The latter has cumulate texture and overlays the Middle olivine pyroxenite sill in the Upper Platreef which displays a poikilitic texture (Fig. 7). This feature is also observed in drill core TN754 (Fig. 5). The occurrence of a cumulate rock overlaying another rock displaying poikilitic texture cannot be explained through fractional crystallisation processes. On this basis, it is therefore concluded that harzburgite and olivine pyroxenite sills in two of the four drill cores studied did not crystallised from the same magma; hence, they are not co-genetic.

4.3.1.3 Pyroxenite (Pyx)

Pyroxenite sills occur only in drill core SS339 (Fig. 7). Drill core SS339 has two sills of ~14 and ~2 m in thickness each from the lower sill to the upper sill. Quarter core samples were collected from each sill (Fig. 6).

In hand specimen, pyroxenites are medium-grained rocks. The upper pyroxenite sill has larger amount of disseminated grains of sulphide ores than the lower sill indicating that BMS mineralisation is top-loaded, as the BMS mineralisation in olivine pyroxenite of the same drill core.

Thin sections show that pyroxenites display equigranular texture (Plate 1e; Table 5). The rocks are dominated by subhedral orthopyroxene primocrysts (>95 vol. %; 1 – 4 mm) which are intergrown with each other (Plate 1e). Orthopyroxene crystals have minor fractures, and some of the crystals have been slightly replaced by tiny biotite along the rim (Plate 1e). The occurrence of hydrous phase (e.g., biotite) in Platreef pyroxenites indicates that fluid–rock interaction occurred (Pronost et al., 2008).

Plagioclase and clinopyroxene (<5 vol. %; <0.5 mm) occur rarely in the interstitial spaces between orthopyroxenes, and plagioclase are completely altered to sericite.

46

The sulphide ores in the rocks occur as disseminated grains of pyrrhotite, pentlandite and chalcopyrite (0.25 – 1.5 mm) with irregular shapes enclosed within orthopyroxene. The ores occur also as smaller veins filling the fractures in orthopyroxene grains (Plate 1e).

4.3.1.4 Feldspathic pyroxenite (FPyx)

Feldspathic pyroxenite sills occur in all four drill cores (i.e., TN754, TN200, SS339 and OY482), and quarter core samples were collected from each sill during sampling (Figs. 5 – 8). Based on the textural and modal mineralogy variations, feldspathic pyroxenite was subdivided into five sub-types (Table 5): Feldspathic pyroxenite Type I, Feldspathic pyroxenite Type II, Feldspathic pyroxenite Type III, Feldspathic pyroxenite Type IV and Feldspathic pyroxenite Type V.

Feldspathic pyroxenite Type I occurs as a single sill in the Upper and Lower Platreef in drill core TN200 (Fig. 6) and also as a single sill in the Upper Platreef in SS339 (Fig. 7). The rocks have cumulate texture with fine- to medium-grained orthopyroxene (~60 – 80 vol. %), plagioclase (~10 – 30 vol. %) and clinopyroxene (~5 – 20 vol. %) (Table 5). Fine to medium-grained orthopyroxene are mainly euhedral, elongated and prismatic with interstitial plagioclase (Plates 1e and f). Clinopyroxene is anhedral and occurs mainly associated with plagioclase interstitial to orthopyroxene crystals. The latter are slightly fractured with few grains having hornblende at their edges (i.e., uralitisation). In the same thin section, there are semi-massive sulphide ores (net-textured) that filled the interstitial spaces and surrounded the pyroxenes (Plate 1e).

Feldspathic pyroxenite Type II occurs as two sills in the Upper Platreef, a single sill in the Lower Platreef in TN754 (Fig. 5) and also as a single sill in the Upper Platreef in OY482 (Fig. 8). The rocks have also cumulate texture with fine- to medium-grained orthopyroxene (~50 – 80 vol. %), plagioclase (~15 – 30 vol. %) and clinopyroxene (~10 – 20 vol. %) (Table 5). Orthopyroxene crystals are euhedral and equant with interstitial plagioclase (Plates 2a and b). In addition, orthopyroxene crystals show blebby exsolution of clinopyroxenes (Plates 2a and b). In TN754, orthopyroxene grains are also partially replaced by biotite along their rims (not shown). This feature has been interpreted as an indication of fluid-rock interaction (Pronost et al., 2008).

47
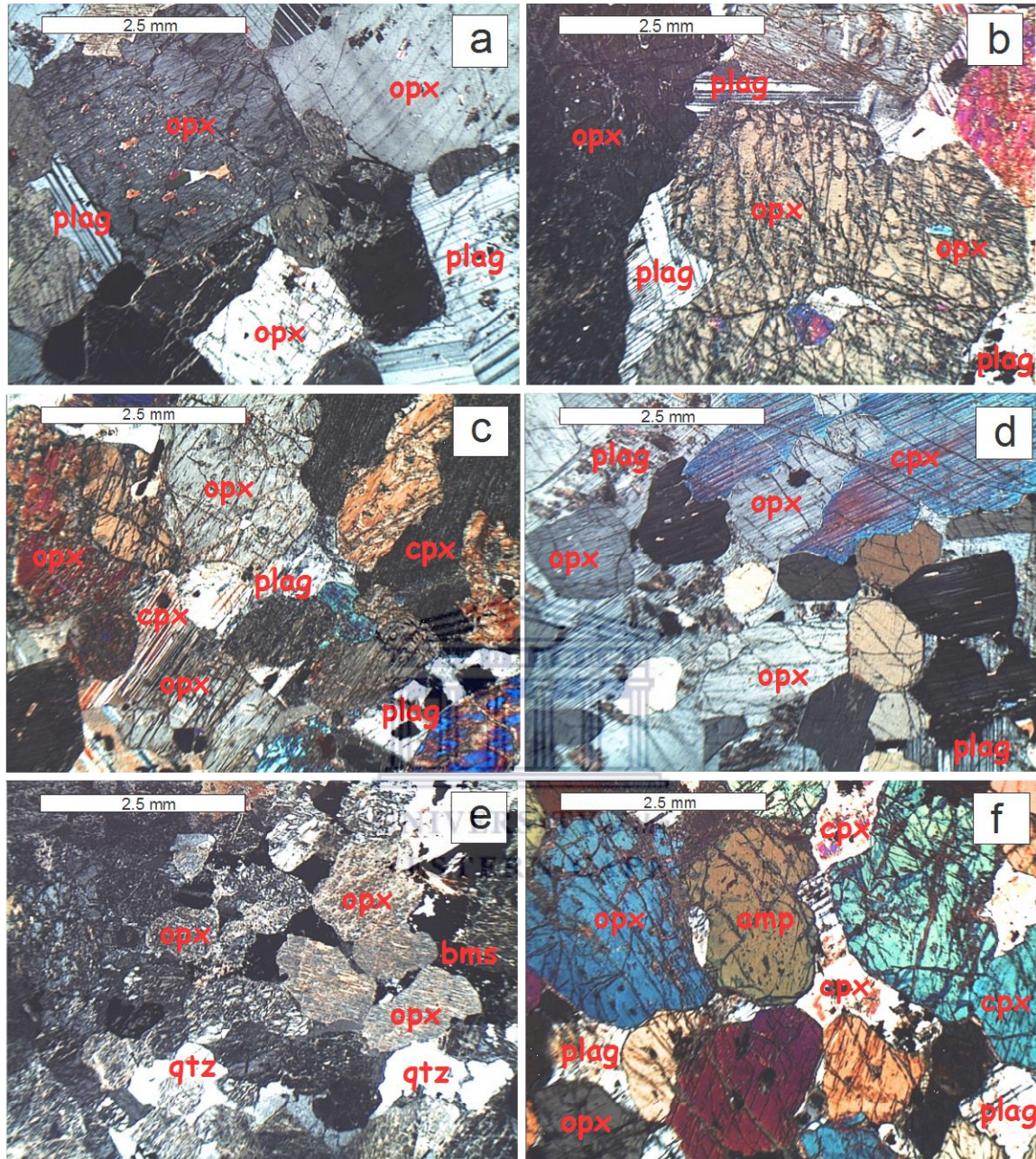
Plate 2: Photomicrographs of selected Platreef rocks. Scale bar: 2.5 mm. Field of view: 6.3 mm across each photomicrograph. A – B) Feldspathic pyroxenite Type II samples OY482-03 and TN754-08, respectively: Note the of blebby exsolution of clinopyroxene in orthopyroxene in sample OY482-03; C – D) Feldspathic pyroxenite Type III samples OY482-30 and TN200-24, respectively: Note clinopyroxene around orthopyroxene; E) Feldspathic pyroxenite Type IV sample OY482-40: The presence of quartz and bms interstitial to orthopyroxene should be noted; F) Feldspathic pyroxenite Type V sample TN200-16: The presence of clinopyroxene as primary and interstitial phases should be noted. The reader is referred to text for more details on the feldspathic pyroxenite Types. Mineral abbreviations: amp: amphibole; bms: base metal sulphides; cpx: clinopyroxene; opx: orthopyroxene; plag: plagioclase; qtz: quartz.

Feldspathic pyroxenite Type III occurs as a single sill in the Upper and Lower Platreef in TN754 (Fig. 5), a single sill in the Lower Platreef in TN200 (Fig. 6) and also as three sills in the Middle Platreef of OY482 (Fig. 8). The rocks have cumulate texture with fine- to medium-grained orthopyroxene (~50 − 80 vol. %), clinopyroxene (~10 − 40 vol. %) and plagioclase (~5 − 30 vol. %) (Table 5). Fine- to medium orthopyroxene crystals are euhedral and elongated (Plates 2c and d). Orthopyroxenes occur mainly intergrown with each other and are also partially enclosed by anhedral clinopyroxene phenocrysts (Plates 2c and d). One of the sills from the Middle Platreef in OY482 shows anhedral quartz grains in between orthopyroxene and euhedral clinopyroxene crystals. The occurrence of feldspathic pyroxenite having interstitial quartz (Plate 2e) between orthopyroxene grains at Overysel indicates assimilation of the granitic materials from the floor rock into the Platreef magma. Such rocks are termed as quartzo-feldspathic pyroxenites, and have been interpreted to be the result of contamination of the Platreef magma with Archaean granite materials (Holwell and McDonald, 2006).

Feldspathic pyroxenite Type IV occurs as a single sill in the Lower Platreef in OY482 (Fig. 8). The rocks have cumulate texture with fine-grained rocks with orthopyroxene (~50 − 80 vol. %), clinopyroxene (~10 − 30 vol. %) and plagioclase (~10 − 30 vol. %) in varying proportions (Table 5). Orthopyroxene crystals (1 mm) are euhedral, prismatic or lath-shaped intergrown with each other having interstitial plagioclase (Plate 2e). There are also anhedral quartz and irregularly-shaped sulphide grains occupying the interstitial spaces between orthopyroxenes and euhedral clinopyroxenes (Plate 2e). These quartz-rich Platreef feldspathic pyroxenite rocks, similar to those observed in Type III, are also interpreted to be the result of contamination of the Platreef magma with Archaean granite materials (Holwell and McDonald, 2006).

Feldspathic pyroxenite Type V occurs as a single sill in the middle part of the Lower Platreef in TN200 (Fig. 6). The rocks have cumulate texture with fine- to medium-grained rocks with orthopyroxene (~80 vol. %), plagioclase (~10 − 20 vol. %) and clinopyroxene (~5 − 10 vol. %) in varying proportions (Table 5).

49
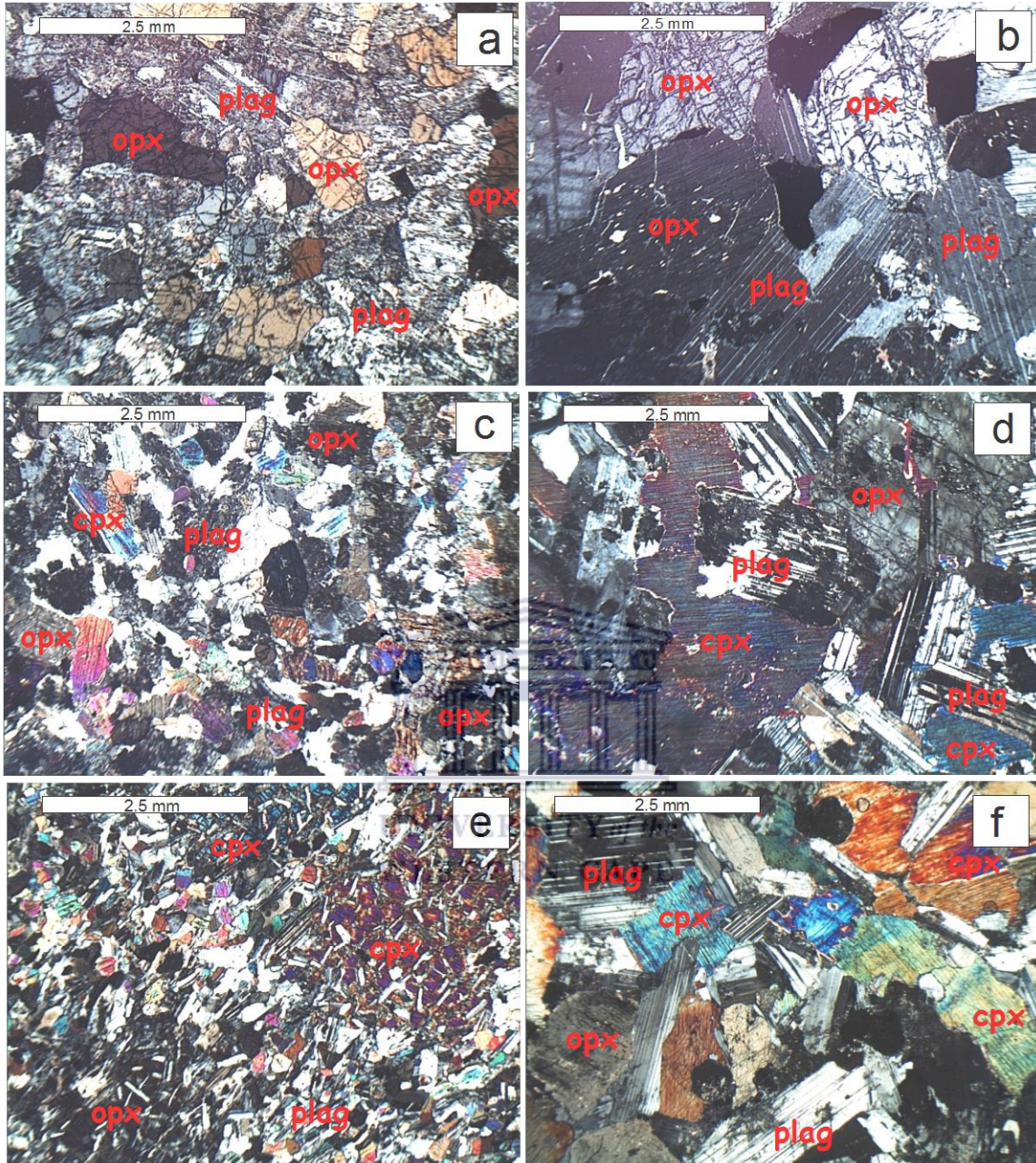
Plate 3: Photomicrographs of selected Platreef and Main Zone rocks. Scale bar: 2.5 mm. Field of view: 6.3 mm across each photomicrograph. A) Norite Type I sample TN200-18; B) Norite Type II sample TN200-12; C) Gabbronorite Type I pyroxenite sample OY482-21; D) Gabbronorite Type II sample OY482-01; E) Gabbronorite Type III sample OY482-14; F) Leucogabbro sample SS339-07. The reader is referred to text for more details on the norite and gabbronorite types. Mineral abbreviations: cpx: clinopyroxene; opx: orthopyroxene; plag: plagioclase.

50

Fine- to medium-grained orthopyroxene and clinopyroxenes are subhedral, intergrown with each other with interstitial plagioclase and clinopyroxene (Plate 2f). There are also medium-grained subhedral amphibole crystals that are intergrown with the pyroxenes (Plate 2f). Within the rock, the interstitial plagioclase is variably altered to sericite.

In overall, the base metal sulphides (e.g., pyrrhotite, pentlandite and chalcopyrite) in the Platreef feldspathic pyroxenite types occurs either as semi-massive (or net-textured) enveloping orthopyroxene grains (Plate 1f), or as irregularly-shaped blebs interstitial to pyroxenes (Plate 2e) or as disseminated grains enclosed within orthopyroxene crystals or associated with the interstitial plagioclase.

4.3.1.5 Norite (NRT)

Norite sills occur only in drill core TN200 and consist of two types: (1) fine- to medium-grained norite (or norite Type I) and (2) medium-grained norite (Norite Type II) (Fig. 6; Table 5). Core samples were also collected from each sill during the sampling campaign (Fig. 6).
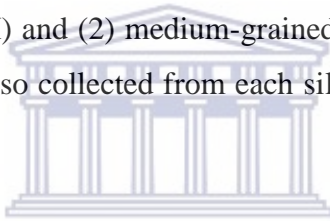
Under the microscope, norite Type I samples have inequigranular texture and are mainly dominated by orthopyroxene crystals intergrown with plagioclase (Plate 3a).

Orthopyroxene crystals are anhedral, small (~50 vol. %; ~1 mm) and fractured mainly in contact with plagioclase and, to some extent, with themselves in some areas of the rocks (Plate 3a). Plagioclase (~50 vol. %; ~1 mm) occurs as laths (Plate 3a) and is partially altered to sericite. Fractured and isolated fine-grained olivine can also be found in the rocks. The base metal sulphides occur as disseminated grains of pyrrhotite, pentlandite and chalcopyrite (~0.25 – 0.5 mm) with irregular shape in contact with the silicates (Plate 3a).

Norite Type II samples, on the other hand, have equigranular texture and are dominated by orthopyroxene crystals intergrown with plagioclase (Plate 3b).

Orthopyroxene crystals are subhedral, medium-grain sized (~50 vol. %; ~2 mm), variably fractured and in contact with plagioclase (Plate 3b). Plagioclase (~50 vol. %; ~2 mm) occurs as laths mainly in contact with orthopyroxene, but also interstitial in between the orthopyroxene crystal (Plate 3b). Anhedral clinopyroxene crystals intergrown with other

51

silicates are present but rare. The base metal sulphides are blebs of pyrrhotite, pentlandite and chalcopyrite (<1 mm) in contact with orthopyroxene and plagioclase (Plate 3b).

4.3.2   Main Zone rocks

4.3.2.1 Gabbronorite/ gabbro (GN)

Gabbronorite sills occur in all four drill cores (Figs. 5, 6, 7 and 8). The rock displays three textural varieties: (1) Fine-grained gabbronorite (Gabbronorite Type I); (2) medium- to coarse-grained gabbronorite (Gabbronorite Type II) and (3) fine- to medium-grained ophimottled gabbronorite (Gabbronorite Type III) (Figs. 5, 6, 7 and 8; Table 5). Gabbronorite Type II occurs in all four drill cores, whereas gabbronorite Types I and III are only present in drill core OY482 (Figs. 5, 6, 7 and 8). Quarter core samples were also collected from all gabbronorite sills (Figs. 5, 6, 7 and 8).

Gabbronorite Type I samples have equigranular texture (Table 5). The rocks have fine-grained clinopyroxene, orthopyroxene and plagioclase primocrysts that are randomly intergrown with each other (Plate 3c). Fine-grained orthopyroxenes (~30 vol. %; <1 mm) are euhedral, prismatic or lath-shaped, and the crystals are variably fractured (Plate 3c). Clinopyroxenes are also fine-grained (~30 vol. %; <1 mm) and euhedral, but elongated and equant (Plate 3c). Plagioclase (~40 – 50 vol. %; <1 mm) commonly occurs as lath and is variably altered to sericite (Plate 3c). The base metal sulphides in the rocks are disseminated grains of pyrrhotite, pentlandite and chalcopyrite (<0.5 mm) in contact with the pyroxenes and plagioclase.

Gabbronorite Type II samples have intergranular texture (Table 5) which is dominated by clinopyroxene and orthopyroxene crystals filling the interstices between plagioclase (Plate 3d). Plagioclase occurs as lath (~30 – 50 vol. %; >2 m), is randomly-oriented in the rocks (Plate 3d), and is also variably altered to sericite in places. Clinopyroxenes are mostly coarse-grained crystals (~30 – 50 vol. %; 1 – >2.5 mm) and anhedral (Plate 3d). Clinopyroxene occurs also as fine-grained crystals since the interstitial spaces between plagioclase laths are small (Plate 3d). Orthopyroxene (~10 – 20 vol. %; <1 mm) are

52

predominantly euhedral and fine-grained crystals with serrated edges (Plate 3d). In these rocks, the base metal sulphides are also disseminated grains of pyrrhotite, pentlandite and chalcopyrite (<0.5 mm) in contact with the silicate minerals.

Gabbronorite Type III samples have ophimottled texture (Table 5) which is dominated by medium-grained clinopyroxene and orthopyroxene crystals (~50 – 60 vol. %; 1 – 4 mm) enclosing smaller and tiny plagioclase laths (~40 – 50 vol. %; <0.1 mm) giving the rock a spotty appearance (Plate 3e). Orthopyroxene and clinopyroxene occur also as very small crystals (<0.1 mm) surrounding the medium-grained pyroxene crystals (Plate 3e). No base metal sulphides grains were identified during the thin section examination.

4.3.2.2 Leucogabbronorite/ Anorthositic leucogabbro (LGN/ ALG)

Leucogabbronorite sills occur in drill cores TN754 and TN200, whereas the anorthositic leucogabbro sill occurs in drill core SS339. Leucogabbronorite sill is ~10 m in thickness in drill core TN754 and 34 m in thickness in TN200 (Figs. 5 and 6). The anorthositic sill in SS339 is ~9 m in thickness (Fig. 7). Quarter core samples were collected from each sill of the three drill cores. These rock types are barren rocks.

In thin section, leucogabbronorite samples have intergranular texture similar to that seen in gabbronorite Type II (Plate 3d). Instead, subhedral orthopyroxene and clinopyroxene are fine- to medium-grained crystals that are interstitial to plagioclase laths of varying sizes. Anorthositic leucogabbro is quite similar to leucogabbronorite in terms of texture (Plate 3 f). The former has negligible amount to no orthopyroxene crystals at all, but instead larger amount of plagioclase lath (~50 – 70 vol. %) than leucogabbronorite (Plate 3f). Despite the presence of the base metal sulphides grains (Plate 3f), these rocks are not mineralised.

4.3.3   Basement rocks (or Floor rock)

The floor rock to the Platreef in drill core OY482 is granite (Fig. 8) and is similar to the Utrecht granite as described by Holwell and McDonald (2006). In drill core SS339, the floor rock is dolomite (Fig. 7). In TN754 and TN200 the hornfelsed BIF/Shale of the Penge iron formation is the floor rock to the Platreef (Figs. 5 & 6).

53

It consists of magnetite-rich chert BIF with few centimetre-sized black shale layers at the bottom of drill cores TN754 and TN200.

4.4 Summary of petrography

The petrography was conducted to identify and classify the different Platreef and Main Zone rocks in the four drill cores of interest. A summary of the petrography for these rocks, from the least to the most differentiated rock, is reported in Table 6 depending on the variation in the modal mineralogy.

Table 6: Summary of findings from the petrography for rock types from the four drill cores.

	Rock type		Mineralogy	BMS	OY482	SS339	TN200	TN754
Main Zone	Leucogabbronorite					x	x	x
	Gabbronorite	Type II	Plag> cpx> opx		x	x	x	
		Type I	Plag> opx≈ cpx		x			
Platreef	Norite	Type II	Opx≈ plag	x			x	
		Type I	Opx≈ plag	x			x	
	Feldspathic pyroxenite	Type V	Opx> plag> cpx	x			x	
		Type IV	Opx> cpx> plag	x	x			
		Type III	Opx> cpx> plag	x	x		x	x
		Type II	Opx> plag> cpx	x	x			x
		Type I	Opx> plag> cpx	x		x	x	
	Pyroxenite		Opx	x		x		
	Olivine pyroxenite		Opx> ol	x		x		x
	Harzburgite		Ol> opx	x		x		x

The major findings from the petrography are:

1. The rock succession, which defines the variation in the modal mineralogy from the least to the most differentiated rocks in the Platreef, consists of harzburgite, olivine pyroxenite, pyroxenite, feldspathic pyroxenite and norite (Tables 5 and 6).

54

2. There are three major groups of feldspathic pyroxenite:

   - The first group includes Types I, II and III which are fine- to medium-grained rocks with abundant orthopyroxene and plagioclase (Tables 5 and 6).

   - The second group includes Type IV which is a fine-grained rock with abundance in orthopyroxene that is slightly lower than Types I and II (Tables 5 and 6).

   - The third group includes Type V which is a fine- to medium-grained rock whose mineralogy is different from the other fine- to medium- grained rocks; i.e., Type I, II and III (Tables 5 and 6).

3. In terms of stratigraphic correlations in the Platreef:

   - There are no single rock type that can be correlated in the four drill cores; i.e., from South (TN754) to North (OY482) (Table 6; Figs. 5, 6, 7, and 8).

   - Harzburgite can be correlated between drill cores TN754 and SS339 (Table 6; Figs. 5 and 7).

   - Olivine pyroxenite can also be correlated between drill cores TN754 and SS339 (Table 6; Figs. 5 and 7).

   - Feldspathic pyroxenite Type I can be correlated between drill cores TN200 and SS339 (Table 6; Figs. 6 and 7).

   - Feldspathic pyroxenite Type II can be correlated between drill cores TN754 and OY482 (Table 6; Figs. 5 and 8).

   - Feldspathic pyroxenite Type III can be correlated between drill cores TN754, TN200 and SS339 (Table 6; Figs. 5, 6 and 7).

4. In terms of stratigraphic correlations in the Main Zone:

   - Not all the rock types from the Main Zone can be correlated in the four drill cores; i.e., from South (TN754) to North (OY482) (Table 6; Figs. 5, 6, 7, and 8).

   - Gabbronorite Type II can be correlated between drill cores TN754 and OY482 (Table 6; Figs. 5 and 8).

   - Leucogabbronorite can be correlated between drill cores TN754, TN200 and SS339 (Table 6; Figs. 5, 6 and 7).

https://etd.uwc.ac.za

5. In terms of mineralisation, most of the Platreef rocks are variably mineralised in base metal sulphides (Tables 5 and 6).

The following chapter presents the whole-rock major and trace elements composition of the Platreef and Main Zone rocks.

5 WHOLE-ROCK GEOCHEMISTRY

As noted earlier in chapter 1.3, the study aims at (1) determining the source of the Platreef magmas and identifying the processes involved in its genesis, and (2) establishing whether a genetic link exists between the Platreef magmas and the magmas from the RLS on the Eastern and Western Limbs of the BIC.

The major element, trace element and Sr–Nd isotope data generated from the Platreef rocks (and few from the MZ) collected from four drill cores are presented in Appendices A, B, C and D, respectively. These data are presented in three main sections:

1. Section 5.1 focuses on major and trace elements for the Platreef and MZ rocks, and presents:
    a. In sub-section 5.1.1: Plots of MgO versus selected major elements to establish the relationship between the modal mineralogy of the rocks and the geochemical data.
    b. In sub-section 5.1.2: REE chondrite-normalised and Primitive Mantle spider diagrams to monitor fractionation and contamination processes.
    c. In sub-section 5.1.3: The summary findings of the whole-rock major and trace elements geochemistry.

2. Section 5.2 focuses on the Sr–Nd isotope data for the Platreef and MZ rocks, and presents the variation patterns in the isotopic compositions using the εNd_{2060} − $^{87}Sr/^{86}Sr_{2060}$ plot. The objective is to determine the source(s) and composition of the magma(s).

3. Section 5.3 focuses on the Cu, Ni and PGE (i.e., Pt and Pd) data for the Platreef rocks, and presents their contents to examine their distributions and determine the style(s) of PGE mineralisation.

5.1 Whole-rock major and trace element geochemistry

5.1.1 Major element geochemistry

The major element compositions for ninety-four whole-rock samples from drill cores TN754, TN200, SS339 and OY482 (Figs. 5 – 8) are reported in Appendix A. The major element data for eight floor rock samples (i.e., five hornfelsed BIF/Shale, two dolomites and only one granite sample) were not included since they are not rock types of interest. Because of this, only the major element data of eighty-six rock samples from the Platreef (i.e., harzburgite, olivine pyroxenite, pyroxenite, feldspathic pyroxenite and norite) and the Main Zone (gabbronorite, leucogabbronorite and anorthositic leucogabbro) will be used to assess whether the chemical composition of the rocks reflects the mineralogy.

Also, the Platreef feldspathic pyroxenite and norite have sub-groups , as identified from the petrography (Table 5), whose chemical composition will be examined separately to asses whether these sub-groups are related to the same magmatic processes.

So, the first step of this exercise involves the use of major elements to assess whether the chemical composition of samples from each Platreef and MZ rock types reflects the rock mineralogy. The second step will involve the use of major elements to assess whether the chemical composition of samples from feldspathic pyroxenite Type I, II, III, IV and V, and norite Type I and II reflects their respective samples mineralogy.

5.1.1.1.1 Platreef and Main Zone rocks

Selected major elements variation diagrams with MgO for the Platreef and MZ samples are shown in Figure 9 (a – f). A statistical summary for the major elements for these rocks, which includes the minimum (Min), maximum (Max) and average (Mean), is reported in Table 7. The Platreef and MZ samples show negative correlations with MgO only for Al_2O_3, CaO and Na_2O, and overall positive correlations for Fe_2O_3 and MnO (excluding harzburgite), whereas TiO_2 shows a quite different trend (Figs. 9a – f).

58
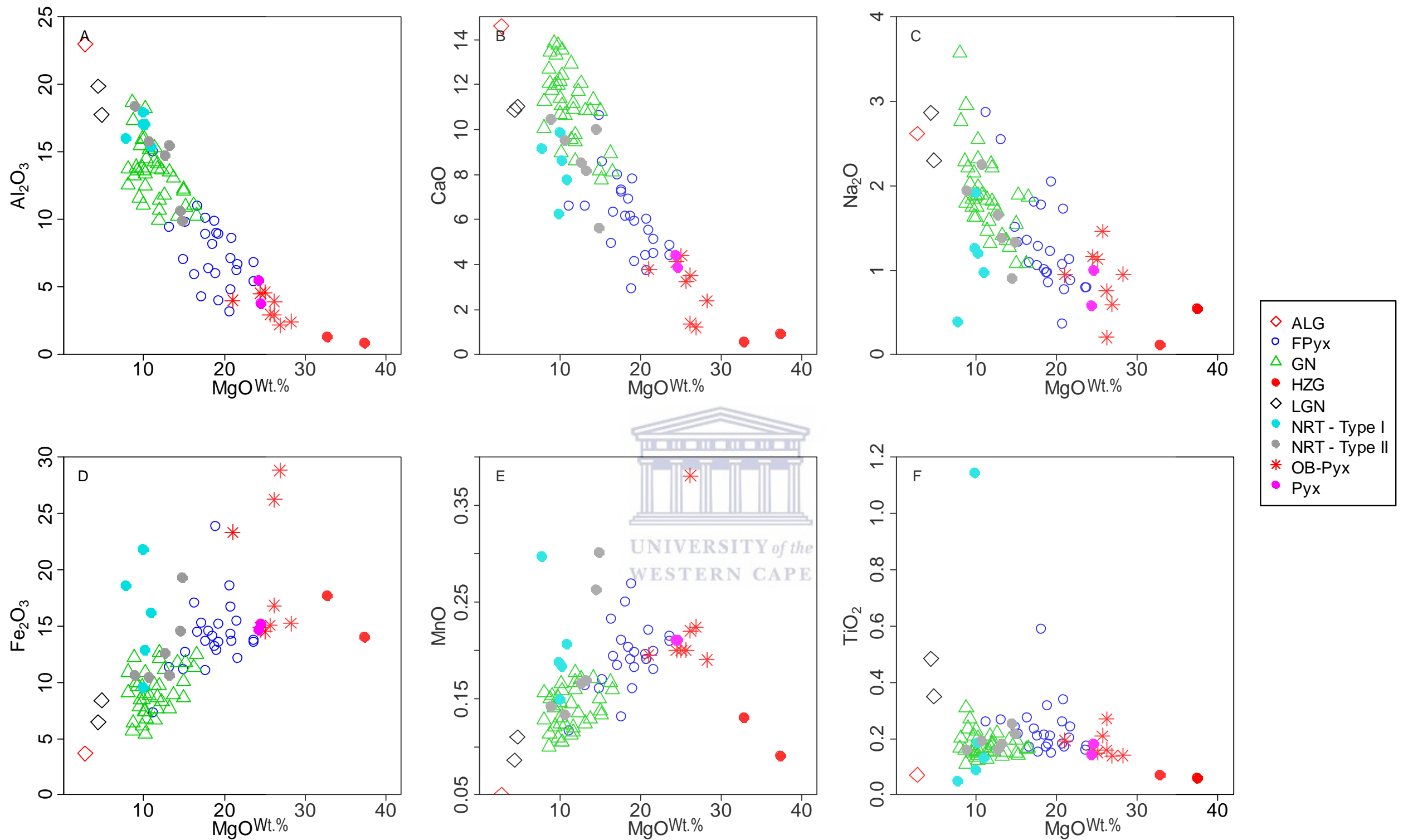
Figure 9 (A – F): Variation of MgO versus selected major elements for the Platreef and Main Zone rocks. Legend abbreviation: ALG: Anorthositic leucogabbro; FPyx: Feldspathic pyroxenite; GN: Gabbronorite; HZG: Harzburgite; LGN: Leucogabbronorite; NRT: Norite; OB-Pyx: Olivine pyroxenite; Pyx: Pyroxenite. All Fe reported as Fe₂O₃ (Total iron contents).

Table 7: Major element statistical summary for the Platreef and Main Zone rocks. All data are expressed in wt. %.

Rock type		SiO_2	TiO_2	Al_2O_3	Fe_2O_3	MnO	MgO	CaO	Na_2O	K_2O	L.O.I.
HZG (n=2)	**Mean**	**37.4**	**0.1**	**1.0**	**15.8**	**0.1**	**35.1**	**0.7**	**0.3**	**0.3**	**8.7**
	Min	36.9	0.1	0.8	14.0	0.1	32.8	0.6	0.1	0.0	8.7
	Max	38.0	0.1	1.3	17.7	0.1	37.4	0.9	0.5	0.5	8.8
OB-Pyx (n=8)	**Mean**	**43.1**	**0.2**	**3.4**	**19.4**	**0.2**	**25.5**	**3.0**	**0.9**	**0.2**	**2.7**
	Min	31.8	0.1	2.2	14.5	0.2	21.0	1.2	0.2	0.0	0.9
	Max	48.9	0.3	4.6	28.8	0.4	28.2	4.4	1.5	1.1	4.7
Pyx (n=2)	**Mean**	**49.5**	**0.2**	**4.6**	**14.9**	**0.2**	**24.5**	**4.1**	**0.8**	**0.0**	**0.9**
	Min	48.6	0.1	3.7	14.6	0.2	24.4	3.9	0.6	0.0	0.4
	Max	50.4	0.2	5.5	15.2	0.2	24.6	4.4	1.0	0.1	1.5
FPyx (n=24)	**Mean**	**48.8**	**0.2**	**7.6**	**14.1**	**0.2**	**18.6**	**6.0**	**1.3**	**0.2**	**2.3**
	Min	43.1	0.1	3.1	7.3	0.1	11.2	2.9	0.4	0.1	0.1
	Max	53.9	0.6	15.0	23.9	0.3	23.7	10.6	2.9	0.7	8.0
NRT (n=11)	**Mean**	**45.7**	**0.3**	**15.3**	**14.3**	**0.2**	**11.3**	**8.5**	**1.4**	**0.8**	**1.6**
	Min	40.5	0.0	9.8	9.5	0.1	7.8	5.6	0.4	0.2	0.6
	Max	49.4	1.1	18.4	21.8	0.3	14.9	10.4	2.2	2.5	2.5
GN (n=36)	**Mean**	**49.5**	**0.2**	**13.4**	**9.1**	**0.1**	**11.3**	**11.1**	**1.9**	**0.4**	**2.7**
	Min	43.4	0.1	10.0	5.4	0.1	8.0	7.8	1.1	0.0	0.6
	Max	56.0	0.3	18.7	12.7	0.2	16.5	13.9	3.6	1.0	7.2
LGN (n=2)	**Mean**	**53.1**	**0.4**	**18.8**	**7.4**	**0.1**	**4.6**	**10.9**	**2.6**	**0.9**	**1.1**
	Min	52.8	0.4	17.8	6.5	0.1	4.4	10.9	2.3	0.8	0.7
	Max	53.5	0.5	19.9	8.4	0.1	4.8	11.0	2.9	1.0	1.4
ALG (n=1)	**Mean**	**49.8**	**0.1**	**23.0**	**3.7**	**0.1**	**2.7**	**14.6**	**2.6**	**1.0**	**2.2**
	Min	49.8	0.1	23.0	3.7	0.1	2.7	14.6	2.6	1.0	2.2
	Max	49.8	0.1	23.0	3.7	0.1	2.7	14.6	2.6	1.0	2.2

Abbreviation: ALG: Anorthositic leucogabbro; FPyx: Feldspathic pyroxenite; GN: Gabbronorite; HZG: Harzburgite; LGN: Leucogabbronorite; NRT: Norite; OB-Pyx: Olivine pyroxenite; Pyx: Pyroxenite.

The positive trend of Fe_2O_3 with MgO (Fig. 9c) is consistent with decreasing modal abundance of pyroxenes and/or olivine from harzburgite to anorthositic leucogabbro, as substantiated from the petrography (Table 5). The negative trends (Figs. 9a – f) are consistent with increasing plagioclase from harzburgite to anorthositic leucogabbro, in support of the petrography (Table 5).

Harzburgite has the highest average contents of MgO (35.1 wt. %) and L.O.I. (8.7 wt. %) (Table 7). Conversely, it has the lowest average contents of SiO_2, Al_2O_3, CaO and Na_2O (Table 7). The rock has the second highest average contents of Fe_2O_3 (15.8 wt. %) after olivine pyroxenite, but also low average contents of TiO_2 (0.1 wt. %) (Table 7). Its average contents of MnO and K_2O are relatively low when compared to other Platreef rock types (Table 7).

Olivine pyroxenite has the second highest average contents of MgO (25.5 wt. %) and the second lowest average contents of SiO_2 (41.3 wt. %) after harzburgite (Table 7). The rock has interestingly the highest average contents of Fe_2O_3 (19.4 wt. %; Table 7), which is due to the high contents of Fe_2O_3 as the result of the presence of semi massive sulphide ores in three olivine pyroxenite samples (23.3 wt. % for TN754-10, 26.3 wt. % for TN754-11 and 28.8 wt. % for TN754-12; Fig. 9d, Appendix A) from the sill above the hornfelsed BIF/Shale floor rock (Fig. 6). The contents of CaO, Na_2O and TiO_2 vary within the rocks (Figs. 9b, c and f; Table 7).

Pyroxenite has lower average contents of MgO (24.5 wt. %) and Fe_2O_3 (14.9 wt. %) than olivine pyroxenite, but higher contents of SiO_2, Al_2O_3 and CaO (Table 7). The rock has negligible average contents of K_2O and L.O.I. than any other rock type from the Platreef (Table 7).

Feldspathic pyroxenite has 48.8 wt. % SiO_2, 18.6 wt. % MgO, 14.1 wt. % Fe_2O_3, 7.6 wt. % Al_2O_3, 6 wt. % CaO and 1.3 wt. % Na_2O average contents (Table 7). The high average contents of Na_2O for feldspathic pyroxenite are due to the high contents of Na_2O in two samples (Fig. 9c) from the Platreef above the floor rock granite (2.6 wt. % for OY482-39 and 2.9 wt. % for OY482-42; Fig. 9c, Appendix A). Sample TN200-16 has the highest contents of Fe_2O_3 reflecting the presence of semi massive sulphide ores in the core.

61

Norite is the Platreef rock with the lowest average contents of MgO (11.3 wt. %), but highest Al_2O_3 (15.3 wt. %), CaO (8.5 wt. %) and Na_2O (1.4 wt. %) (Table 7). The rock has also 45.7 wt. % SiO_2 and 0.3 wt. % TiO_2 average contents (Table 7).

For the Main Zone rocks, gabbronorite has the highest average contents of MgO (11.3 wt. %) and Fe_2O_3 (9.1 wt. %), and the lowest average contents of Al_2O_3 (15.3 wt. %) and Na_2O (1.9 wt. %) (Table 7). Leucogabbronorite has higher average contents of SiO_2 (53.1 wt. %), Al_2O_3 (18.8 wt. %), Na_2O (2.6 wt. %) and K_2O (0.9 wt. %) than gabbronorite (Table 7). Anorthositic leucogabbro has the highest average contents of Al_2O_3 (23 wt. %), CaO (14.6 wt. %) and the lowest average contents of MgO (2.7 wt. %) and Fe_2O_3 (3.7 wt. %) from any rock of the Platreef and the Main Zone (Table 7).

Table 8: Major element statistical summary for feldspathic pyroxenite (FPyx) types. All data are expressed in wt. %.

Rock sub-type		SiO_2	TiO_2	Al_2O_3	Fe_2O_3	MnO	MgO	CaO	Na_2O	K_2O	L.O.I.
FPyx - Type I (n=8)	**Mean**	**48.3**	**0.2**	**8.0**	**14.0**	**0.2**	**20.7**	**5.5**	**1.1**	**0.1**	**1.2**
	Min	46.2	0.1	5.4	13.2	0.2	16.6	4.4	0.8	0.1	0.1
	Max	50.1	0.2	11.0	15.4	0.2	23.7	6.3	2.0	0.2	2.5
FPyx - Type II (n=4)	**Mean**	**49.9**	**0.2**	**8.4**	**12.7**	**0.2**	**18.9**	**6.5**	**1.1**	**0.4**	**1.4**
	Min	49.0	0.2	6.7	11.0	0.1	17.6	4.5	0.9	0.1	1.1
	Max	52.1	0.2	10.1	14.1	0.2	21.7	7.3	1.3	0.7	2.1
FPyx - Type III (n=8)	**Mean**	**48.4**	**0.3**	**6.3**	**14.8**	**0.2**	**17.8**	**6.8**	**1.3**	**0.2**	**3.4**
	Min	43.6	0.2	3.1	11.1	0.2	14.9	3.7	0.4	0.1	0.9
	Max	52.4	0.6	9.8	18.6	0.3	20.8	10.6	1.8	0.4	8.0
FPyx - Type IV (n=3)	**Mean**	**52.0**	**0.2**	**9.5**	**11.3**	**0.2**	**14.5**	**5.8**	**2.2**	**0.3**	**3.6**
	Min	49.2	0.2	3.9	7.3	0.1	11.2	4.1	1.2	0.1	1.8
	Max	53.9	0.3	15.0	15.1	0.2	19.3	6.6	2.9	0.4	6.1
FPyx - Type V (n=1)	**Mean**	**43.1**	**0.3**	**6.0**	**23.9**	**0.3**	**18.9**	**2.9**	**1.0**	**0.3**	**2.2**
	Min	43.1	0.3	6.0	23.9	0.3	18.9	2.9	1.0	0.3	2.2
	Max	43.1	0.3	6.0	23.9	0.3	18.9	2.9	1.0	0.3	2.2
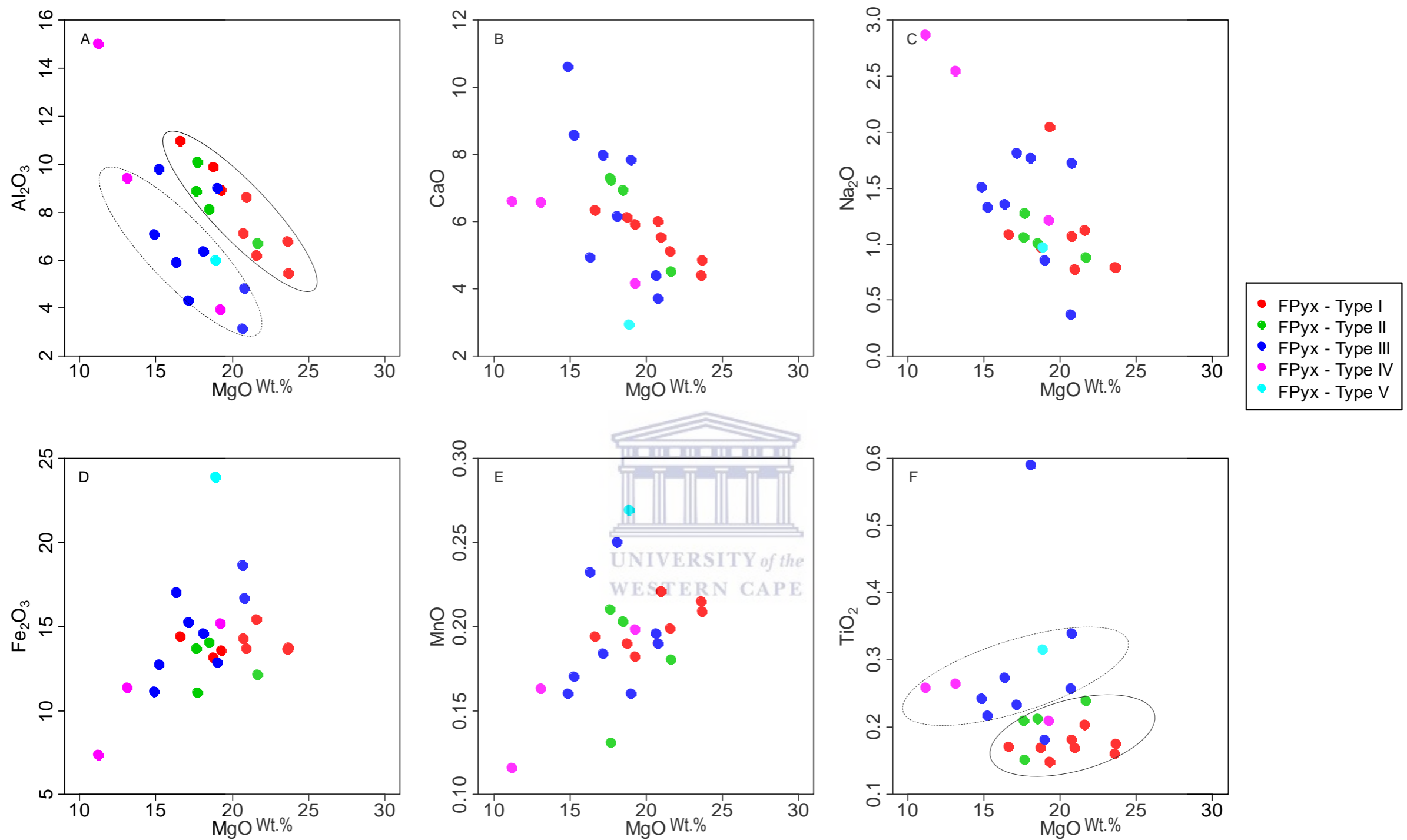
Figure 10 (A – F): Variation of MgO versus selected major elements for the Platreef feldspathic pyroxenite (FPyx) types. Closed circle: Feldspathic pyroxenite Type I and II. Dashed circle: Feldspathic pyroxenite Type III and IV.

5.1.1.1.2 *Platreef feldspathic pyroxenite and norite types*

The chemical compositions of samples from feldspathic pyroxenite Type I, II, III, IV and V are shown in Figure 10 (a – f). A statistical summary for the major elements for Type I, II, III, IV and V, which includes the minimum, maximum and average is reported in Table 8. There are overall negative correlations for MgO with Al_2O_3, CaO and Na_2O, and positive correlations with Fe_2O_3 and MnO for feldspathic pyroxenite samples (Figs. 10a – e) reflecting the variation in abundance of orthopyroxene and plagioclase in these rocks, as reported from the petrography (Table 5).

Despite the scattering of feldspathic pyroxenite samples from different types, there are two parallel trends on variation diagrams of MgO with Al_2O_3 and TiO_2 (Figs. 10a – f). There is negative correlation between MgO and Al_2O_3 (Fig. 10a), and positive correlation between MgO and TiO_2 (Fig. 10f). The two parallel and negatively correlated trends are defined mainly by feldspathic pyroxenite (1) Type I and II having a high slope, and (2) Type III and IV having a low slope (Fig. 10a). The two parallel and positively correlated trends are also defined mainly by feldspathic pyroxenite (1) Type I and II having a low slope, and (2) Type III and IV having a high slope (Fig. 10f). These trends are consistent with the petrography which has shown that feldspathic pyroxenite Type I and II have abundant orthopyroxene and are least differentiated than Type III and IV (Table 5). This can also be seen from Table 8 which shows a decrease in the average contents of MgO from feldspathic pyroxenite Type I to IV.

Feldspathic pyroxenite Type V, which consists of one sample (Table 8), shows a different composition. The contents of MgO in this sample are within range with MgO contents of feldspathic pyroxenite Type I, II, III and IV (Table 8; Figs. 10a – f). Its modal mineralogy for orthopyroxene is also within range with Type I, II, III and IV (Table 5). However, on variation diagrams of MgO versus Al_2O_3 and TiO_2, feldspathic pyroxenite Type V plots together with Type III and IV (Figs. 10a and f). This trend is compatible with the existence of a genetic link that may exist between feldspathic pyroxenite samples from Type III, IV and V.

64

For norite, Type I has lower average contents of SiO_2, MgO, CaO and Na_2O than Norite Type II (Figs. 9a – f; Table 9). Conversely, Norite Type I has higher average contents of TiO_2, Al_2O_3, Fe_2O_3 and L.O.I. (Figs. 9a – f; Table 9). It is worth mentioning that samples from norite Type I and II have different textures (i.e., fine- to medium-grained versus medium-grained rock; Plates 3a and b) which explain the variation in their compositions (Table 9).

Table 9: Major element statistical summary for norite (NRT) types. All data are expressed in wt. %.

Rock sub-type		SiO_2	TiO_2	Al_2O_3	Fe_2O_3	MnO	MgO	CaO	Na_2O	K_2O	L.O.I.
NRT-Type I (n=5)	**Mean**	**44.1**	**0.3**	**16.7**	**15.8**	**0.2**	**9.8**	**8.3**	**1.1**	**1.3**	**1.9**
	Min	40.5	0.0	15.4	9.5	0.1	7.8	6.2	0.4	0.4	1.0
	Max	48.0	1.1	17.9	21.8	0.3	11.0	9.9	1.9	2.5	2.5
NRT-Type II (n=6)	**Mean**	**47.1**	**0.2**	**14.1**	**13.0**	**0.2**	**12.5**	**8.7**	**1.6**	**0.4**	**1.4**
	Min	45.4	0.2	9.8	10.5	0.1	8.9	5.6	0.9	0.2	0.6
	Max	49.4	0.3	18.4	19.3	0.3	14.9	10.4	2.2	0.7	2.3

5.1.2   Trace element geochemistry

5.1.2.1 Harzburgite

On REE chondrite-normalised diagram, harzburgite samples show similar patterns which are not fractionated (Average La_N/Yb_N= 1.1; ranging: 0.4 – 1.9) (Fig. 11a; Table 10). Europium anomaly varies from negative to positive (Eu/Eu* = 0.8 – 1.4), and the rocks are poorly-enriched in REE contents (Average ΣREE= 4.1) (Table 10). On the Primitive mantle-normalised (PMN) trace elements diagram, harzburgite samples also have relatively similar patterns showing a slight enrichment of the large ion lithophile elements (LILE) relative to the high field strength elements (HFSE) with peaks at U and Pb, and negative anomalies at Th and Ti (Fig. 11d).
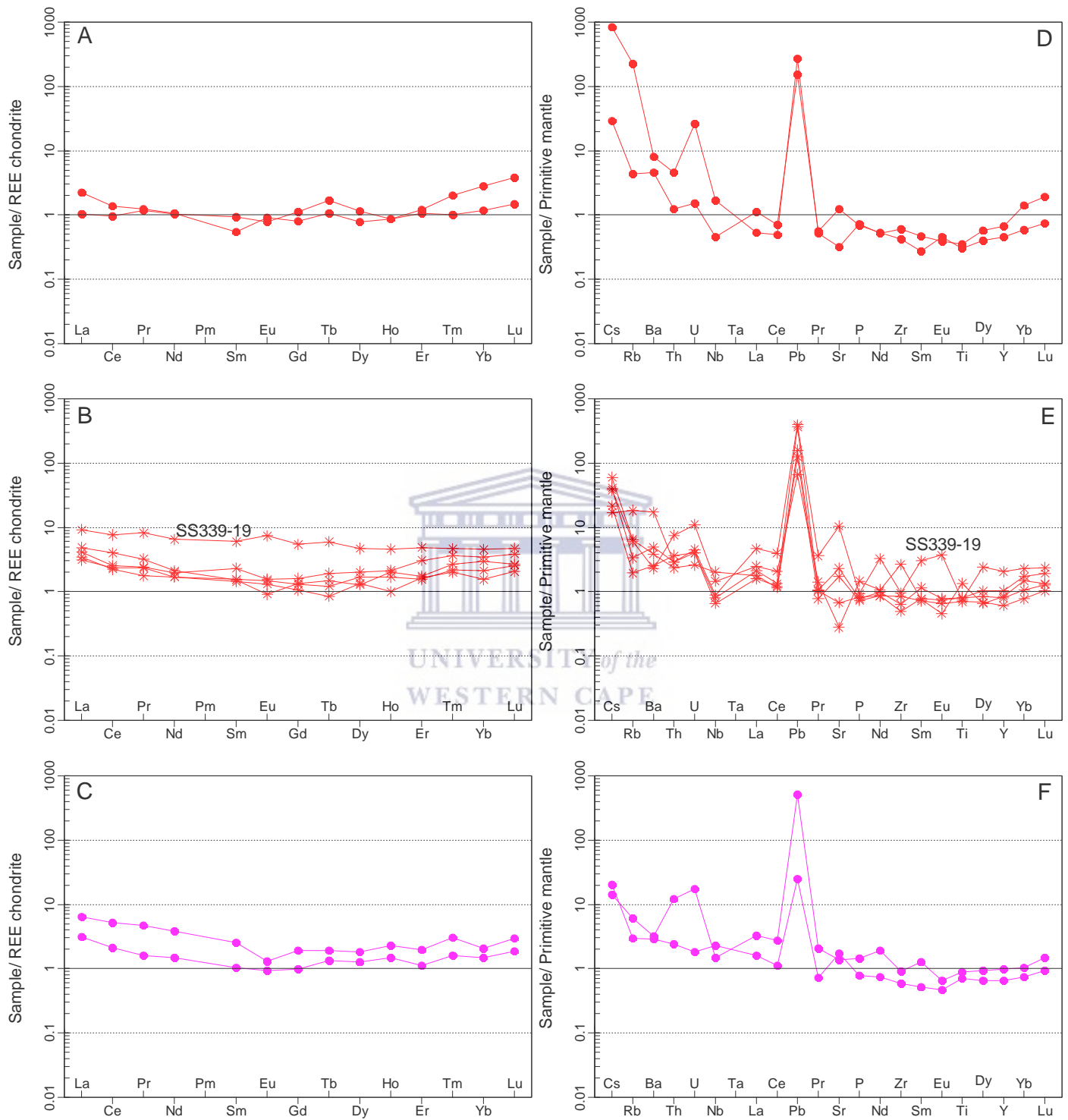
Figure 11: REE chondrite–normalised patterns for harzburgite (A), olivine pyroxenite (B) and pyroxenite (C). REE normalising values are from Nakamura (1974). Primitive mantle–normalised trace elements patterns for harzburgite (D), olivine pyroxenite (E) and pyroxenite (F). Normalisation values are from McDonough and Sun (1995).

66

Table 10: REEs statistical summary for harzburgite (HZG), olivine pyroxenite (OB-Pyx) and pyroxenite (Pyx).

Rock type		Eu/Eu*	La_N/Yb_N	La_N/Sm_N	Gd_N/Yb_N	ΣREE
	Mean	**1.1**	**1.1**	**2.6**	**0.5**	**4.1**
HZG (n=2)	Min	0.8	0.4	1.1	0.4	4.1
	Max	1.4	1.9	4.1	0.7	4.1
	Mean	**0.9**	**1.6**	**2.3**	**0.6**	**7.9**
OB-Pyx (n=4)	Min	0.6	1.2	1.8	0.5	6.5
	Max	1.1	2.0	3.2	0.7	9.4
	Mean	**0.8**	**2.6**	**2.8**	**0.8**	**9.2**
Pyx (n=2)	Min	0.6	2.1	2.6	0.7	5.8
	Max	0.9	3.1	3.0	0.9	12.7

OB-Pyx SS339-19: Eu/Eu= 1.3; La_N/Yb_N 2.0; La_N/Sm_N 1.5; Gd_N/Yb_N= 1.2; ΣREE= 22.5*

5.1.2.2 Olivine pyroxenite

Olivine pyroxenites have U-shaped patterns (aver. La_N/Sm_N= 2.3; aver. Gd_N/Yb_N= 0.6; Table 10) on the REE chondrite-normalised diagram, with exception for sample SS339-19 (Fig. 11b). In comparison to harzburgite samples, they are slightly fractionated (aver. La_N/Yb_N= 1.6; ranging: 1.2 – 2.0) (Fig. 11b; Table 10).

Olivine pyroxenites have also negative and positive Eu anomalies (Eu/Eu* = 0.6 – 1.1; excluding SS339-19), and the rocks are slightly enriched in REE contents (aver. ΣREE= 7.9; excluding SS339-19) than harzburgite (Table 10). On the PMN trace elements diagram, olivine pyroxenites have higher contents of trace elements than harzburgites (Excluding SS339-19; Figs. 11d and e). Although olivine pyroxenite samples do not have relatively similar patterns, they are also characterised with LILE that are enriched relative to the HFSE with peaks at U, La and Pb, and negative anomalies at Nd (Excluding SS339-19; Fig. 11e).
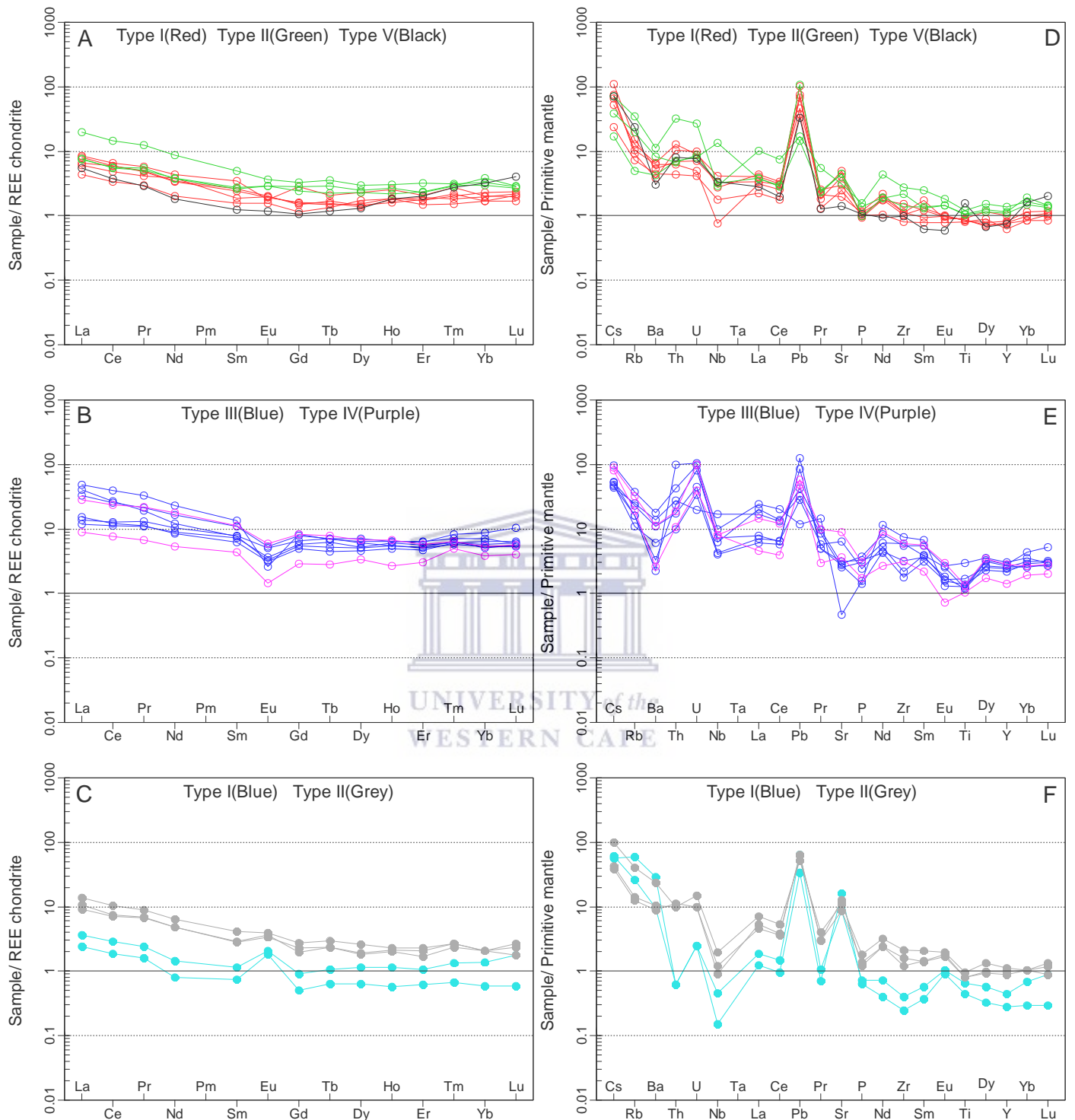
Figure 12: REE chondrite–normalised patterns for feldspathic pyroxenite samples from Type I, II and V (A), feldspathic pyroxenite Type III and IV (B), norite Type I and II (C). REE normalising values are from Nakamura (1974). Primitive mantle–normalised trace elements patterns for feldspathic pyroxenite samples from Type I, II and V (D), feldspathic pyroxenite Type III and IV (E), norite Type I and II (F). Normalisation values are from McDonough and Sun (1995).

68

5.1.2.3 Pyroxenite

Pyroxenites have similar patterns on the REE chondrite-normalised diagram (Fig. 11c). Relative to olivine pyroxenites, pyroxenites are fractionated (aver. La_N/Yb_N= 2.6; aver. Gd_N/Yb_N= 0.8) (Table 10). They are characterised by negative Eu anomalies (Eu/Eu* = 0.6 – 0.9), and are slightly enriched in REE contents (aver. ΣREE= 9.2) than olivine pyroxenites (Table 10). On the PMN trace elements diagram, pyroxenites are also characterised with enrichment of the LILE relative to the HFSE with peaks at Pb and Nd (Fig. 11f).

Table 11: REEs statistical summary for feldspathic pyroxenite (FPyx) types.

Rock sub-type		Eu/Eu*	La_N/Yb_N	La_N/Sm_N	Gd_N/Yb_N	ΣREE
FPyx - Type I (n=5)	**Mean**	**1.0**	**3.5**	**2.8**	**0.9**	**12.3**
	Min	0.6	2.6	2.4	0.7	8.3
	Max	1.2	4.7	3.2	1.4	15.5
FPyx - Type II (n=3)	**Mean**	**1.0**	**3.5**	**3.2**	**0.8**	**19.9**
	Min	0.9	1.9	2.8	0.7	14.0
	Max	1.1	6.0	4.0	1.0	31.1
FPyx - Type III (n=6)	**Mean**	**0.5**	**4.2**	**3.0**	**1.0**	**47.4**
	Min	0.2	1.9	1.6	0.8	29.3
	Max	0.7	7.6	5.3	1.3	80.4
FPyx - Type IV (n=2)	**Mean**	**0.5**	**3.9**	**2.3**	**1.2**	**36.6**
	Min	0.4	2.3	2.0	0.8	18.8
	Max	0.6	5.4	2.5	1.6	54.4
FPyx - Type V (n=1)	**Mean**	**1.0**	**1.7**	**4.5**	**0.3**	**9.2**
	Min	1.0	1.7	4.5	0.3	9.2
	Max	1.0	1.7	4.5	0.3	9.2

5.1.2.4 Feldspathic pyroxenite

Most feldspathic pyroxenite samples are fractionated than pyroxenite samples (aver. La_N/Sm_N> 2.6; aver. Gd_N/Yb_N> 0.8) (Tables 10 and 11), with exception for feldspathic pyroxenite Type V which shows a U-shaped pattern (Fig. 12a) (aver. La_N/Sm_N= 1.7; aver.

69

Gd_N/Yb_N= 0.3; Table 11) similar to olivine pyroxenites (Fig. 11b). Feldspathic pyroxenite Type I and II samples have positive and negative Eu anomalies ($Eu/Eu^* = 0.6 - 1.2$; $Eu/Eu^* = 0.9 - 1.2$, respectively) (Table 11). Feldspathic pyroxenite Type III and IV have negative Eu anomalies ($Eu/Eu^* = 0.2 - 0.7$; $Eu/Eu^* = 0.4 - 0.6$, respectively) and Type V sample has no Eu anomaly ($Eu/Eu^* = 1$) (Fig. 12a; Table 11). With the exception for feldspathic pyroxenite Type V which has the same average contents of REE with olivine pyroxenite (aver. $\Sigma REE = 9.2$), all other feldspathic pyroxenite types have average contents of REE (aver. $\Sigma REE > 9.2$) that is higher than olivine pyroxenite (Tables 10 and 11). Amongst feldspathic pyroxenite types, there is a gradual increase in the average contents of ΣREE from the least differentiated Type I to the most differentiated Type III and IV (Table 11) which is consistent with the petrography (Table 5).

On the PMN trace elements diagram, all feldspathic pyroxenite types are also characterised with enrichment of the LILE relative to the HFSE (Figs. 12d and e). Most samples have peaks at Th, U, La, Pb, Sr and Nd, and negative anomalies at Ba, Nb, P, Zr and Ti, with exception for Type V which has a positive anomaly for Ti (Figs. 12d and e). Overall, there is also a gradual increase in the average contents of trace elements from the least differentiated Type I to the most differentiated Type III and IV which is also consistent with the petrography (Table 5).

Table 12: REEs statistical summary for norite (NRT) types.

Rock sub-type		Eu/Eu^*	La_N/Yb_N	La_N/Sm_N	Gd_N/Yb_N	ΣREE
	Mean	**2.5**	**3.4**	**3.2**	**0.8**	**5.4**
NRT - Type I (n=2)	Min	2.1	2.7	3.2	0.7	4.1
	Max	3.0	4.1	3.3	0.9	6.7
	Mean	**1.3**	**5.4**	**3.5**	**1.1**	**18.7**
NRT - Type II (n=3)	Min	1.2	4.3	3.2	0.9	16.3
	Max	1.5	6.7	3.7	1.3	22.8

5.1.2.5 Norite

On the REE chondrite-normalised diagram, norite Type I and II samples are fractionated with average La_N/Sm_N of 3.4 and 5.4, and average Gd_N/Yb_N of 0.8 and 1.1, respectively (Fig. 12c; Table 12). These rock also have pronounced positive Eu anomalies (Eu/Eu*= 2.1 – 3.0 for Type I; Eu/Eu*= 1.2 – 1.5 for Type II) than feldspathic pyroxenites, olivine pyroxenites and harzburgites (Tables 10, 11 and 12). Norite Type I has average contents of REE (aver. ΣREE= 5.4) that is lower than norite Type II and all pyroxenitic rocks, but still higher than harzburgites (Tables 10, 11 and 12).
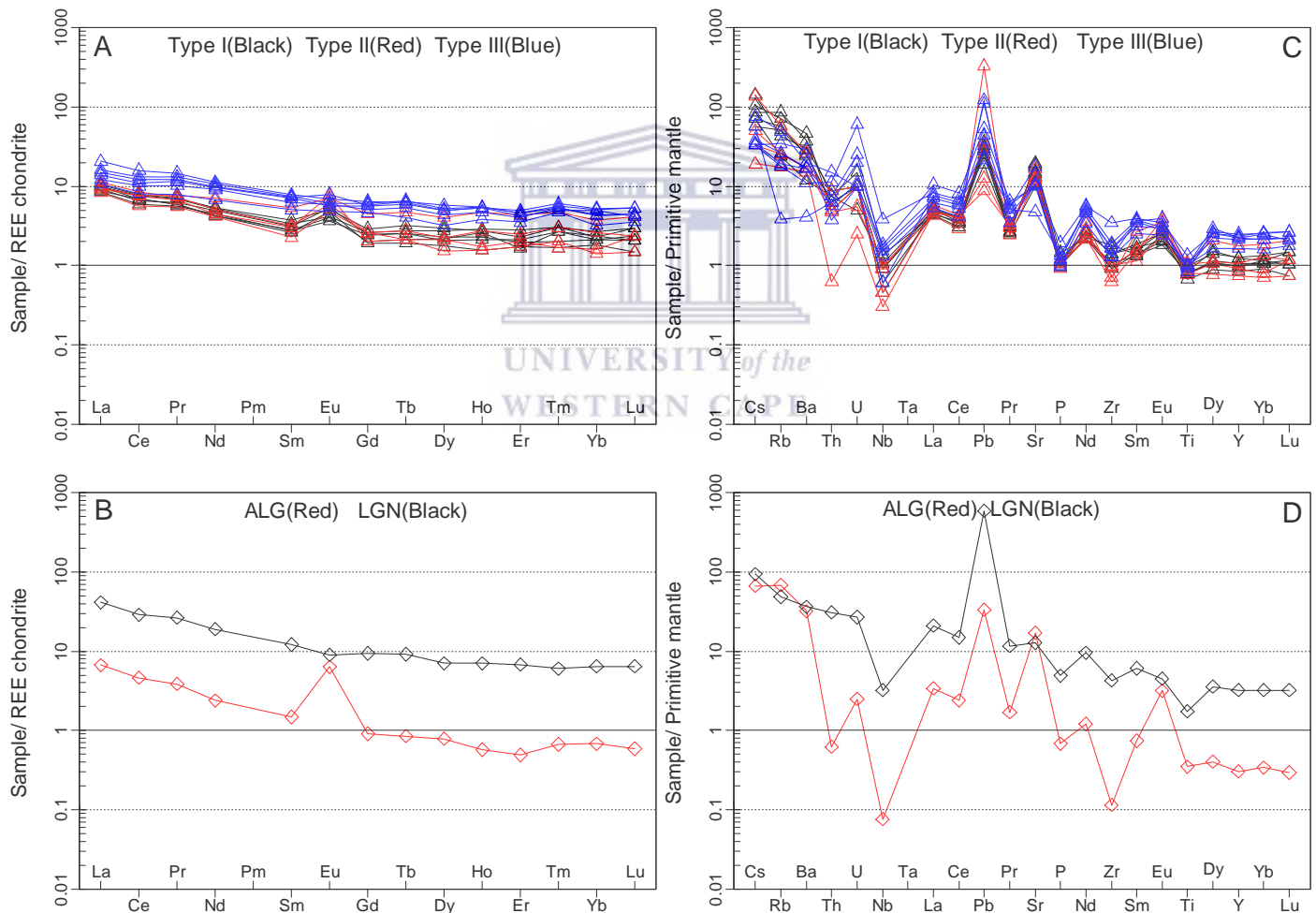
Figure 13: REE chondrite–normalised patterns for gabbronorite Type I, II and III (A), leucogabbronorite (LGN) and anorthositic leucogabbro (ALG) (B). REE normalising values are from Nakamura (1974). Primitive mantle–normalised trace elements patterns for gabbronorite Type I, II and III (C), leucogabbronorite (LGN) and anorthositic leucogabbro (ALG) (D). Normalisation values are from McDonough and Sun (1995).

71

On the PMN trace elements diagram, they have also LILE that are enriched relative to HFSE with peaks at U, La, Pb, Sr and Eu, and negative anomalies at Th, Nb and Zr (Fig. 12f). Norite Type II has also a peak at Nd, and has higher trace elements contents than norite Type I (Fig. 12f).

5.1.2.6 Gabbronorite and leucogabbroic rocks

All gabbronorite samples (i.e., Type I, II and III) are fractionated (aver. $La_N/Sm_N \geq 2.4$; aver. $Gd_N/Yb_N \geq 0.8$) with most of them having a positive Eu anomaly (Eu/Eu* = 0.9 – 3.1) (Table 13). They are also variably enriched in REE contents (aver. ΣREE = 14.3 – 37.8) as norites and feldspathic pyroxenites (Tables 11, 12 and 13).

Gabbronorite Type I and II have average contents of REE (aver. ΣREE= 16.7 and 18, respectively) that is lower than gabbronorite Type III (aver. ΣREE= 16.7) (Fig. 13a; Table 13). The latter has a weakly negative to positive Eu anomaly (Eu/Eu* = 0.9 – 1.2) than gabbronorite Type I and II (Eu/Eu* = 1.4 – 3.1) (Fig. 13; Table 13).
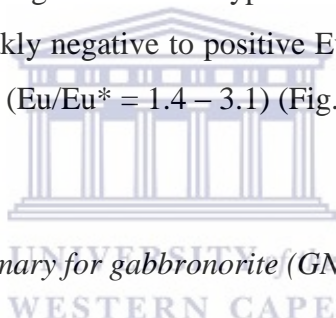
Table 13: REEs statistical summary for gabbronorite (GN) types.

Rock sub-type		Eu/Eu*	La_N/Yb_N	La_N/Sm_N	Gd_N/Yb_N	ΣREE
	Mean	**1.7**	**4.3**	**3.1**	**1.1**	**16.7**
GN - Type I (n=6)	Min	1.4	3.7	2.8	0.9	14.9
	Max	2.1	5.5	3.8	1.3	18.9
	Mean	**2.1**	**4.7**	**3.0**	**1.3**	**18.0**
GN - Type II (n=4)	Min	1.4	2.4	1.7	1.0	14.3
	Max	3.1	6.9	3.7	1.6	21.9
	Mean	**1.0**	**3.3**	**2.1**	**1.3**	**30.2**
GN - Type III (n=6)	Min	0.9	2.7	1.9	1.1	21.6
	Max	1.2	4.1	2.6	1.4	37.8

On the PMN trace elements diagram (Fig. 13c); all gabbronorite types are also characterised with enrichment of the LILE relative to the HFSE. Most gabbronorite samples have peaks at U, La, Pb, Sr, Nd and Eu, and negative anomalies at Th, Nb, P, Zr and Ti (Fig. 13c).

72

Although gabbronorite Type I and II have lower contents for most trace elements than gabbronorite III, gabbronorite Type II has LILE (e.g., Cs, Rb and Ba) contents that are overlapping with gabbronorite Type III whereas gabbronorite Type I has slightly higher LILE contents than gabbronorite Type III (Fig. 13c).

Leucogabbronorite and anorthositic leucogabbro have light REE that are fractionated relative to the heavy REE (La_N/Sm_N= 6.4 and 9.8; aver. Gd_N/Yb_N= 1.5 and 1.3, in that order) (Table 14). Anorthositic leucogabbro has a very pronounced positive Eu anomaly (Eu/Eu*= 5.5), but lower contents of REE (ΣREE = 9.8) and other trace elements than leucogabbronorite (ΣREE = 65.9) (Table 13) (Figs. 13b and d.)

Table 14: REEs statistical summary for anorthositic leucogabbro (ALG) and leucogabbronorite (LGN).

Rock type		Eu/Eu*	La_N/Yb_N	La_N/Sm_N	Gd_N/Yb_N	ΣREE
	Mean	**5.5**	**9.8**	**4.5**	**1.3**	**9.8**
ALG (n=1)	Min	5.5	9.8	4.5	1.3	9.8
	Max	5.5	9.8	4.5	1.3	9.8
	Mean	**0.8**	**6.4**	**3.4**	**1.5**	**65.9**
LGN (n=1)	Min	0.8	6.4	3.4	1.5	65.9
	Max	0.8	6.4	3.4	1.5	65.9

5.1.3   Summary of geochemical findings

Whole-rock geochemistry was conducted to establish the relationship between the modal mineralogy of the Platreef rocks and the geochemical data, and to monitor fractionation and contamination processes in the four drill cores of interest. A statistical summary showing average MgO, La_N/Yb_N and ΣREE for the Platreef and Main Zone rocks, from the least to the most differentiated rock as suggested from the petrography, is reported in Table 15.

73

Table 15: Summary of findings from the major and trace element geochemistry.

	Rock type		Mineralogy	Av. MgO	Av. La$_N$/Yb$_N$	Av. ΣREE
Main Zone	Leucogabbronorite			4.58	6.38	65.85
	Gabbronorite	Type II	Plag> cpx> opx	10.57	4.73	18.00
		Type I	Plag> opx≈ cpx	11.99	4.30	3.12
Platreef	Norite	Type II	Opx≈ plag	12.48	5.36	18.69
		Type I	Opx≈ plag	9.78	3.38	5.39
	Feldspathic pyroxenite	Type V	Opx> plag> cpx	18.89	1.69	9.19
		Type IV	Opx> cpx> plag	14.53	3.85	36.59
		Type III	Opx> cpx> plag	17.78	4.17	47.44
		Type II	Opx> plag> cpx	18.88	3.48	19.86
		Type I	Opx> plag> cpx	20.67	3.51	12.31
	Pyroxenite		Opx	24.47	2.59	9.25
	Olivine pyroxenite*		Opx> ol	25.52	1.63	7.86
	Harzburgite		Ol> opx	35.12	1.12	4.09

* Excluded OB-Pyx SS339-19: MgO= 25.03; La$_N$/Yb$_N$ 2.0; ΣREE= 22.5

The major findings from the major and trace elements geochemistry are:

1. The decrease in the average contents of MgO accompanied with the increase in the average contents of La$_N$/Yb$_N$ and ΣREE from harzburgite to olivine pyroxenite, pyroxenite, and feldspathic pyroxenite Type I, II and III (Table 15), which is consistent with the variation in the modal mineralogy of the Platreef rocks, may be an indication that :

   - A genetic link exists between some of these Platreef rocks.
   - Magmatic differentiation processes; such as contamination and fractionation, may have played an important role during the genesis of these Platreef rocks.

2. The average contents of MgO, La$_N$/Yb$_N$ and ΣREE for feldspathic pyroxenite Type IV when compared to those from feldspathic pyroxenite Type I, II and III (Table 15) may be an indication that the magmatic processes involved in their genesis are not linked to the same processes although they may share the same origin.

74

3. The average contents of MgO, La_N/Yb_N and ΣREE for feldspathic pyroxenite Type V when compared also to those from feldspathic pyroxenite Type I, II, III and IV (Table 15) may also be an indication that the magmatic processes involved in their genesis are not the same although they may also share the same origin.

4. Norite Type I and II are not genetically related to the same magmatic processes or to any that resulted in the genesis of the Platreef feldspathic pyroxenite types.

5. The genesis of the Platreef is not related to the same magmatic processes that have resulted in the genesis of the Main Zone.

In conclusion, these major findings provide the basis upon which the link between the major and trace elements geochemistry and the isotope geochemistry will be established in order to understand the genesis of the Platreef. In the following sub-chapter, we present the Sr–Nd isotopic composition of the Platreef (and few Main Zone) rocks.
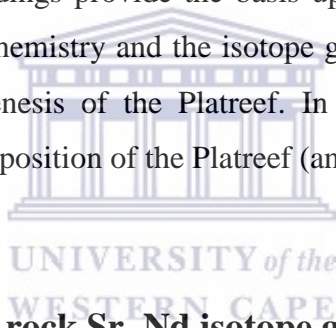
5.2   Whole-rock Sr–Nd isotope geochemistry

As stated earlier, the measured Sr–Nd isotope data generated from the Platreef rocks (and few from the MZ) collected from four drill cores are presented in Appendix D. The initial Sr–Nd ratios for the Platreef and MZ rocks, calculated at the nearest round off age of 2.06 Ga for the BIC (Zeh et al., 2015; Yudovskaya et al., 2013b; Buick et al., 2001), are reported in Table 16.

The isotopic compositions for the Platreef and MZ rocks vary widely with $^{87}Sr/^{86}Sr_{2060}$ ranging from 0.707281 to 0.760885, $^{143}Nd/^{144}Nd_{2060}$ ranging from 0.508803 to 0.510003, and the rocks yield εNd_{2060} ranging from –22.9 to +0.7 (Table 16). Olivine pyroxenite, pyroxenite and feldspathic pyroxenite samples from the Platreef have εNd_{2060} ranging between –22.9 and –2.9 (Table 16).

For the Main Zone rocks, gabbronorite Type II sample OY482-01 has positive εNd_{2060} (+0.7), whereas gabbronorite Type III sample OY482-20 has negative εNd_{2060} (−5.8) (Table 16). Leucogabbronorite sample TN754-01 has also negative εNd_{2060} (−7.2) (Table 16).

Table 16: Sr–Nd isotope systematic for selected Platreef and Main Zone rocks (This study). $^{87}Sr/^{86}Sr$ and εNd were calculated at 2060 Ma.

Sample	Rock type	$^{87}Rb/^{86}Sr$	$^{147}Sm/^{144}Nd$	$^{87}Sr/^{86}Sr_{2060}$	$^{143}Nd/^{144}Nd_{2060}$	εNd_{2060}
OY482-01	GN-II	0.19	0.11	0.711746 ±14	0.510003	+0.7 ±0.2
OY482-03	FPyx-II	0.10	0.14	0.711050 ±13	0.509722	−4.9 ±0.2
OY482-20	GN-III	0.16	0.15	0.715021 ±13	0.509673	−5.8 ±0.2
OY482-30	FPyx-III	0.46	0.14	0.721956 ±13	0.509618	−6.9 ±0.2
OY482-35	FPyx-III	0.35	0.16	0.719761 ±15	0.509520	−8.8 ±0.2
OY482-40	FPyx-IV	0.47	0.16	0.742252 ±11	0.509420	−10.8 ±0.2
SS339-08	OB-Pyx	0.25	0.16	0.710042 ±11	0.509340	−12.4 ±0.3
SS339-09	Pyx	0.39	0.13	0.710492 ±12	0.509779	−3.8 ±0.2
SS339-12	OB-Pyx	0.33	0.18	0.708406 ±13	0.509363	−11.9 ±0.3
SS339-13	Pyx	0.15	0.14	0.709177 ±10	0.509822	−2.9 ±0.3
SS339-15	OB-Pyx	0.13	0.23	0.709493 ±22	0.508803	−22.9 ±0.3
SS339-19	OB-Pyx	0.15	0.18	0.709173 ±10	0.509418	−10.8 ±0.2
TN200-03	FPyx-I	0.27	0.16	0.708374 ±15	0.509326	−12.6 ±0.2
TN200-04	FPyx-I	0.68	0.14	0.708570 ±15	0.509380	−11.6 ±0.2
TN200-05	FPyx-I	0.26	0.15	0.707545 ±11	0.509386	−11.5 ±0.2
TN200-09	FPyx-I	0.23	0.15	0.708742 ±20	0.509240	−14.3 ±0.2
TN200-16	FPyx-V	1.47	0.13	0.712106 ±12	0.509591	−7.4 ±0.2
TN200-24	FPyx-III	3.07	0.11	0.711998 ±18	0.509680	−5.7 ±0.2
TN754-01	LGN	0.33	0.13	0.709322 ±11	0.509603	−7.2 ±0.2
TN754-02	FPyx-III	1.30	0.12	0.709816 ±20	0.509542	−8.4 ±0.2
TN754-03	FPyx-II	0.99	0.11	0.707281 ±20	0.509702	−5.3 ±0.2
TN754-06	FPyx-III	0.76	0.13	0.711523 ±12	0.509562	−8.0 ±0.2
TN754-08	FPyx-II	0.38	0.14	0.711031 ±12	0.509711	−5.1 ±0.3
TN754-11	OB-Pyx	1.93	0.14	0.760885 ±41	0.509499	−9.2 ±0.2

Epsilon Nd (or εNd_{2060}) was calculated after Liew and Hofmann (1988). All isotopes are calculated at the nearest round-off age of 2.06 Ga (or 2060 Ma) for the BIC (Buick et al., 2001; Yudovskaya et al., 2013b; Zeh et al., 2015). Errors (2σ) correspond to the last two digits of the Sr isotope values and the last digit of the εNd values.
Abbreviation: FPyx: Feldspathic pyroxenite; GN: Gabbronorite; LGN: Leucogabbronorite; OB-Pyx: Olivine pyroxenite; Pyx: Pyroxenite.
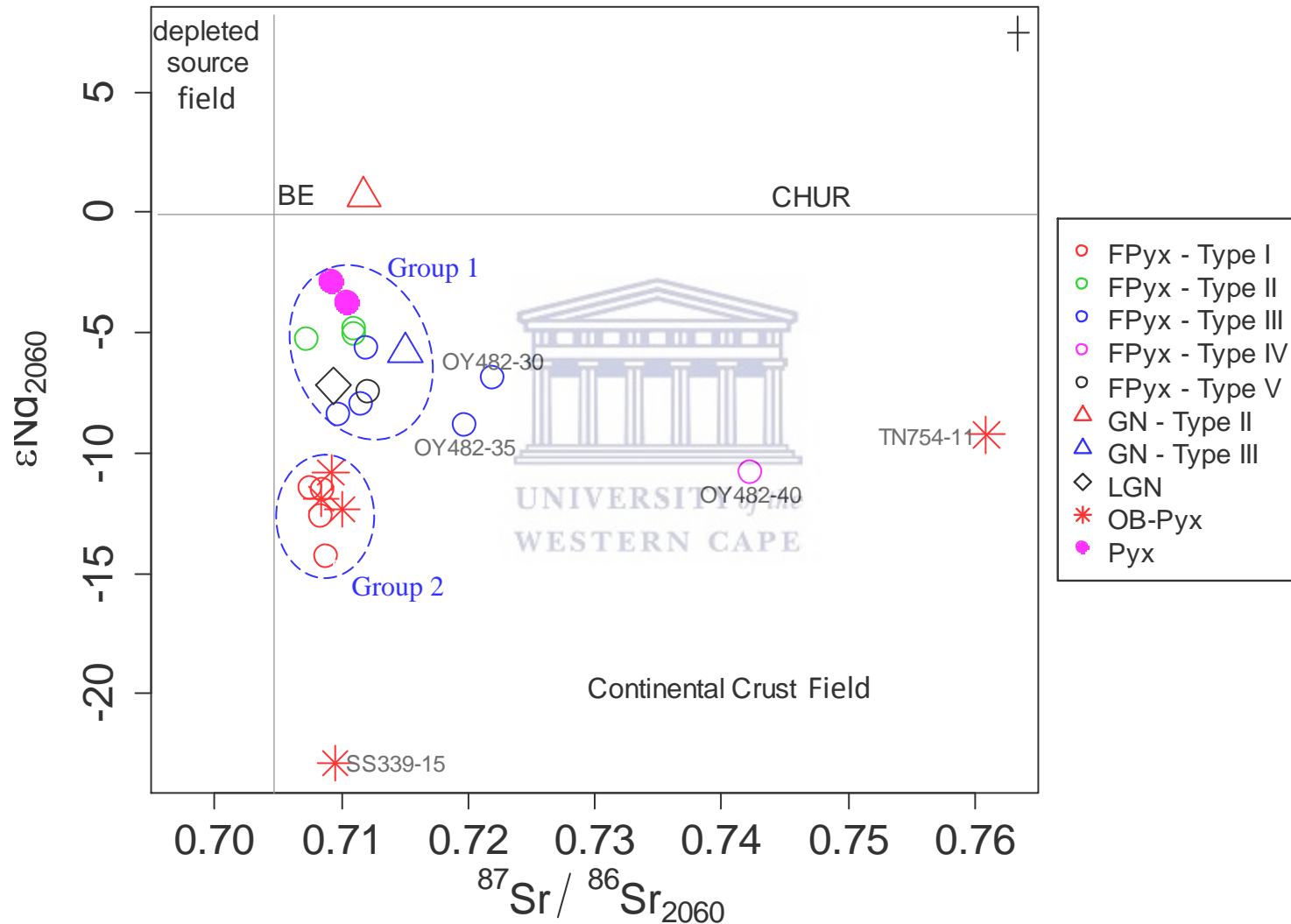
Figure 14: Plot of $^{87}Sr/^{86}Sr_{2060}$ versus εNd_{2060} for the Platreef and Main Zone rock samples from the four drill cores. Chondrite Uniform Reservoir (CHUR) present day $^{143}Nd/^{144}Nd$ of 0.512638 (or $\varepsilon Nd= 0$) after Wasserburg et al. (1981). Bulk Earth (BE) present day $^{87}Sr/^{86}Sr$ of 0.7045 after Faure (1986). All isotopes are calculated at the nearest round-off age of 2.06 Ga for the BIC (Buick et al., 2001; Yudovskaya et al., 2013b; Zeh et al., 2015). The reader is referred to text for more details on the isotopic groups (1 and 2) for the Platreef rocks. Legend abbreviation: FPyx: Feldspathic pyroxenite; GN: Gabbronorite; LGN: Leucogabbronorite; OB-Pyx: Olivine pyroxenite; Pyx: Pyroxenite. The error bars (top right corner) are ±2σ.

77

Table 17: Sr–Nd isotopic compositional ranges for the Platreef and Main Zone rocks in decreasing εNd$_{2060}$.

Unit	Rock type	Sub-type	$^{87}Sr/^{86}Sr_{2060}$		εNd_{2060}	
			Min	Max	Min	Max
Platreef	Pyroxenite (n=2)		0.709177±10	0.710492±12	−3.8±0.2	−2.9±0.3
	Feldspathic pyroxenite	Type II (n=3)	0.707281±20	0.711050±13	−5.3±0.2	−4.9±0.2
		Type III (n=5)	0.709816±20	0.721956±13	−8.8±0.2	−5.7±0.2
		Type V (n=1)	0.712106±12	0.712106±12	−7.4±0.2	−7.4±0.2
	Olivine pyroxenite (n=5)		0.708406±13	0.760885±41	−22.9±0.3	−9.2±0.2
	Feldspathic pyroxenite	Type IV (n=1)	0.742252±11	0.742252±11	−10.8±0.2	−10.8±0.2
		Type I (n=4)	0.707545±11	0.708742±20	−14.3±0.2	−11.5±0.2
Main Zone	Gabbronorite	Type II (n=1)	0.711746±14	0.711746±14	+0.7±0.2	+0.7±0.2
		Type III (n=1)	0.715021±13	0.715021±13	−5.8±0.2	−5.8±0.2
	Leucogabbronorite (n=1)		0.709322±11	0.709322±11	−7.2±0.2	−7.2±0.2

Figure 14 and Table 17 show the variation in the Sr–Nd isotopic composition for the Platreef and MZ rock samples. Table 17 above shows the isotopic compositional's ranges for the Platreef and Main Zone rocks with decreasing εNd$_{2060}$. The results for the Platreef rocks show the following (in decreasing εNd$_{2060}$ order):

1. Pyroxenites have εNd$_{2060}$ ranging between −3.8±0.2 and −2.9±0.3, and $^{87}Sr/^{86}Sr_{2060}$ between 0.709177±10 and 0.710492±12 (Fig. 14; Table 17).

2. Feldspathic pyroxenite Type II has εNd$_{2060}$ ranging between −5.3±0.2 and −4.9±0.2, and $^{87}Sr/^{86}Sr_{2060}$ between 0.707281±20 and 0.711050±13 (Fig. 14; Table 17).

3. Feldspathic pyroxenite Type III has εNd$_{2060}$ ranging between −8.8±0.2 and −5.7±0.2, and $^{87}Sr/^{86}Sr_{2060}$ between 0.709816±20 and 0.721956±13 (Fig. 14; Table 17).

4. Feldspathic pyroxenite Type V has εNd$_{2060}$ of −7.4±0.2 and $^{87}Sr/^{86}Sr_{2060}$ of 0.712106±12 (Fig. 14; Table 17).

5. Olivine pyroxenites have εNd$_{2060}$ ranging between −22.9±0.3 and −9.2±0.2, and $^{87}Sr/^{86}Sr_{2060}$ between 0.708406±13 and 0.760885±41 (Fig. 14; Table 17).

6. Feldspathic pyroxenite Type IV has εNd$_{2060}$ of −10.8±0.2 and $^{87}Sr/^{86}Sr_{2060}$ of 0.742252±11 (Fig. 14; Table 17).

7. Feldspathic pyroxenite Type I has εNd_{2060} ranging from -14.3 ± 0.2 to -11.5 ± 0.2, and $^{87}Sr/^{86}Sr_{2060}$ between 0.707545 ± 11 and 0.708742 ± 20 (Fig. 14; Table 17).

The results for the Main Zone rocks show (in decreasing εNd_{2060} order; Table 17):

1. Gabbronorite II has εNd_{2060} of $+0.7\pm0.2$ and $^{87}Sr/^{86}Sr_{2060}$ of 0.711746 (Fig. 14; Table 17).
2. Gabbronorite III has εNd_{2060} of -5.8 ± 0.2 and $^{87}Sr/^{86}Sr_{2060}$ of 0.715021 (Fig. 14; Table 17).
3. Leucogabbronorite has εNd_{2060} of -7.2 ± 0.2 and $^{87}Sr/^{86}Sr_{2060}$ of 0.709322 (Fig. 14; Table 17).

In Figure 14, the isotopic composition for the Platreef rock samples shows that most pyroxenite, feldspathic pyroxenite type II, III and IV samples have higher initial Sr ratios and higher negative εNd_{2060} than most olivine pyroxenite and feldspathic pyroxenite type I samples which have lower initial Sr ratios and lower negative εNd_{2060}.

On the basis of the trends (Table 17 and Figure 14), the Sr–Nd isotopic compositions of the Platreef rocks show two distinct groups of samples:

1. Group 1 consists of rock samples having εNd_{2060} ranging between -8.4 ± 0.2 to -2.9 ± 0.3, and $^{87}Sr/^{86}Sr_{2060}$ between 0.707281 ± 20 to 0.712106 ± 12; i.e. pyroxenite and feldspathic pyroxenite II, III and V (Fig. 14; Table 16).
2. Group 2 consists of rock samples having εNd_{2060} ranging between -12.6 ± 0.2 to -10.8 ± 0.2, and $^{87}Sr/^{86}Sr_{2060}$ between 0.707545 ± 11 to 0.710042 ± 11; i.e. olivine pyroxenite and feldspathic pyroxenite I (Fig. 14; Table 16).

It should be also noted that there are olivine pyroxenite (TN745-11 and SS339-15) and feldspathic pyroxenite (OY482-30, OY482-35 and OY482-40) samples which could not be included in any of the two groups because they have anomalously high initial Sr or Nd isotopic compositions (Fig. 14) which will be discussed in chapter 6.

5.3   Base metal sulphides and PGE contents in the Platreef rocks

PGE-bearing minerals in the Platreef rocks of this study could not be identified through ore microscopy studies. However, the petrography has revealed the presence of the BMS (pentlandite, pyrrhotite and chalcopyrite) in these rocks. For these reasons, the contents of SO_3, Cu, Cu+Ni and Pt+Pd (Table 18) were used to determine the styles of the PGE mineralisation in the Platreef rocks.

Although S, Cu and Ni are chalcophile metals and predominantly reside in sulphides, Ni resides also in silicates (e.g. olivine and orthopyroxene). Therefore, the contents of SO_3 and Cu were used as proxies to assess the sulphide (BMS) contents, whereas the content of Pt+Pd was used as a proxy to assess the contents of the PGE in the Platreef rocks.

In terms of the BMS contents, the Platreef feldspathic pyroxenite Type V has the highest average contents of SO_3 (1.2 wt. %), followed by olivine pyroxenite (0.8 wt. %) and then feldspathic pyroxenite Type I (0.7 wt. %) (Table 18). Feldspathic pyroxenite Type III and IV have average SO_3 contents of 0.6 and 0.5 wt. %, respectively (Table 18). Harzburgite, pyroxenite and feldspathic pyroxenite Type II have average SO_3 contents of 0.3, 0.3 and 0.2 wt. %, respectively (Table 18). Norite Type I and II have average SO_3 contents of 0.7 and 0.8 wt. %, respectively (Table 18).

In addition, the Platreef feldspathic pyroxenite Type IV has the highest average contents of Cu (1970.6 ppm), followed by olivine pyroxenite (1614.7 ppm) and then feldspathic pyroxenite Type III (1427.6 ppm) (Table 18). Harzburgite, pyroxenite, feldspathic pyroxenite Type I and V, and norite II have average Cu contents ranging between ~500 and ~1000 ppm (Table 18). Feldspathic pyroxenite Type II and norite I have average contents of Cu lower than 500 ppm (Table 18).

In terms of the PGE contents for the Platreef rocks, olivine pyroxenite has the highest average contents of Pt+Pd (2.7 g. t^{-1}) (Table 18). Feldspathic pyroxenite Type IV has the lowest average contents of Pt+Pd (0.1 g. t^{-1}), whereas harzburgite, feldspathic pyroxenite Type II and III have average contents of Pt+Pd ranging between 3.0 and 0.8 g. t^{-1} (Table 18).

Table 18: Mean, minimum and maximum contents of BMS (Cu+Ni) and PGE (Pt+Pd) in the Platreef rocks.

HZG	Mean	Min	Max		OB-Pyx	Mean	Min	Max
SO$_3$ (n=2)	0.3	0.1	0.5		SO$_3$ (n=5)	0.8	0.4	1.3
Cu (n=2)	701.3	212.2	1190.4		Cu (n=5)	1614.7	275.5	3380.4
Cu+Ni (n=2)	2474.4	1498.8	3450.0		Cu+Ni (n=5)	4714.4	1367.8	8697.5
Pt+Pd (n=2)	0.5	0.5	0.5		Pt+Pd (n=3)	2.7	1.8	3.6

Pyx	Mean	Min	Max		FPyx-I	Mean	Min	Max
SO$_3$ (n=2)	0.3	0.1	0.4		SO$_3$ (n=5)	0.7	0.5	1.0
Cu (n=2)	682.0	421.6	942.4		Cu (n=5)	612.7	299.5	1143.5
Cu+Ni (n=2)	2484.6	1487.1	3482.1		Cu+Ni (n=5)	2363.5	1285.9	4085.0
Pt+Pd (n=0)	-	-	-		Pt+Pd (n=0)	-	-	-

FPyx-II	Mean	Min	Max		FPyx-III	Mean	Min	Max
SO$_3$ (n=3)	0.2	0.1	0.3		SO$_3$ (n=6)	0.6	0.4	1.2
Cu (n=3)	409.2	213.2	620.0		Cu (n=6)	1427.6	374.6	2768.6
Cu+Ni (n=3)	1229.0	950.7	1562.0		Cu+Ni (n=6)	3888.9	1404.1	8519.5
Pt+Pd (n=3)	0.8	0.1	1.4		Pt+Pd (n=1)	0.3	0.3	0.3

FPyx-IV	Mean	Min	Max		FPyx-V	Mean	Min	Max
SO$_3$ (n=2)	0.5	0.4	0.5		SO$_3$ (n=1)	1.2	1.2	1.2
Cu (n=2)	1970.6	1839.2	2102.2		Cu (n=1)	875.0	875.0	875.0
Cu+Ni (n=2)	4897.2	3556.3	6238.0		Cu+Ni (n=1)	2817.5	2817.5	2817.5
Pt+Pd (n=1)	0.1	0.1	0.1		Pt+Pd (n=0)	-	-	-

NRT-I	Mean	Min	Max		NRT-II	Mean	Min	Max
SO$_3$ (n=2)	0.7	0.4	1.0		SO$_3$ (n=3)	0.8	0.7	0.9
Cu (n=2)	460.6	446.6	474.6		Cu (n=3)	922.0	611.1	1314.9
Cu+Ni (n=2)	1283.7	1113.7	1453.6		Cu+Ni (n=3)	2481.7	1990.7	2844.1
Pt+Pd (n=0)	-	-	-		Pt+Pd (n=0)	-	-	-

<u>Note</u>: FPyx: feldspathic pyroxenite; HZG: harzburgite; OB-Pyx: olivine-bearing pyroxenite; NRT: Norite. "-": Not analysed.

On the basis of the average contents of SO_3, Cu and Pt+Pd in the Platreef rocks, this study has noted that:

1. Olivine pyroxenite has high average contents of SO_3, Cu and Pt+Pd (Table 18); therefore the rock is PGE and BMS mineralised.

2. Feldspathic pyroxenite Type III and IV have high average contents of SO_3 and Cu but low average contents of Pt+Pd (Table 18); therefore these rocks are only BMS mineralised.

3. Feldspathic pyroxenite Type II and harzburgite have low average contents of SO_3, Cu and Pt+Pd (Table 18); therefore the rocks are barren.

This study therefore concludes that the Platreef in the four drill cores host two styles of mineralisation; i.e., PGE-BMS mineralisation and BMS mineralisation.

82

6   DISCUSSION

The Platreef rocks analysed from the studied drill cores were at most slightly weathered. The petrography has revealed that two harzburgite and three olivine pyroxenite samples (SS339-10, TN754-09, TN754-10, TN754-11 and TN754-12) are variably serpentinised (L.O.I: ~3.4 – 8.8 wt. %), and five feldspathic pyroxenite samples (OY482-29, OY482-34, OY482-35, OY482-40 and TN200-24) are highly altered (L.O.I: ~3.4 – 8 wt. %). The LOI values of < 3.0 wt. % for the Platreef rocks indicate therefore well-preserved minerals. As a result, the major and trace elements and the Sr–Nd isotopic compositions of the Platreef rocks most likely reflect those of corresponding parental magmas and can thus be used in the following discussion on the genesis of the Platreef.

6.1   Drill core stratigraphy and magmatic differentiation

Core logging in combination with the petrography have revealed that the rock succession in the Platreef is different from one drill core to the other (Figs. 5 – 8). This is evidenced by the occurrence of (1) harzburgite and olivine pyroxenite only in TN754 and SS339, (2) feldspathic pyroxenite Type I in TN200 and SS339 and (3) feldspathic pyroxenite Type II in TN754 and OY482 (Figs. 5 – 8), and indicates that lithostratigraphic correlations between the four drill cores are not consistent with a single magmatic injection. It is therefore evident that multiple magmas were involved in the genesis of the Platreef, as previously noted (Kinnaird, 2005; Manyeruke et al., 2005; Yudovskaya and Kinnaird, 2010; Mitchell and Scoon, 2012).

The plots in Figure 9 (a – f) show the variation of selected major elements versus MgO for the Platreef rocks. The trends in the major elements for the Platreef rocks (Figs. 9a – f) are consistent with the change in the modal mineralogy of olivine, orthopyroxene and plagioclase from harzburgite to olivine pyroxenite, pyroxenite, feldspathic pyroxenite and norite.

83
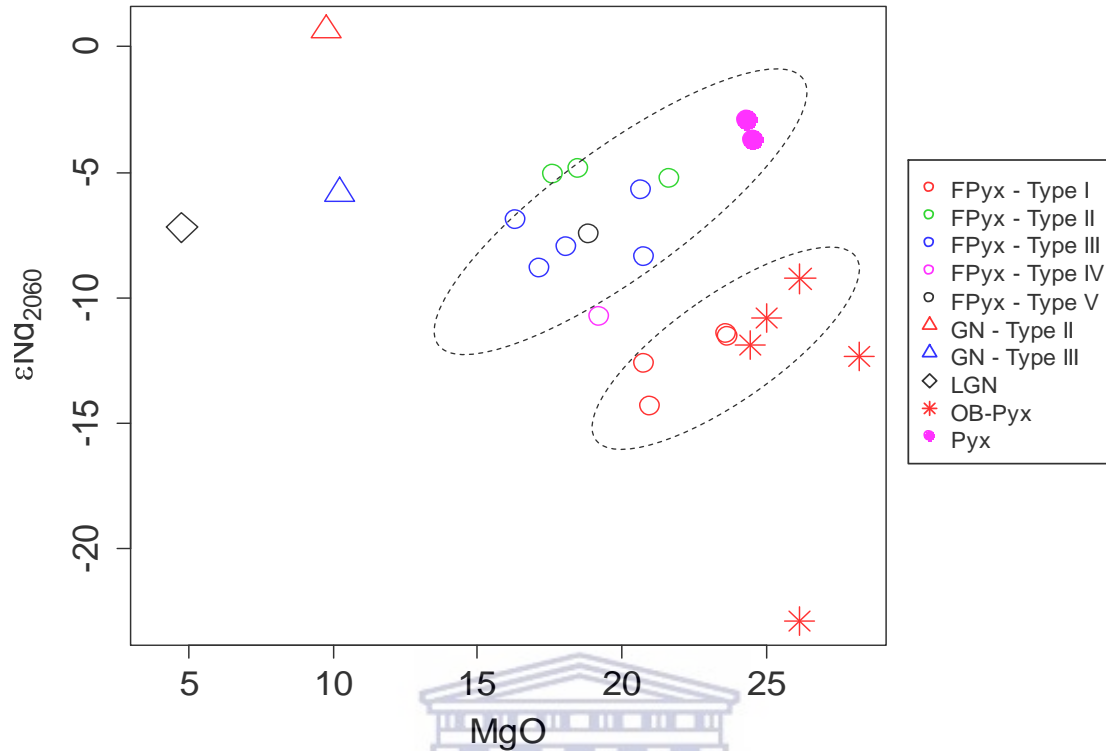
Figure 15: Plot of εNd$_{2060}$ versus MgO for the Platreef rocks from the four drill cores.

The investigation conducted using the Sr–Nd isotope data of the Platreef has revealed two groups of rocks (Fig. 14; Table 17). There is a trend for the Platreef rocks of group 1 which is marked by the decrease in negative εNd$_{2060}$ coupled with an overall increase in $^{87}Sr/^{86}Sr_{2060}$ from pyroxenite to feldspathic pyroxenite Type II and III samples (Table 17). In addition, these rocks display a positive correlation between MgO and εNd$_{2060}$ such that pyroxenites have the highest values and feldspathic pyroxenites Type III have the lowest values (Fig. 15). Moreover, the ΣREE contents show a gradual increase from pyroxenites to feldspathic pyroxenite Type II and III (Fig. 16a).

On the other hand, the Platreef rocks of group 2 overlap in εNd$_{2060}$ values with most olivine pyroxenite samples having higher $^{87}Sr/^{86}Sr_{2060}$ values than feldspathic pyroxenite Type I samples (Table 17). These rocks also display a positive correlation between MgO and εNd$_{2060}$ such that olivine pyroxenites have higher values than feldspathic pyroxenite Type I samples (Fig. 15), and their ΣREE contents increase from olivine pyroxenites to feldspathic pyroxenite Type I (Fig. 16b).

84
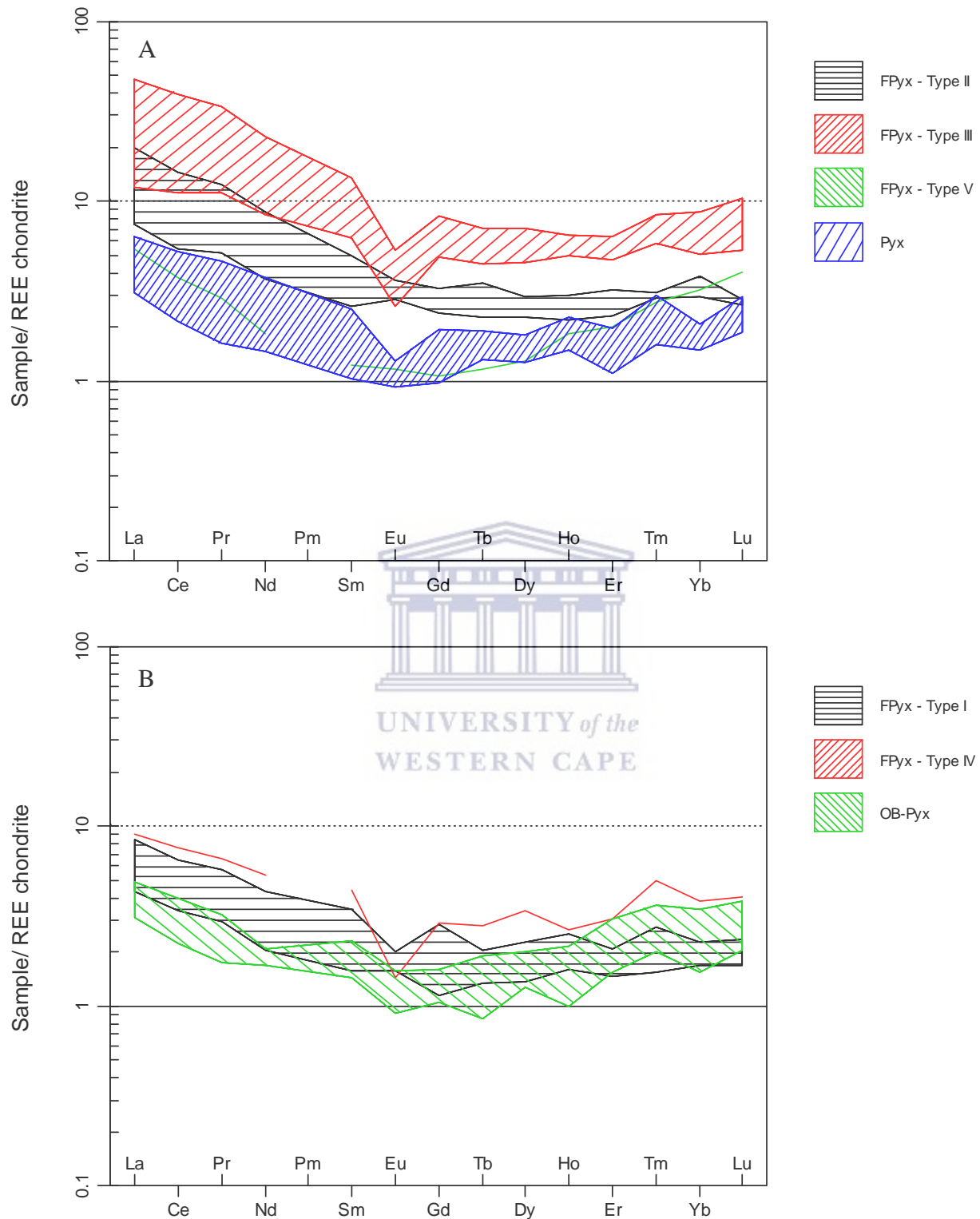
Figure 16: A) REE chondrite–normalised patterns for the Platreef rocks in group 1; B) REE chondrite–normalised patterns for the Platreef rocks in group 2 with feldspathic pyroxenite Type IV sample OY482-40. The REE normalising values are from Nakamura (1974).

Positive correlations between εNd and Mg#, and negative correlations between εNd and $^{87}Sr/^{86}Sr$ in mafic rocks have been generally attributed to AFC processes (Stewart and DePaolo, 1990; Geist et al., 1990; Chung et al., 1997; Maier et al., 2000; Huang et al., 2015). Since MgO is used as a differentiation index (Figs. 9a – f), the magmas for the Platreef rocks of group 1 were therefore subjected to assimilation and fractionation processes in agreement with previous studies (Rudnick et al., 1986; Chen et al., 2001). The increase in the ΣREE contents for the Platreef rocks of group 2; i.e. from olivine pyroxenites to feldspathic pyroxenite Type I (Fig. 16b), as opposed to the lack of trends between εNd and Mg#, and between εNd and $^{87}Sr/^{86}Sr$, may only suggest fractionation processes. It should be reminded that the variation in εNd and $^{87}Sr/^{86}Sr$ for the Platreef rocks as a whole (Fig. 14) coupled with the lack of similarity for the stratigraphy of the Platreef in each drill core (Figs. 5 – 8) is not consistent with a single magmatic injection. Thus, these attributes suggest the involvement of multiple magmas in the genesis of the Platreef each subjected to separate differentiation mechanism at shallow depth and from different set of staging chambers as earlier suggestions (Yudovskaya et al., 2017a) based on the two parallel trends shown in Figure 15.
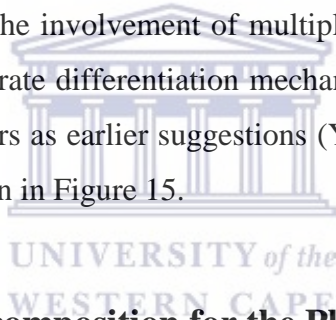
6.2   Sr–Nd isotopic composition for the Platreef and RLS rocks

The Sr–Nd isotope data of the Platreef (Group 1 and 2) and Main Zone rocks are reported in Table 19, and those of rocks from the Platreef, LZ, CZ and MZ of the BIC in previous studies are reported in Table 20. Figure 17 shows the Sr–Nd isotopic compositions of the Platreef and Main Zone rocks (in this study) plotted with those of rocks from previous studies (Maier et al., 2000; Pronost et al., 2008; Roelofse and Ashwal, 2012).

There are a number of important differences between the Sr–Nd isotopic composition of the Platreef rocks in this study and those from rocks in previous studies.
In Figure 17, the rocks from the LZ, CZ and MZ of the BIC (Maier et al., 2000; Roelofse and Ashwal, 2012) show clustered data points with all having negative εNd values which vary between –8.5 and –5.1, and $^{87}Sr/^{86}Sr$ varying between 0.704400 and 0.709671 (Table 20).

86

Table 19: Whole-rock εNd and $^{87}Sr/^{86}Sr$ for the Platreef (including group 1 and 2) and Main Zone rocks in the studied drill cores. $^{87}Sr/^{86}Sr$ and εNd were calculated at 2060 Ma.

Unit	Sample	Rock type	Group	$^{87}Sr/^{86}Sr_{2060}$	$εNd_{2060}$
Platreef	SS339-13	Pyx	1	0.709177 ±10	−2.9 ±0.3
	SS339-09	Pyx	1	0.710492 ±12	−3.8 ±0.2
	OY482-03	FPyx-II	1	0.711050 ±13	−4.9 ±0.2
	TN754-08	FPyx-II	1	0.711031 ±12	−5.1 ±0.3
	TN754-03	FPyx-II	1	0.707281 ±20	−5.3 ±0.2
	TN200-24	FPyx-III	1	0.711998 ±18	−5.7 ±0.2
	OY482-30	FPyx-III	1?	0.721956 ±13	−6.9 ±0.2
	TN200-16	FPyx-V	1	0.712106 ±12	−7.4 ±0.2
	TN754-06	FPyx-III	1	0.711523 ±12	−8.0 ±0.2
	TN754-02	FPyx-III	1	0.709816 ±20	−8.4 ±0.2
	OY482-35	FPyx-III	1?	0.719761 ±15	−8.8 ±0.2
	TN754-11	OB-Pyx	2?	0.760885 ±41	−9.2 ±0.2
	OY482-40	FPyx-IV	2?	0.742252 ±11	−10.8 ±0.2
	SS339-19	OB-Pyx	2	0.709173 ±10	−10.8 ±0.2
	TN200-05	FPyx-I	2	0.707545 ±11	−11.5 ±0.2
	TN200-04	FPyx-I	2	0.708570 ±15	−11.6 ±0.2
	SS339-12	OB-Pyx	2	0.708406 ±13	−11.9 ±0.3
	SS339-08	OB-Pyx	2	0.710042 ±11	−12.4 ±0.3
	TN200-03	FPyx-I	2	0.708374 ±15	−12.6 ±0.2
	TN200-09	FPyx-I	2	0.708742 ±20	−14.3 ±0.2
	SS339-15	OB-Pyx	?	0.709493 ±22	−22.9 ±0.3
Main Zone	OY482-01	GN-II		0.711746 ±14	+0.7 ±0.2
	OY482-20	GN-III		0.715021 ±13	−5.8 ±0.2
	TN754-01	LGN		0.709322 ±11	−7.2 ±0.2

Epsilon Nd (or $εNd_{2060}$) was calculated after Liew and Hofmann (1988). All isotopes are calculated at the nearest round-off age of 2.06 Ga (or 2060 Ma) for the BIC (Buick et al., 2001; Yudovskaya et al., 2013b; Zeh et al., 2015). The isotopic groups (1 and 2) for the Platreef rocks are the same as in Figure 14. The errors (2σ) correspond to the last two digits of the Sr isotope values and the last digit of the εNd values.

Abbreviation: FPyx: Feldspathic pyroxenite; GN: Gabbronorite; LGN: Leucogabbronorite; OB-Pyx: Olivine pyroxenite; Pyx: Pyroxenite.

Table 20: Published whole-rock εNd and $^{87}Sr/^{86}Sr$ for the Bushveld rocks. Platreef and MZ data in the Northern Limb are from Pronost et al. (2008), and Roelofse and Ashwal (2012). Data from the Western Limb are from Maier et al. (2000) and references therein.

Bushveld	Zone	Sample ID	Rock type	εNd_{2060}	$^{87}Sr/^{86}Sr_{2060}$
Northern Limb (Pronost et al., 2008)					
	PL	OY47-8B	P	−7.2±0.2	0.718256±22
	PL	PP7a	P	−7.0±0.2	0.713693±21
	PL	PP12a	P	−7.4±0.2	0.712479±15
Northern Limb (Roelofse & Ashwal, 2012)					
	MZ	MO-2063.66	Gn	−6.6	0.708313
	MZ	MO-2108.08	Gn	−7.8	0.707945
	MZ	MO-2115.7	Gn	−7.9	0.707999
	MZ	MO-2150.15	Gn	−6.6	0.708192
	MZ	MO-2169	Gn	−7.0	0.708230
	MZ	MO-2212.63	Gn	−7.2	0.707846
	MZ	MO-2547.91	Gn	−7.2	0.708146
	MZ	MO-2577.02	Gn	−7.5	0.708350
	MZ	MO-2591.7	Gn	−7.8	0.707974
	MZ	MO-2625.7	Gn	−8.5	0.708512
	MZ	MO-2662.7	Gn	−7.1	0.709671
	MZ	MO-2696.44	Gn	−8.4	0.708637
Western Limb (Maier et al., 2000)					
	MZ	MZ7	Gn	−6.3	0.707000
	MZ	A1	Gn	−7.1	0.708200
	MZ	A 168	Gn	−6.4	0.708500
	MZ	A 254	Gn	−7.4	0.708400
	C_UZ	UA 2	An	−7.6	0.707800
	C_UZ	UA25	Px	−6.5	0.707300
	C_UZ	UA 31	An	−7.3	0.707400
	C_UZ	UA 41	Px	−6.3	0.706900
	C_UZ	UA 48	An	−6.4	0.706400
	C_UZ	B 235/36	Px	−6.4	0.706700
	C_UZ	S 11	No	−6.4	0.706100
	C_UZ	NG3 159.4	Px	−6.9	0.705900
	C_LZ	NG1 25	Px	−5.3	0.705600
	C_LZ	NG1 327.45	Px	−5.1	0.704900
	C_LZ	NG1 528.5	Px	−5.3	0.704800
	LZ	NG2 171.5	Px	−6.0	0.707400
	LZ	NG2 557.1	Hz	−5.4	0.704400

The εNd and $^{87}Sr/^{86}Sr$ values were calculated at 2060 Ma. The errors (2σ) correspond to the last two digits of the Sr isotope values and the last digit of the εNd values for the data after Pronost et al. (2008).

Abbreviations: PL: Platreef. An: Anorthosite; Gn: Gabbronorite; Hz: Harzburgite; N-No: Norite; P or Px: Pyroxenite. PL: Platreef; MZ: Main Zone; C_UZ: Upper Critical Zone; C_LZ: Lower Critical Zone; LZ: Lower Zone.
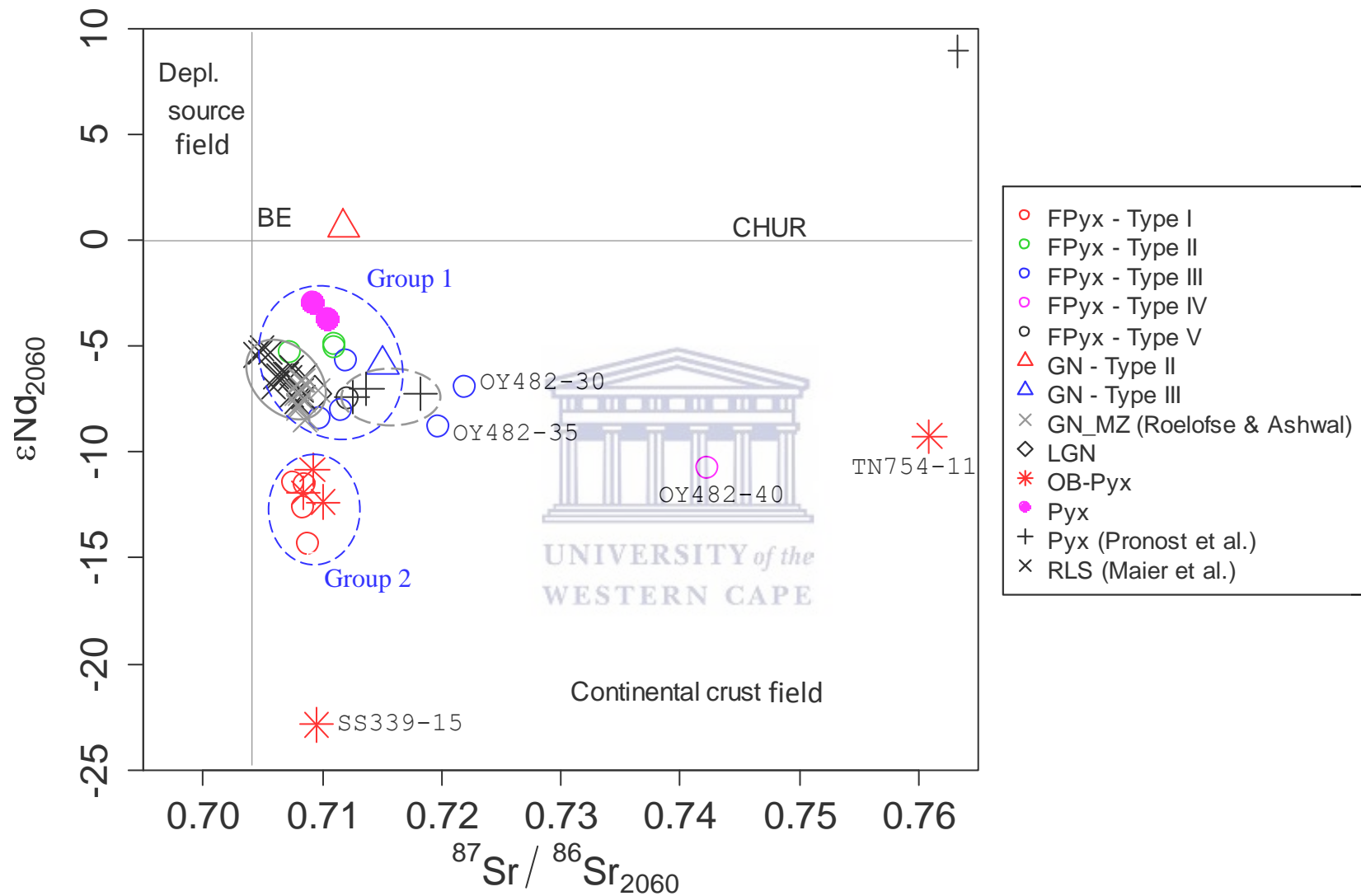
Figure 17: Plot of $^{87}Sr/^{86}Sr_{2060}$ versus εNd_{2060} for the Platreef and Main Zone samples (This study) and for the Platreef, LZ, CZ and MZ (Maier et al., 2000; Pronost et al., 2008; Roelofse and Ashwal, 2012). Chondrite Uniform Reservoir (CHUR) present day $^{143}Nd/^{144}Nd$ of 0.512638 (or $\varepsilon Nd= 0$) after Wasserburg et al. (1981). Bulk Earth (BE) present day $^{87}Sr/^{86}Sr$ of 0.7045 after Faure (1986). All isotopes are calculated at the nearest round-off age of 2060 Ma for the BIC (Buick et al., 2001; Yudovskaya et al., 2013b; Zeh et al., 2015). The isotopic groups (1 and 2) for the Platreef rocks are the same as in Figure 14. Closed grey circle: LZ, CZ and MZ roks of the BIC (Maier et al., 2000; Roelofse and Ashwal, 2012); Dashed grey circle: Platreef pyroxenites (Pronost et al., 2008). Legend abbreviation: FPyx: Feldspathic pyroxenite; GN: Gabbronorite; LGN: Leucogabbronorite; OB-Pyx: Olivine pyroxenite; Pyx: Pyroxenite. The error bars (top right corner) are ±2σ.

89

In their studies, Maier et al. (2000) showed a general decrease in εNd coupled with the increase in $^{87}Sr/^{86}Sr$ with height from the LZ and C_LZ to the C_UZ and MZ in the BIC (Fig. 3b). They suggested the Sr–Nd isotopic trends, which are associated with change in the composition of the rocks from the basal ultramafic portion to the upper gabbronoritic MZ, reflect both progressive differentiation and contamination as the result of the varying nature of the crustal materials assimilated by the BIC magmas (Maier et al., 2000).

The Platreef pyroxenites studied by Pronost et al. (2008), which show also clustering of the data points (Fig. 17), have also negative εNd (–7.4±0.2 to –7.0±0.2) in range with those of rocks from the C_UZ and MZ of the BIC (–8.5 to –6.4; Table 20). On the other hand, these pyroxenites have higher initial $^{87}Sr/^{86}Sr$ (0.712479±15 to 0.718256±22) than those from the LZ, CZ and MZ (0.704400 to 0.709671) reported by Maier et al. (2000) and Roelofse and Ashwal (2012) (Table 20; Fig. 17). In their studies, Pronost et al. (2008) suggested that the Platreef shares a common origin with the Merensky reef in the Eastern and Western Limbs of the Bushveld Complex, and its proximity to the country rocks has enhanced crustal contamination processes.

In this study, the Platreef olivine pyroxenite, pyroxenite and feldspathic pyroxenite also have negative εNd (–22.9±0.3 to –2.9±0.3; Table 19) as the rocks from the Platreef, LZ, CZ and MZ from previous studies (Maier et al., 2000; Pronost et al., 2008; Roelofse and Ashwal, 2012) (Table 20; Fig. 17). However, these rocks show scattering of their data points on the $^{87}Sr/^{86}Sr$ versus εNd plot (Fig. 17) relative to those of rocks from previous studies (Maier et al., 2000; Pronost et al., 2008; Roelofse and Ashwal, 2012).

Interestingly, some Platreef rocks of group 1 show some similarities with rocks from the LZ, CZ and MZ of the BIC. Platreef feldspathic pyroxenite Type II, III and V have εNd (–8.4±0.2 to –4.9±0.2; Table 19) in range with those of rocks from the LZ, CZ and MZ (– 8.5 to –5.1; Table 20) (Fig. 17). On the other side, most feldspathic pyroxenite samples (Type II, III and V) have $^{87}Sr/^{86}Sr$ values (0.709816±20 to 0.712106±12, excluding type II sample TN754-03 having 0.707281±20; Table 19) that are higher than those of rocks from the LZ, CZ and MZ (0.704800 to 0.709671; Table 20) (Fig. 17). The overlap in the

90

εNd values between the Platreef feldspathic pyroxenite Type II, III and the rocks from the LZ, CZ and MZ (Fig. 17) suggests there is a relationship between the Platreef magmas and the RLS magmas. The high $^{87}Sr/^{86}Sr$ for our Platreef feldspathic pyroxenites than the rocks of the LZ, CZ and MZ indicates the Platreef magmas were more contaminated than the RLS magmas during ascent, as previously suggested on the basis of the O, Sr and Os isotopes studies (Harris and Chaumba, 2001; Pronost et al., 2008; Reisberg et al., 2011; Yudovskaya et al., 2017b).

More interestingly, Platreef feldspathic pyroxenite Type II samples OY482-03, TN754-03 and TN754-08 have εNd (–5.3±0.2 to –4.9±0.2; Table 19) slightly close in range with those of rocks from the LZ and C_LZ of the Bushveld (–6.0 to –5.3; Table 20) (Fig. 17). Although the feldspathic pyroxenite Type III sample TN200-24 has also εNd (–5.7±0.2; Table 19) in range with those from the LZ and C_LZ (–6.0 to –5.3; Table 20), Type III samples (TN754-02 and TN754-06) have εNd (–8.4±0.2 to –8.0±0.2; Table 19) in range with those from the MZ (–8.5 to –6.3; Table 20) (Fig. 17). Instead, the Type V sample (TN200-16) has εNd (–7.4±0.2; Table 19) in range with those from the C_UZ and MZ (–8.5 to –6.3; Table 20) (Fig. 17). As a result of the variation in εNd for the Platreef feldspathic pyroxenites in group 1, it is suggested that the magmas which formed Types II and III (i.e. OY482-03, TN754-03, TN754-08 and TN200-24) share the same parental magma with those of the LZ and C_LZ; the Type V magma (TN200-16) shares the same parental magma with those of the C_UZ and MZ, whereas the Type III magma (TN754-02 and TN754-06) share the same parental magma with the MZ.

However, there are also feldspathic pyroxenite Type III samples (OY482-30 and OY482-35) which are not parts of group 1 (Fig. 17). They have εNd in range with rocks from the LZ, CZ and MZ, but also have the highest $^{87}Sr/^{86}Sr$ values (Fig. 17). Sample OY482-30 has εNd (–6.9±0.2; Table 19) in range with those from the C_UZ (–7.6 to –6.3; Table 20), and sample OY482-35 has εNd (–8.8±0.2; Table 19) that is slightly close with those from the MZ (–8.5 to –6.3; Table 20) suggesting their magmas share the same parental magma. Their high $^{87}Sr/^{86}Sr$ also indicates their magmas were also contaminated than the magmas of both the Platreef of group 1 and 2, and the RLS.

91

Surprisingly, the Platreef pyroxenites (i.e. SS339-09 and SS339-13) have higher εNd (−3.8±0.2 to −2.9±0.3; Table 19) than the feldspathic pyroxenites of group 1, pyroxenites studied by Pronost et al. (2008) and rocks from the LZ, CZ and MZ (Fig. 17) indicating a different source for their magmas, which will be discussed later. Despite having lower ^{87}Sr/^{86}Sr (0.709177±10 to 0.710492±12; Table 19) than the feldspathic pyroxenites of group 1 and pyroxenites (Pronost et al., 2008), which suggests their magmas were least contaminated, Platreef pyroxenites have higher ^{87}Sr/^{86}Sr than most LZ, CZ and MZ rocks (Fig. 17) confirming the Platreef magmas were contamined than the RLS magmas during ascent, as stated earlier.

More surprisingly, Platreef olivine pyroxenite and feldspathic pyroxenite Type I of group 2 have lower εNd values (−14.3±0.2 to −10.8±0.2; Table 19) than the Platreef rocks in group 1, the Platreef pyroxenites studied by Pronost et al. (2008) and (3) the rocks from the LZ, CZ and MZ (Fig. 17) also indicating different sources for their magmas, which will be discussed later. Most Platreef rocks of group 2 have lower ^{87}Sr/^{86}Sr values than most Platreef rocks in group 1 and pyroxenites from studies by Pronost et al. (2008) (Fig. 17) indicate their magmas are less contaminated than those of group 1. In contrast, the ^{87}Sr/^{86}Sr values for the Platreef rocks of group 2 (0.707545±11 to 0.710042±11; Table 19) are higher than those from rocks of the LZ and C_LZ, and most rocks from the C_UZ (Table 20) (Fig. 17) confirming furthermore that the Platreef magmas are contaminated than the RLS magmas. Yet, the ^{87}Sr/^{86}Sr values of the Platreef rocks of group 2 overlap with those from rocks of the MZ of the BIC (Tables 19 and 20) (Fig. 17) suggesting their magmas were equally contaminated.

Similarly, the olivine pyroxenite sample (SS339-15) has the lowest εNd (Fig. 17) indicating a different source for its magma relative to the RLS magmas. The fact that its ^{87}Sr/^{86}Sr (0.709493±22) overlaps with rocks of the Platreef group 2 (Fig. 17) indicates its magma was less contaminated than those of group 1, but more contaminated than the LZ, C_LZ and C_UZ magmas. Yet, its ^{87}Sr/^{86}Sr value suggests its magma was equally contaminated as the MZ magma. There are also Platreef olivine pyroxenite (TN754-11) and feldspathic pyroxenite Type IV (OY482-40) having lower εNd (−9.2±0.2 and −

10.8±0.2) and higher $^{87}Sr/^{86}Sr$ values than most rocks of the RLS (Fig. 17). This indicates their magmas derived from different sources and were contaminated than the magmas of both the Platreef of group 1 and 2, and the RLS.

In overall, the Sr–Nd isotopic composition of the Platreef rocks from the four drill cores shows that contamination played a significant role in the genesis of the Platreef. This may have occurred either in the sources or during magma ascent and differentiation or during magma emplacement.

In the following sub-chapter, this study will examine the possible contaminants that may have interacted with the Platreef magmas.

6.3 Contamination of the Platreef

6.3.1 Crustal versus floor rock contamination

Geochemical evidence for crustal and floor rock contamination of the Platreef magmas have been previous reported in several studies. While some studies have focused on the role that crustal contamination played during ore-forming processes (Sharman-Harris et al., 2005; Manyeruke et al., 2005; Holwell et al., 2007; Penniston-Dorland et al., 2008; Sharman et al., 2013; Smith et al., 2016), others studies (Cawthorn et al., 1985; Barton et al., 1986; Harris and Chaumba, 2001; Pronost et al., 2008; Ihlenfeld and Keays, 2011) have focused on issues related to bulk contamination of the Platreef magmas. It has been proposed that the Platreef was emplaced due to multiple magmatic injections (Kinnaird, 2005; Manyeruke et al., 2005; Yudovskaya and Kinnaird, 2010), and it is widely agreed that two episodes of contamination took place; i.e., one episode at depth by assimilation of wall rock materials (i.e., crustal contamination during ascent) and the other episode during emplacement through assimilation of the country rocks (floor rock contamination) (Ihlenfeld and Keays, 2011; Smith et al., 2016).

Although negative εNd values for mafic and ultramafic rocks of the RLS of the BIC have been interpreted as the result of crustal contamination (Maier et al., 2000), studies have

93

also suggested that the Sr isotope signature of the Platreef has been affected as a result of the interaction between its magmas and the floor rock, particularly where it is granite such as the floor rock at Overysel (Cawthorn et al., 1985; Barton et al., 1986).

The petrography has shown that the Platreef sills, from which the feldspathic pyroxenite Type III samples (OY482-30 and OY482-35) and olivine pyroxenite sample TN754-11 were taken, have orthopyroxene with interstitial quartz as the sill in direct contact with the Archaean granite floor rock (Feldspathic pyroxenite Type IV sample OY482-40; Plate 2e). The presence of quartz coupled with the high $^{87}Sr/^{86}Sr$ in these samples are indicative of assimilation of granite by the Platreef magmas interpreted as floor rock contamination in agreement with previous studies (Cawthorn et al., 1985; Barton et al., 1986; Holwell and McDonald, 2006). It should be noted that the quartz grains in the olivine pyroxenite sample TN754-11 is interpreted as having derived from later granitic intrusions (Fig. 5).

Pronost et al. (2008) reported geochemical data of the floor rock dolomite (TG03 – Rb: 2.4 ppm; Sr: 685 ppm; $^{87}Sr/^{86}Sr$ 0.70384±26) that show much lower $^{87}Sr/^{86}Sr$ value than any of the $^{87}Sr/^{86}Sr$ values for the BIC rocks reported in this study (Tables 19 and 20). On the basis of the stable isotope studies, Pronost et al. (2008) concluded that the Platreef magmas which have assimilated BIF/shale and/or dolomite materials from the floor rock would not have their $^{87}Sr/^{86}Sr$ affected as the magmas that assimilated granitic materials because BIF/shale and dolomite are Sr-poor rocks. Taking the above into account and our earlier interpretation that the high $^{87}Sr/^{86}Sr_{2060}$ values in samples OY482-30, OY482-35, OY482-40 and TN754-11 are due to floor rock contamination, this study can therefore concluded that the Sr isotopic compositions for the remaining Platreef rock samples are the results of crustal contamination.

From the variation in the isotopic compositions of the Platreef rocks (Fig. 17; excluding the samples affected due to floor rock interaction), crustal contamination of the Platreef magmas occurred either in the mantle sources or during magma ascent. The latter option is first examined since (1) this study has established there is a relationship between the Platreef magmas and the RLS magmas, and (2) previous studies (Maier et al., 2000;

94

Roelofse and Ashwal, 2012) have suggested that different crustal rocks of the Kaapvaal Craton (KC; De Wit et al., 1992) may have influenced the isotopic compositions of the BIC magmas. Some of the components of the KC are rocks from the Upper and Lower crust which have high and low radiogenic Sr, respectively (Hart et al., 1981; 1990). Other studies have also suggested that mixing of mantle-derived magma with Lower crust rocks produces magmas with high negative εNd and low ^{87}Sr/^{86}Sr (De Paolo and Wasserburg, 1979; Amelin et al., 1996; Jahn et al., 1999; Duan et al., 2016) whereas with Upper crust rocks produces magmas having low negative εNd and high ^{87}Sr/^{86}Sr (De Paolo and Wasserburg, 1979).

Studies have shown that mixing of two end-members produces a single hyperbolic trend on the εNd versus ^{87}Sr/^{86}Sr plot, which is marked by a decrease in εNd coupled with an increase in ^{87}Sr/^{86}Sr values (DePaolo and Wasserburg, 1979; Amelin and Semenov, 1996; Howarth and Prevec, 2013; Mao et al., 2016). Given the fact that a single hyperbolic trend cannot be roughly fitted through the Platreef samples (of group 1 and 2; Fig. 17), it is likely that the parental magma had mixed with crustal components of different Sr–Nd isotopic compositions, as suggested in other mafic intrusions (Chen et al., 2001; Geist et al., 1990).

On these bases, a quantitative isotopic model for crustal contamination of the Platreef that shows mixing between the parental magma and different crustal rocks of the KC, which host the BIC, is suggested in the following sub-chapter.

6.3.2   Isotopic modelling for crustal contamination

The bulk mixing model to explain the variation in the isotopic compositions of the Platreef rocks of group 2 and 3 is presented in Figure 18. This mixing approach was chosen because it is simple and does not yield unambiguous solutions. It focuses on the nature of the contaminants and the effect it has on the composition of the hybrid magma even if the results cannot be applied quantitatively, and the major elements composition

may not be reproduced (Maier et al., 2000). In the absence of Sr–Nd isotope data for the parental magma to the Platreef, the isotopic composition of the mantle-derived magma (MDM) for the BIC (Maier et al., 2000) was considered in the mixing model (Fig. 18).
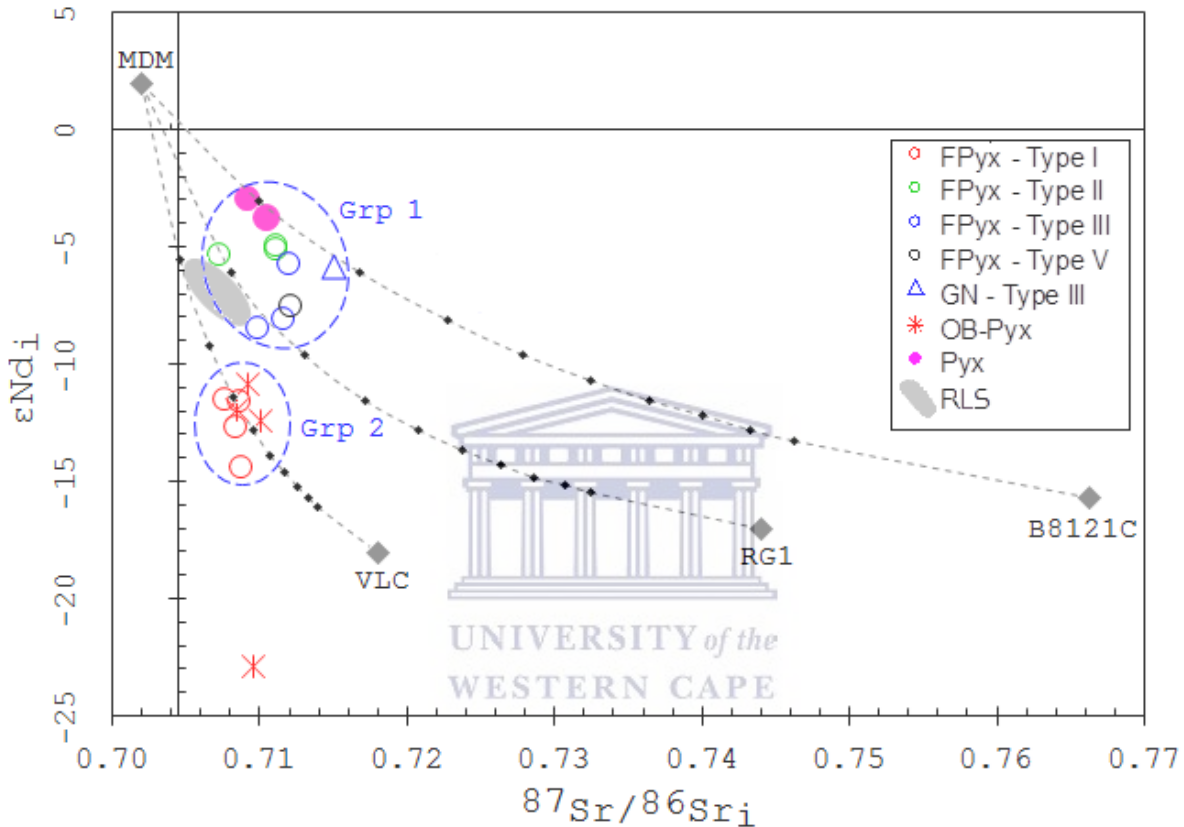
Figure 18: Sr–Nd isotopic mixing model for the Platreef rocks from the four drill cores. Samples affected by floor rock contamination (i.e. OY482-30, OY482-35, OY482-40 and TN754-11) are not included in the model. The mixing lines represent mixtures between Mantle-derived magma (MDM: Nd= 3.4 ppm; Sr = 52 ppm; $^{87}Sr/^{86}Sr$ = 0.702, εNd = +2; after Maier et al., 2000) and crustal contaminant rocks from the Kaapvaal Craton. The contaminant end-members are: (1) Granitoids from the Johannesburg dome – Sample B8121C: Nd= 25.5 ppm, Sr= 140 ppm, $^{87}Sr/^{86}Sr$= 0.766366, εNd= –15.7 (Barton et al., 1999); (2) Granitoids from the Vredefort dome – Sample RG1: Nd= 48.02 ppm, Sr= 167.3 ppm, $^{87}Sr/^{86}Sr$= 0.744045, εNd= –17 (Reimold et al., 2017); (3) Granitoids from the Vredefort Lower Crust – VLC: Nd= 39 ppm, Sr= 189 ppm, $^{87}Sr/^{86}Sr$= 0.718, εNd= – 18.7 (Maier et al., 2000). Tick marks on mixing lines give the weight % of crustal rocks in the mixture. The tick increments on the mixing lines are 5 %. The dashed circles show the Platreef groups as in Figures 14 and 15. Filled grey oval represents field for the RLS of the BIC. All isotopes were calculated at the nearest round-off age of 2.06 Ga for the BIC (Buick et al., 2001; Yudovskaya et al., 2013b; Zeh et al., 2015).

96

Table 21: Whole-rock Sr–Nd isotopic data compilation of granitoids from the Kaapvaal Craton

Block	Unit	Samples	$^{87}Sr/^{86}Sr$	$^{143}Nd/^{144}Nd$	$^{87}Sr/^{86}Sr_{2060}$	εNd_{2060}
	MB	96/201	n.a	0.510495	n.a	−13.1
	MB	96/233	n.a	0.510475	n.a	−13.5
	PB	96/239	n.a	0.510662	n.a	−11.4
	PB	96/247	n.a	0.510965	n.a	−8.7
	RK	96/210	n.a	0.510709	n.a	−11.0
	SB	96/228	n.a	0.510596	n.a	−13.0
Pietersburg	GH	B-79-26A	0.711600	0.510557	0.704264	−10.8
	TB	T1E	0.721350	0.510875	0.706879	−9.3
	TB	T-3	0.732970	0.510484	0.709258	−11.2
	TB	T-4	0.740820	0.510440	0.712361	−11.6
	TB	T-5	0.839650	0.510801	0.733496	−10.0
	TB	T-7	0.905070	0.512278	0.748002	−2.8
	TB	T-9	0.787710	0.510658	0.723714	−11.3
	TB	T-14	0.865910	0.510874	0.766387	−9.9
	Basement	Meta-granite	0.839558	0.511133	0.738816	−16.7
Witwatersrand	VD	RG1*	0.846587	0.510233	0.744045	−17.0
	VD	TMW39	0.772406	0.510827	0.721649	−12.9
	VD	TMW144	0.748179	0.510606	0.714267	−14.3
	VD	VPU20	0.718748	0.510058	0.707534	−17.5
	JD	B8121B	0.891800	0.510884	0.764581	−13.2
	JD	B8121C*	0.898900	0.510994	0.766366	−15.7
	JD	B8121G	0.892300	0.510905	0.762947	−13.3
	JD	B8121I	0.882300	0.510932	0.756951	−16.3
	JD	N130	0.772900	0.510864	0.723708	−13.1
	JD	HG114	0.709300	0.511015	0.704086	−11.2
	JD	HG117	0.716900	0.510942	0.706229	−12.1
	JD	HG118	0.708400	0.511028	0.705144	−12.0

MB: Murchison Belt; PB: Pietersburg Belt; RK: Rhenosterkoppies; SB: Sutherland Belt (Kreissig et al., 2000); GH: Goutplaats Hout gneiss suite (Barton et al., 1992); TB: Turfloop Batholith (Henderson et al., 2000); VD: Vredefort Dome (Reimold et al., 2017); JD: Johannesburg Dome (Barton et al., 1999). Meta-granite (Frimmel et al., 2009). All isotopes are calculated at 2.06 Ga. The asterix (*) denotes samples used in the isotope mixing model to reflect the isotopic composition of the crustal contaminants.

There are several radiogenic isotope studies conducted on Archaean granitoids from the KC (Walraven, 1989; Barton et al., 1992; De Wit et al., 1993; Brandl and Kröner, 1993; Poujol et al., 1996; Poujol and Robb, 1999; Poujol, 2001; Kreissig et al., 2000; Henderson et al., 2000; Kröner et al., 2000; Anhaeusser and Poujol, 2004; Zeh et al., 2009; 2013; Laurent et al., 2013, 2017; Vezinet et al., 2018), but only those with whole-rock Sr–Nd isotope data (Barton et al., 1992; Henderson et al., 2000) were considered in the mixing model for this study.

A compilation of whole-rock Sr–Nd isotope data for Archaean granitoids from the KC, calculated at 2.06 Ga, is presented in Table 21. For the isotope modelling, granitoids samples from the Johannesburg dome (i.e. B8121C; Barton et al., 1999), the Vredefort dome (RG1; Reimold et al., 2017 and reference therein) and the Vredefort Lower crust (VLC; Maier et al., 2000) were selected because their isotopic compositions reflect the best possible contaminants of the parental magma to the Platreef (Fig. 18).

The Sr–Nd isotope modelling is presented in Figure 18. The results show that the Platreef pyroxenites (i.e. SS339-09 and SS339-13) plot on the mixing line between the MDM and granitoids from the Johannesburg dome, whereas feldspathic pyroxenite samples Type II (OY482-03 and TN754-08) and III (TN200-24) plot close to the mixing line between the MDM and granitoids from the Johannesburg dome (Fig. 18). Instead, the feldspathic pyroxenite sample Type II (TN754-03) plots on the mixing line between the MDM and granitoids from the Vredefort dome, and the Type III samples (TN200-16, TN754-06 and TN754-02) plot in proximity to the mixing line between the MDM and granitoids from the Vredefort dome (Fig. 18). As a whole, these results can be interpreted as between 5 to 10 % of granitoid melts from the Vredefort dome or the Johannesburg dome are required to reproduce the isotopic composition of the Platreef rock samples of group 1 (Fig. 18).

On the other hand, most Platreef samples of group 2 plot close to and on the mixing line between the MDM and granitoids from the Vredefort Lower crust while two samples plot below the mixing line (Fig. 18). As a whole, the amount needed to reproduce the Sr–Nd isotopic composition of the Platreef rock samples of group 2 is between 15 to 20 % using granitoid melts from the Vredefort Lower crust (Fig. 18).

6.4   Source of the Platreef magmas

The Platreef rocks in the four studied drill cores (Figs. 5–8) have $^{87}Sr/^{86}Sr$ (0.707281±20 to 0.760885±41) and negative εNd (–22.9±0.3 to –2.9±0.3) values (Table 19) indicating their magmas were contaminated, as it has been suggested in many igneous intrusions (Amelin and Semenov, 1996; Casquet et al., 1998, 2001; Chen et al., 2001; Zhong et al., 2004; Howarth and Prevec, 2013; Duan et al., 2016). The high $^{87}Sr/^{86}Sr$ values for the bulk of the Platreef rocks relative to those from the LZ, CZ and MZ (Tables 19 and 20) suggests that the Platreef magmas are more contaminated than the RLS magmas, which is consistent with earlier studies (Harris and Chaumba, 2001; Pronost et al., 2008; Reisberg et al., 2011; Yudovskaya et al., 2017b; Grobler et al., 2018). In addition, the variation in the Sr–Nd isotopic compositions of the Platreef rocks in this study, when compared to the LZ, CZ and MZ rocks of the BIC, is remarkably striking. Not only the Platreef rocks data points are scattered than those of the RLS, which are close to one another, most rocks of group 1 can be related to the RLS, while those of group 2 cannot (Fig. 17).

Previous studies have shown that the Platreef magmas share some similarities with those that formed the LZ or the CZ (Yudovskaya et al., 2017a, 2017b; Gobler et al., 2018), the LZ or the MZ (McDonald et al., 2005), the CZ or the MZ (Kruger, 2005; Pronost et al., 2008; Reisberg et al., 2011) and the $C_U Z$ or the MZ (Maier et al., 2008). Our Nd isotope data are consistent with the Platreef having formed from magmas that are similar to those that formed the LZ, $C_L Z$, $C_U Z$ and MZ in agreement with previous researchers (Kruger, 2005; McDonald et al., 2005; Pronost et al., 2008; Maier et al., 2008; Reisberg et al., 2011; Yudovskaya et al., 2017a, 2017b; Gobler et al., 2018). On the basis of Os isotope data, Reisberg et al. (2011) suggested that a significant contribution of the LZ magmas into the genesis of the Platreef seemed unlikely, but also admitted that this possibility could not be ruled out until Os isotope data from the LZ are available. This study shows that the overlap in εNd values of some of the Platreef rocks in group 1 (Fig. 17) and those from the LZ (Tables 19 and 20) suggests there exists a relationship between the Platreef magmas and the LZ magmas.

On the basis of the major and trace elements, and the O, S, Os, Sr and Nd isotopes data, it has been established that contamination of the Platreef occurred before its emplacement (Harris and Chaumba, 2001: Holwell et al., 2007; McDonald and Holwell, 2007; Penniston-Dorland et al., 2008; Reisberg et al., 2011; Ihlenfeld and Keays, 2011; Smith et al., 2016) and due to the interaction with the floor rock (Cawthorn et al., 1985; Barton et al., 1986; Harris and Chaumba, 2001; Sharman-Harris et al., 2005; Manyeruke et al., 2005; Holwell et al., 2007; Penniston-Dorland et al., 2008; Pronost et al., 2008; Ihlenfeld and Keays, 2011; Sharman et al., 2013; Smith et al., 2016). Our data are consistent with the contamination of the Platreef by the Archaean granite as the floor rock and by crustal rocks prior its emplacement, as argued earlier.

However, this study has shown that floor rock contamination did not significantly affect the bulk of the Sr–Nd isopotic composition of the Platreef rocks. It is therefore believed that contamination prior emplacement is considered as the possible cause of the Sr–Nd isotopic compositions of the Platreef rocks of group 1 and 2 (Fig. 17). Figure 18 shows the mixing curves of a mantle-derived magma that has been subjected to contamination by three different crustal contaminants of the KC. To change the Nd isotopic composition of a mantle-derived magma from εNd of +2 to –2.9±0.3 to –8.4±0.2, it requires an assimilation of 5 – 10 wt. % of the Vredefort or Johannesburg granitoid melts.

Such amount of assimilation is reasonable as it would not affect much of the major and trace elements composition of the magma. This is also in agreement with the Sr isotopic compositions of the RLS which required a less radiogenic Sr contaminant. However, in order to change the Nd isotopic composition of a mantle-derived magma from εNd of +2 to –10.8±0.2 to –14.3±0.2, it requires an assimilation of 15 – 20 wt. % of the Vredefort Lower crust. Such amount of assimilation would modify to some extend the major and trace elements composition of the magmas and, thus, would not suffice to explain the lower contents of trace elements for feldspathic pyroxenite Type I than Type II, III and IV (Figs. 12a, b, d and e). Also, this amount would not explain the highly negative εNd of feldspathic pyroxenite Type I (Fig. 17). Furthermore, this is also not in agreement with the Sr isotopic compositions of the RLS which would then required more radiogenic Sr contaminants.

100

The low negative εNd values for the Platreef pyroxenites in this study than the LZ and $C_L Z$ rocks of the BIC (Fig. 17) suggest their mantle-derived magmas were more primitive than the B1 magma of the BIC. To this day, no other studies have reported the occurrence of magmas that are more primitive than the B1 magma in the Northern Limb since it was reported in the Eastern and Western Limbs of the BIC (Wilson, 2015; Maier et al., 2016). Therefore, this study believes that such mantle-derived magmas ascended via different conduit systems than those that produced the RLS magmas and interacted with different crustal rocks (highly radiogenic in Sr) to have acquired such high $^{87}Sr/^{86}Sr$ values. It is also not possible to determine whether a relationship exists between the more primitive magma in the Northern Limb (in this study) and those from the Eastern and Western Limbs of the BIC (Wilson, 2015; Maier et al., 2016) due to the lack of Sr–Nd isotope data for the BUS. The magmas that produced the feldspathic pyroxenites of group 1 on the other hand ascended to form the RLS rocks on one side and the Platreef rocks on the other side after having also interacted with highly radiogenic Sr crustal rocks to explain for their high $^{87}Sr/^{86}Sr$ values. This is consistent with the suggestion that the Platreef and the CZ magmas were the same and originated from melts of the LZ komatiitic lineage (Yudovskaya et al., 2017b).
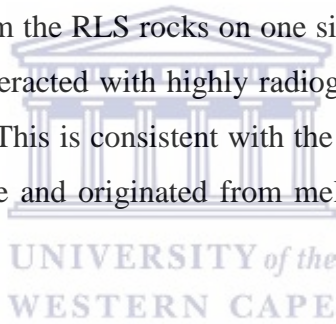
The highly negative εNd values for the Platreef rocks of group 2 (Table 19) indicate their magmas were either contaminated from the mantle source or derived from an enriched mantle source, as suggested in other igneous intrusions (Amelin et al., 1996; Jahn et al., 1999; Chen et al., 2001; Li et al., 2006; Zhang et al., 2011; Xu et al., 2017).

On the PMN trace elements diagrams (Figs. 11e and 12e), the Platreef rocks of group 2 (i.e. olivine pyroxenite and feldspathic pyroxenite Type I samples) have distinctive negative anomalies in Nb, P and Ti, and positive Pb anomalies. Previous studies have shown that negative Nb and Ta anomalies are most characteristic of subduction zone volcanic rocks or typical continental crust (Jahn et al., 1999; Li et al., 2006; Zhang et al., 2011). The Platreef rocks of group 2 are enriched in the LILE (e.g. Cs, Rb, Ba and Sr) relative to the HFSE (Nb, Ta, Zr and Ti) (Figs. 11e and 12e) suggesting they have higher LILE/HFSE values than the primitive mantle.
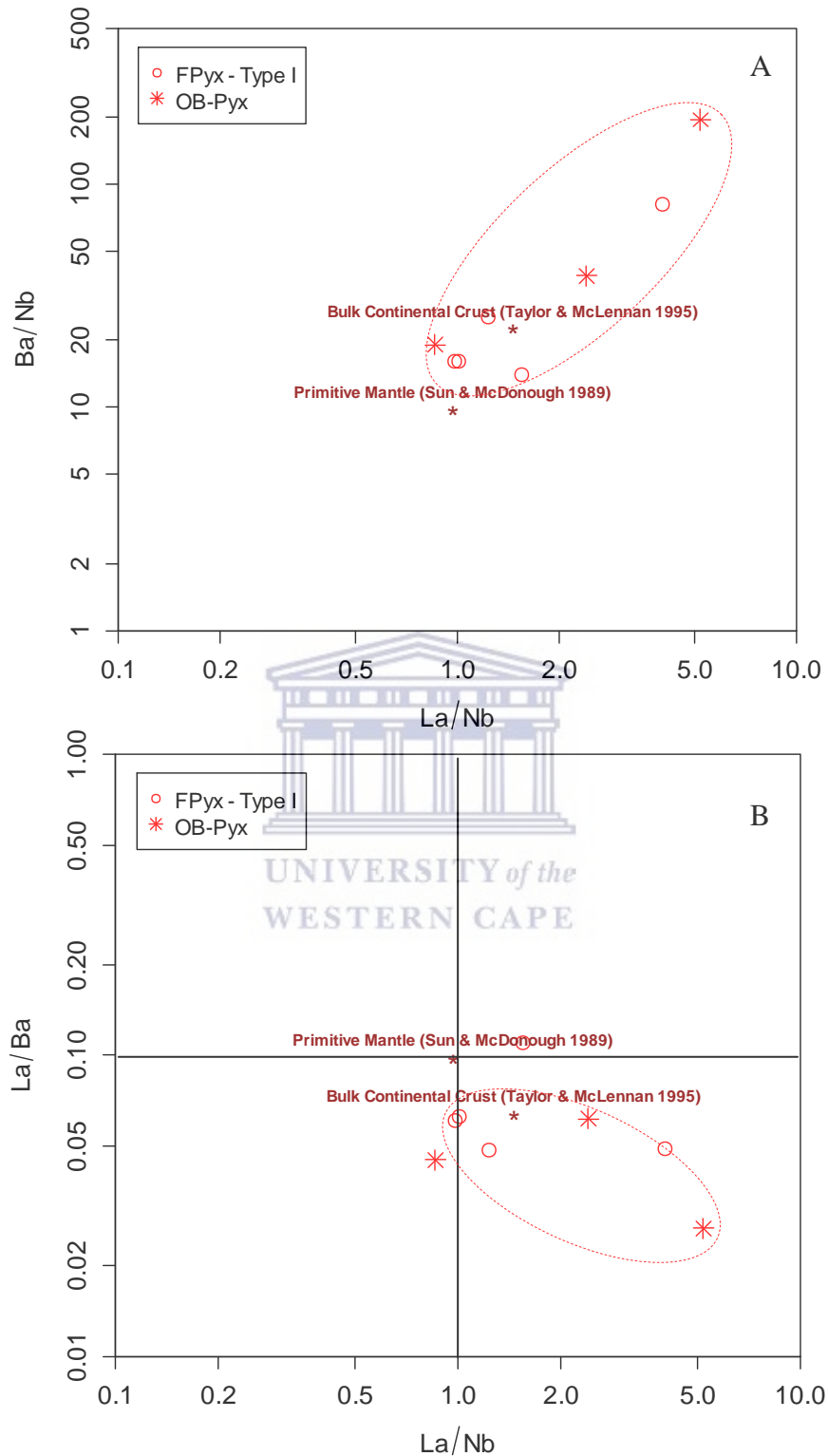
Figure 19: Plots of A) La/Nb versus Ba/Nb and B) La/Nb versus La/Ba for the Platreef rocks of group 2. Data source of the Primitive mantle (Sun and McDonough, 1989) and Bulk Continental Crust (Taylor and McLennan, 1995) are also plotted for comparison purposes.
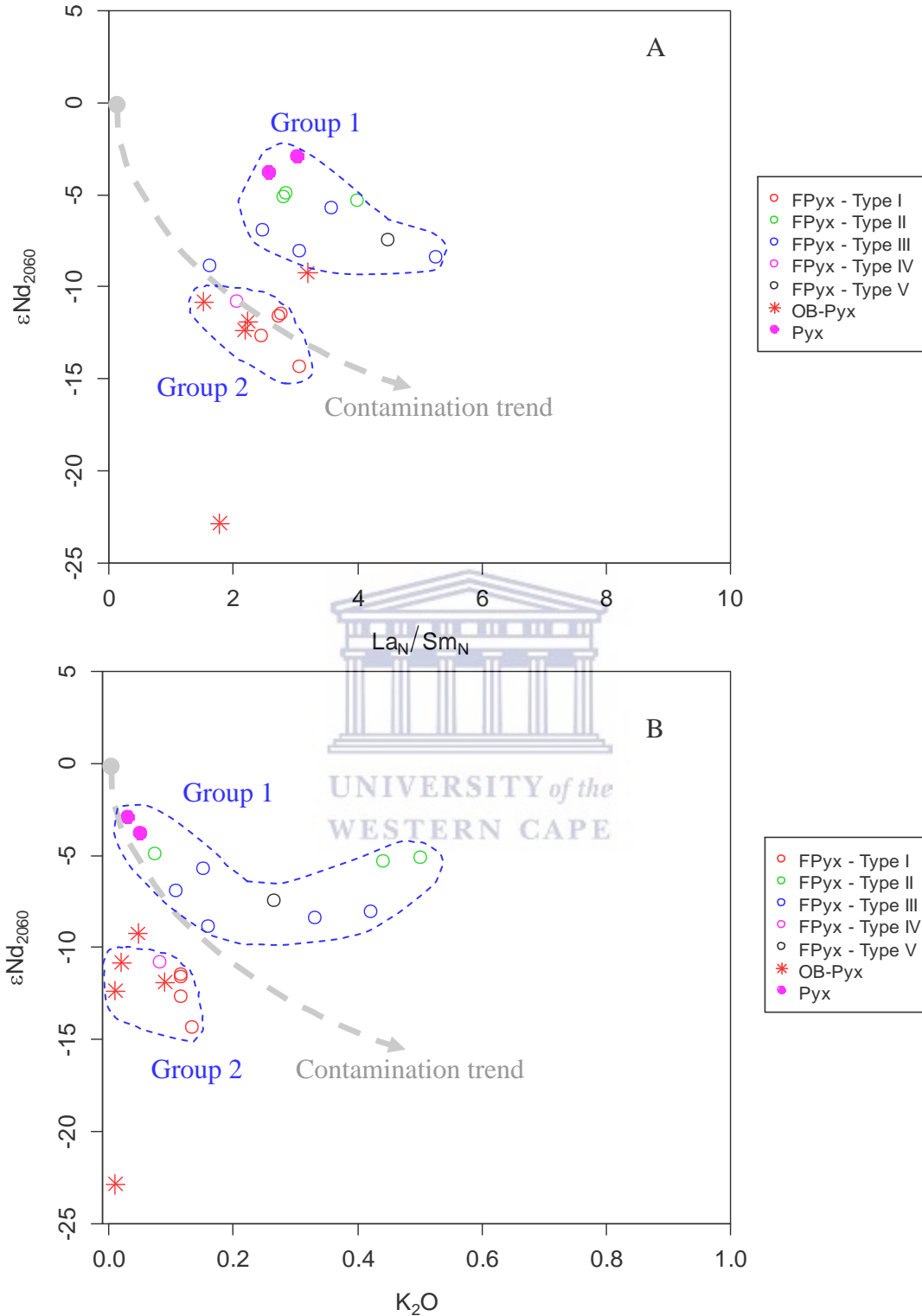
Figure 20: Plots of εNd$_{2060}$ versus La$_N$/Sm$_N$ (in A) and K$_2$O (in B) for the Platreef rocks in this study. The εNd are calculated at 2060 Ma for the BIC (Buick et al., 2001; Yudovskaya et al., 2013b; Zeh et al., 2015). The isotopic groups (1 and 2) for the Platreef rocks are the same as in Figure 14. Legend abbreviation: FPyx: Feldspathic pyroxenite; OB-Pyx: Olivine pyroxenite; Pyx: Pyroxenite.

103

In addition, these Platreef rocks are enriched in LREE and have low HREE contents which could also indicate addition of crustal material or subduction-related fluids (Zhang et al., 2011). In Figure 19a, some Platreef samples have La/Nb and Ba/Nb ratios that are higher than the bulk continental crust, but other samples have ratios that are intermediate between the primitive mantle and the bulk continental crust suggesting they probably derived from a mantle source strongly modified by hydrous fluids rather than crustal materials and/or sediments (Zhang et al., 2011). In addition, the Platreef rocks of group 2 have lower La/Ba values (<0.1) than the primitive mantle, but also high La/Nb values (>1) (Fig. 19b) that are characteristics of slab-metasomatized sub-continental lithospheric mantle (Jahn et al., 1999; Zhang et al., 2011).

Studies have shown that crustal contamination in mafic/ultramafic magmas (1) decreases the εNd values while increasing the La/Sm ratios and K_2O contents at the same time (Li et al., 2006; Xu et al., 2017). Figure 20 (a and b) shows there is a decrease in the εNd values from most of the Platreef rocks of group 1 to those of group 2 with decreasing La/Sm ratios and K_2O contents, not consistent with the interaction between the mantle-derived magmas and the crust-derived felsic melts (Xu et al., 2017). In addition, the TiO_2, P_2O_5, Nb, Ti, Zr, Th and U contents decrease with decreasing εNd values from rocks of group 1 to those of group 2 (Figs. 22 – 27 in Appendix E). Since the continental crust is typically low in Ti, and P, and depleted in Nb, it seems unlikely that the Platreef magmas of rocks of group 2 were contaminated from the mantle source.

Therefore, this study suggests that the highly negative εNd values, low $^{87}Sr/^{86}Sr$ and trace elements (i.e. LILE and LREE) signature of the Platreef magmas that produced the rocks of group 2 reflect the enrichment of the mantle source as a result of partial melting of an enriched subcontinental lithospheric mantle (SCLM) metasomatized by subduction-slab-released fluids since subduction events played major roles during terrane accretion of the KC (Zeh et al., 2013). This is consistent with previous studies (Zirakparvar et al., 2014; Zeh et al., 2015) which suggest the involvement of the SCLM in the genesis of the RLS magmas in the Eastern and Western Limbs of the Bushveld based on Hf and U-Pb isotope

data. It is also worth mentioning that no other studies have reported the involvement of an enriched mantle source in the genesis of the Platreef.

However, this study suggests that the variation in the isotopic compositions between the Platreef of group 2 and those of the RLS (Fig. 17) is possibly due to the heterogeneity of the SCLM (which is made up of depleted mantle rocks, abundant eclogites and domains enriched by subduction zone; Zeh et al., 2015). This study further suggests that such enriched magmas ascended using different conduit systems than those that produced the magmas of the Platreef pyroxenite and feldspathic pyroxenite of group 1. The latter were derived from magmas that share a common source with the magmas that produced the RLS rocks.

In summary, this study concludes that the Platreef magmas were derived from the partial melting of heterogeneous mantle source comprising depleted mantle melts (DMM) and both metasomatized SCLM slightly unradiogenic Nd enriched melts (Slightly-Nd UEM) and highly unradiogenic Nd enriched melts (highly-Nd UEM).
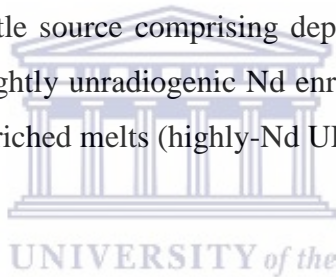
6.5   Mineralisation in the Platreef

In terms of the PGE and BMS mineralisation in the Platreef, there is a general consensus that these are magmatic in origin (Pronost et al., 2008). However, crustal contamination is said to have played an important role in the ore-forming process based on previous S isotope studies. The latter have suggested that sulphide saturation occurred at depth in the chamber and during emplacement through assimilation of the floor rock materials into the Platreef (Sharman-Harris et al., 2005; Manyeruke et al., 2005; Holwell et al., 2007; Penniston-Dorland et al., 2008; Sharman et al., 2013; Smith et al., 2016).

Strontium and Nd are lithophile elements, and because of this, they will not be partitioned into any immiscible sulphide in a magma that has reached sulphide saturation (Sproule et al., 2002). Therefore, this study can only examine the relationship between the PGE and BMS contents and the Platreef rocks (Table 18).

105

Table 22: Downhole contents of SO₃, BMS elements (Cu and Ni), Au, Pt and Pt in the Platreef rocks from the four drill cores. The contents of SO₃ is expressed in wt. %, and those of Cu, Ni, Au, Pd and Pt are in ppm.

Sample	Depth (m)	Rock type	Group	SO_3	Cu	Ni	Au	Pd	Pt
OY482-03	284.85	FPyx-II	1	0.12	394	780	0.08	0.93	0.46
OY482-30	415.72	FPyx-III	1?	0.38	967	1206	-	-	-
OY482-35	426.95	FPyx-III	1?	0.51	2769	2246	-	-	-
OY482-40	459.81	FPyx-IV	2?	0.46	2102	4136	0.05	0.03	0.03
SS339-08	60.72	OB-Pyx	2	1.04	3380	4859	0.24	1.93	1.62
SS339-09	61.93	Pyx	1	0.41	942	2540	-	-	-
SS339-12	73.15	OB-Pyx	2	0.62	2664	6034	-	-	-
SS339-13	82.24	Pyx	1	0.11	422	1066	-	-	-
SS339-15	99.36	OB-Pyx	?	0.71	1256	2070	0.07	0.95	0.81
SS339-19	131.07	OB-Pyx	2	0.43	497	871	0.20	1.53	1.30
TN200-03	230.77	FPyx-I	2	1.01	1143	2942	-	-	-
TN200-04	235.2	Fpyx-I	2	0.49	695	1785	-	-	-
TN200-05	235.95	Fpyx-I	2	0.58	581	1443	-	-	-
TN200-08	249.17	Fpyx-I	2	0.93	300	986	-	-	-
TN200-09	254.87	Fpyx-I	2	0.51	345	1599	-	-	-
TN200-16	278.02	FPyx-V	1	1.19	875	1943	-	-	-
TN200-24	303.8	FPyx-III	1	0.50	375	1030	0.05	0.20	0.12
TN754-02	223.34	FPyx-III	1	1.23	1870	6650	-	-	-
TN754-03	231.17	FPyx-II	1	0.08	213	738	0.05	0.03	0.08
TN754-06	264	FPyx-III	1	0.53	1195	2117	-	-	-
TN754-08	279.85	FPyx-II	1	0.31	620	942	0.05	0.35	0.43
TN754-11	321.74	OB-Pyx	2?	1.27	275	1666	-	-	-

<u>Note</u>: FPyx: feldspathic pyroxenite; OB-Pyx: olivine-bearing pyroxenite; Pyx: pyroxenite. "-": Not analysed.

The data in this study (Table 22) show that high BMS contents in the Platreef rocks do not always correlate with high PGE contents and vice versa, as earlier suggested (Gain and Mostert, 1982; Armitage et al., 2002; Kinnaird et al., 2005; Hutchinson and Kinnaird, 2005; Holwell and McDonald, 2006; Holwell et al., 2007; Hutchinson and McDonald, 2008; Mitchell and Scoon, 2012).

In addition, Table 22 shows that the upper most Platreef sills (away from the floor rock) in drill cores TN754, TN200 and SS339 have the highest Cu contents. However in drill core OY482, there are high Cu contents in the Platreef sill above the floor rock (OY482-40 has Cu of 2102 ppm; Table 22). Furthermore, feldspathic pyroxenite Type III samples from the Upper and Lower Platreef in TN754 have the highest Cu contents (1870 ppm Cu for TN754-02; 1195 ppm Cu for TN754-06) (Table 22).

On the basis of these observations, this study speculates that sulphide saturation was not reached through assimilation of the floor rock during the emplacement of the Platreef, but instead at depth as previously noted (McDonald and Holwell, 2007; Ihlenfeld and Keays, 2011; Smith et al., 2016). This study further speculates that (1) the Platreef magmas were subjected to varying sulphide saturation processes at depth and (2) the varying contents of the PGE in the rocks (Table 22) reflect the heterogeneous nature of the source for these magmas and/or the fertility of each magma as suggested in previous studies (McDonald and Holwell, 2007; McDonald et al., 2009).
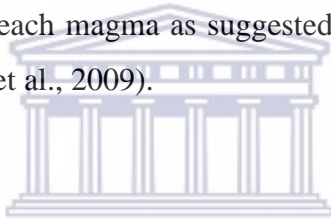
6.6 Model for the genesis of the Platreef

On the basis of the isotopic study, a model for the genesis of the Platreef is proposed in three principal steps (Fig. 21). In step one, this study suggests that the parental magmas to the Platreef were derived from depleted mantle melts (DMM) and metasomatized slightly and highly unradiogenic Nd enriched melts (slightly-Nd and highly-Nd UEM) from the SCLM (Fig. 21) (Richardson and Shirey, 2008; Zirakparvar et al., 2014; Zeh et al., 2015).

In step two, these parental magmas ascended via the continental crust using different paths (Fig. 21). Parental magmas which derived from the DMM most likely assimilated less amount of radiogenic Sr crustal rocks into the staging chambers resulting into the formation of hybrid magmas (HM-I; Fig. 21) having the Sr–Nd isotopic compositions of pyroxenite (Table 19; Fig. 18). The slightly-Nd UEM parental magmas have most likely assimilated a slightly high amount of radiogenic Sr crustal rocks into staging chambers which resulted into the formation of hybrid magmas (HM-II; Fig. 21).
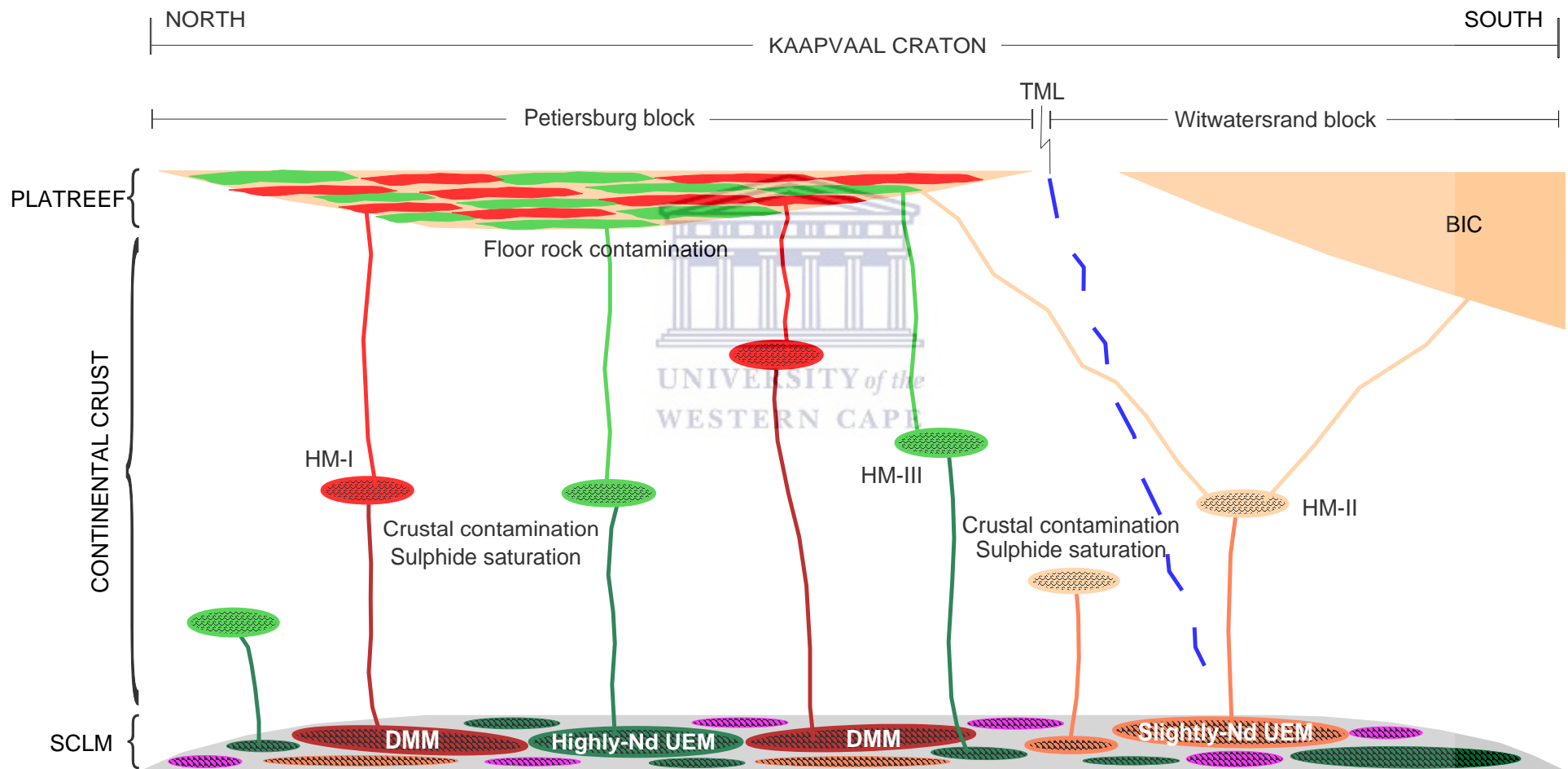
Figure 21: Simplified model for the genesis of the Platreef. Stage 1 – Formation of the parental magmas to the Platreef as a result of the partial melting of depleted mantle rocks (producing depleted mantle melts "DMM") and unradiogenic Nd enriched domains (producing highly-Nd and slightly-Nd enriched melts "UEM") from the subcontinental lithopsheric mantle (SCLM) underneath the Kaapvaal Craton. Stage 2 – Ascent of parental magmas through the continental crust and formation of the Platreef hybrid magmas (HM-I, HM-II and HM-III). Stage 3 – Injection and emplacement of the Platreef hybrid magmas into the country rock of the Northern limb of the Bushveld Igneous Complex (BIC). TML: Thabazimbi-Murchison Lineament.

This HM-II (Fig. 21) has produced the Platreef rocks of group 1 which have inherited its isotopic compositions (Table 19; Fig. 18). In this case, the parental magmas for LZ, CZ and MZ of the RLS that originated from unradiogenic enriched melts (Richardson and Shirey, 2008; Zirakparvar et al., 2014; Zeh et al., 2015) must have had interacted with crustal rocks that were less radiogenic in Sr than the parental magmas of the Platreef rocks of group 1 considering the difference in their Sr isotopic compositions (Fig. 18) and the variation in the Sr–Nd isotopic composition of crustal rocks of the KC (Table 21).

On the other side, the parental magmas which derived from highly-Nd UEM have most likely assimilated crustal rocks that were less radiogenic in Sr, as those assimilated by the parental magmas for LZ, CZ and MZ of the RLS, considering the overlapping in their Sr isotopic compositions (Fig. 18). Such interactions produced hybrid magmas (HM-III) into staging chambers that are different from those in which the parental magmas derived from slightly-Nd UEM interacted with the crust (Fig. 21).

During the interaction with crustal rocks of the KC in the staging chambers, the Platreef hybrid magmas (HM-I, HM-II and HM-III) were subjected to varying degree of sulphide saturation processes (Fig. 21).

In step three, the Platreef hybrid magmas (HM-I, HM-II and HM-III) ascended and were emplaced into the Northern limb of the BIC (Fig. 21) as a result of the multiple magmatic injections (Kinnaird, 2005; Manyeruke et al., 2005; Yudovskaya and Kinnaird, 2010; Mitchell and Scoon, 2012). During emplacement, the assimilation of Archaean granite into the Platreef magmas (Floor rock contamination; Fig. 21) took place and resulted in some feldspathic pyroxenite samples from Overysel having anomalously high initial Sr ratio values (Table 19; Fig. 18). The sequence of intrusion of the hybrid magmas to form the Platreef was not sequential (Fig. 21) considering the rock succession in the four drill cores of interest (Figs. 5 – 8). Furthermore, the variation in the styles of the PGE and BMS mineralisation with depth and along strike reflect the heterogeneous nature of the source of the Platreef magmas.

7 CONCLUSIONS & RECOMMENDATIONS

7.1 Conclusions

On the basis of the Sr–Nd isotope data obtained from the Platreef rocks from the four drill cores, the following can be concluded:

1. The bulk of the Platreef rocks in the four drill cores are not genetically related to rocks from the LZ, CZ and MZ of the RLS in the Eastern and Western Limbs of the BIC.

2. The Platreef magmas were derived from partial melting of a heterogeneous mantle source comprising depleted mantle melts and metasomatized slightly and highly unradiogenic Nd enriched melts.

3. The varying styles of the PGE and BMS mineralisation in the Platreef rocks are possibly due to the heterogeneous nature of the source of the magmas which were subjected to varying saturation processes at depth.

In conclusion, the genesis of the Platreef is much more complex and should be considered very much independent from processes involved in the genesis of the RLS in the Eastern and Western Limbs of BIC, as earlier suggestions (McDonald et al., 2005).

7.2 Recommendations

This study brought new evidence which contribute to our understanding on the magmas sources and processes involved in the genesis of the Platreef using four drill cores arrayed along 30 km of strike length. It is therefore recommended that further research be done to establish the extent of the processes involved in the genesis of the Platreef.

8 REFERENCES

A

Amelin, Y.V., Neymark, L.A., Ritsk, E.Y., Nemchin, A.A., 1996, "Enriched Nd–Sr–Pb isotopic signatures in the Dovyren layered intrusion eastern Siberia, Russia: evidence for source contamination by ancient upper-crustal material", *Chemical Geology,* vol. 129, pp. 39–69.

Amelin, Y.V. & Semenov, V.S. 1996, "Nd and Sr isotopic geochemistry of mafic layered intrusions in the eastern Baltic shield: implications for the evolution of Paleoproterozoic continental mafic magmas", *Contributions to Mineralogy and Petrology,* vol. 124, no. 3, pp. 255-272.

Anhaeusser, C. & Poujol, M. 2004, "Petrological, geochemical and U-Pb isotopic studies of Archaean granitoid rocks of the Makoppa Dome, northwest Limpopo Province, South Africa", *South African Journal of Geology,* vol. 107, no. 4, pp. 521-544.

Armitage, P., McDonald, I., Edwards, S. & Manby, G. 2002, "Platinum-group element mineralization in the Platreef and calc-silicate footwall at Sandsloot, Potgietersrus District, South Africa", *Applied Earth Science: Transactions of the Institutions of Mining and Metallurgy: Section B,* vol. 111, no. 1, pp. 36-45.

Ashwal, L.D., Webb, S.J. & Knoper, M.W. 2005, "Magmatic stratigraphy in the Bushveld Northern Lobe: continuous geophysical and mineralogical data from the 2950 m Bellevue drillcore", *South African Journal of Geology,* vol. 108, no. 2, pp. 199-232.

B

Barton Jr, J., Doig, R., Smith, C., Bohlender, F. & Van Reenen, D. 1992, "Isotopic and REE characteristics of the intrusive charnoenderbite and enderbite geographically associated with the Matok Pluton, Limpopo Belt, southern Africa", *Precambrian Research,* vol. 55, no. 1-4, pp. 451-467.

Barton, J., Barton, E. & Kröner, A. 1999, "Age and isotopic evidence for the origin of the Archaean granitoid intrusives of the Johannesburg Dome, South Africa", *Journal of African Earth Sciences,* vol. 28, no. 3, pp. 693-702.

Barton, J., Cawthorn, R.G. & White, J. 1986, "The role of contamination in the evolution of the Platreef of the Bushveld Complex", *Economic Geology,* vol. 81, no. 5, pp. 1096-1104.

Begemann, F., Ludwig, K., Lugmair, G., Min, K., Nyquist, L., Patchett, P., Renne, P., Shih, C., Villa, I.M. & Walker, R. 2001, "Call for an improved set of decay constants for geochronological use", *Geochimica et Cosmochimica Acta,* vol. 65, no. 1, pp. 111-121.

Begg, G., Griffin, W., Natapov, L., O'Reilly, S.Y., Grand, S., O'Neill, C., Hronsky, J., Djomani, Y.P., Swain, C. & Deen, T. 2009, "The lithospheric architecture of Africa: Seismic tomography, mantle petrology, and tectonic evolution", *Geosphere,* vol. 5, no. 1, pp. 23-50.

Brandl, G. & Kröner, A. 1993, "Preliminary results of single zircon studies from various Archaean rocks of the Northeastern Transvaal", *Ext. Abstr. 16th International Colloquium of African Geology, Mb, Swaziland*, pp. 54.

Buchanan, D. 1975, "The petrography of the Bushveld Complex intersected by boreholes in the Bethal area", *Trans Geol Soc S Afr,* vol. 78, pp. 335-348.

Buick, I.S., Maas, R. & Gibson, R. 2001, "Precise U–Pb titanite age constraints on the emplacement of the Bushveld Complex, South Africa", *Journal of the Geological Society,* vol. 158, no. 1, pp. 3-6.

C

Casquet, C., Eguiluz, L., Galindo, C., Tornos, F. & Velasco, F. 1998, "The Aguablanca Cu–Ni (PGE) intraplutonic ore deposit (Extremadura, Spain). Isotope (Sr, Nd, S) constraints on the source and evolution of magmas and sulfides", *Geogaceta,* vol. 24, pp. 71-74.

Casquet, C., Galindo, C., Tornos, F., Velasco, F. & Canales, A. 2001, "The Aguablanca Cu–Ni ore deposit (Extremadura, Spain), a case of synorogenic orthomagmatic mineralization: age and isotope composition of magmas (Sr, Nd) and ore (S)", *Ore Geology Reviews,* vol. 18, no. 3-4, pp. 237-250.

Cawthorn, R.G., Barton, J. & Viljoen, M.J. 1985, "Interaction of floor rocks with the Platreef on Overysel, Potgietersrus, northern Transvaal", *Economic Geology,* vol. 80, no. 4, pp. 988-1006.

Cawthorn, R.G. & Walraven, F. 1998, "Emplacement and crystallization time for the Bushveld Complex", *Journal of Petrology,* vol. 39, no. 9, pp. 1669-1687.

Cawthorn, R., Cooper, G. & Webb, S. 1998, "Connectivity between the western and eastern limbs of the Bushveld Complex", *South African Journal of Geology,* vol. 101, no. 4, pp. 291-298.

Chen, J., Yan, J., Xie, Z., Xu, X. & Xing, F. 2001, "Nd and Sr isotopic compositions of igneous rocks from the Lower Yangtze region in eastern China: constraints on sources", *Physics and Chemistry of the Earth, Part A: Solid Earth and Geodesy,* vol. 26, no. 9-10, pp. 719-731.

Chung, S., Cheng, H., Jahn, B., O'Reilly, S.Y. & Zhu, B. 1997, "Major and trace element, and Sr-Nd isotope constraints on the origin of Paleogene volcanism in South China prior to the South China Sea opening", *Lithos,* vol. 40, no. 2, pp. 203-220.

D

De Wit, M.J., Armstrong, R.A., Kamo, S.L. & Erlank, A.J. 1993, "Gold-bearing sediments in the Pietersburg greenstone belt; age equivalents of the Witwatersrand Supergroup sediments, South Africa", *Economic geology,* vol. 88, no. 5, pp. 1242-1252.

De Wit, M.J., de Ronde, C.E., Tredoux, M., Roering, C., Hart, R.J., Armstrong, R.A., Green, R.W., Peberdy, E. & Hart, R.A. 1992, "Formation of an Archaean continent", *Nature,* vol. 357, no. 6379, pp. 553-562.

DePaolo, D. & Wasserburg, G. 1979, "Petrogenetic mixing models and Nd-Sr isotopic patterns", *Geochimica et Cosmochimica Acta,* vol. 43, no. 4, pp. 615-627.

Duan, J., Li, C., Qian, Z., Jiao, J., Ripley, E.M. & Feng, Y. 2016, "Multiple S isotopes, zircon Hf isotopes, whole-rock Sr-Nd isotopes, and spatial variations of PGE tenors in the Jinchuan Ni-Cu-PGE deposit, NW China", *Mineralium Deposita,* vol. 51, no. 4, pp. 557-574.

E

Eales, H., Botha, W., Hattingh, P., De Klerk, W., Maier, W. & Odgers, A. 1993, "The mafic rocks of the Bushveld Complex: a review of emplacement and crystallization history, and mineralization, in the light of recent data", *Journal of African Earth Sciences (and the Middle East),* vol. 16, no. 1, pp. 121-142.

Eales, H. & Cawthorn, R. 1996, "The Bushveld Complex", *Developments in Petrology,* vol. 15, pp. 181-229.

Eales, H., De Klerk, W. & Teigler, B. 1990, "Evidence for magma mixing processes within the Critical and Lower Zones of the northwestern Bushveld Complex, South Africa", *Chemical Geology,* vol. 88, no. 3-4, pp. 261-278.

Eglington, B. & Armstrong, R. 2004, "The Kaapvaal Craton and adjacent orogens, southern Africa: a geochronological database and overview of the geological development of the craton", *South African Journal of Geology,* vol. 107, no. 1-2, pp. 13-32.

F

Faure, G. 1986, Principles of isotope Geology, 2nd edition. John Wiley & Sons. New York.

Frimmel, H., Zeh, A., Lehrmann, B., Hallbauer, D. & Frank, W. 2009, "Geochemical and geochronological constraints on the nature of the immediate basement next to the Mesoarchaean auriferous Witwatersrand Basin, South Africa", *Journal of Petrology,* vol. 50, no. 12, pp. 2187-2220.

G

Gain, S.B. & Mostert, A. 1982, "The geological setting of the platinoid and base metal sulfide mineralization in the Platreef of the Bushveld Complex in Drenthe, north of Potgietersrus", *Economic Geology,* vol. 77, no. 6, pp. 1395-1404.

Geist, D.J., Frost, C.D. & Kolker, A. 1990, "Sr and Nd isotopic constraints on the origin of the Laramie anorthosite complex, Wyoming", *American Mineralogist,* vol. 75, no. 1-2, pp. 13-20.

Grobler, D.F., Brits, J.A.N., Maier, W.D., & Crossingham, A. 2018, "Litho- and chemostratigraphy of the Flatreef PGE deposit, northern Bushveld Complex", *Mineralium Deposita,* vol. 54, no. 1, pp. 3-58.

H

Hall, G., Pelchat, J. & Dunn, C. 1990, "The determination of Au, Pd and Pt in ashed vegetation by ICP-mass spectrometry and graphite furnace atomic absorption spectrometry", *Journal of Geochemical Exploration,* vol. 37, no. 1, pp. 1-23.

Hamilton, J. 1977, "Sr isotope and trace element studies of the Great Dyke and Bushveld mafic phase and their relation to early Proterozoic magma genesis in southern Africa", *Journal of Petrology,* vol. 18, no. 1, pp. 24-52.

Harmer, R. & Sharpe, M.R. 1985, "Field relations and strontium isotope systematics of the marginal rocks of the eastern Bushveld Complex", *Economic Geology,* vol. 80, no. 4, pp. 813-837.

Harris, C. & Chaumba, J.B. 2001, "Crustal contamination and fluid–rock interaction during the formation of the Platreef, northern limb of the Bushveld Complex, South Africa", *Journal of Petrology,* vol. 42, no. 7, pp. 1321-1347.

Hart, R., Welke, H. & Nicolaysen, L. 1981, "Geochronology of the deep profile through Archean basement at Vredefort, with implications for early crustal evolution", *Journal of Geophysical Research: Solid Earth,* vol. 86, no. B11, pp. 10663-10680.

Hart, R.J., Andreoli, M.A., Tredoux, M. & De Wit, M.J. 1990, "Geochemistry across an exposed section of Archaean crust at Vredefort, South Africa: with implications for mid-crustal discontinuities", *Chemical Geology,* vol. 82, pp. 21-50.

Henderson, D., Long, L. & Barton Jr, J. 2000, "Isotopic ages and chemical and isotopic composition of the Archaean Turfloop Batholith, Pietersburg granite—greenstone terrane, Kaapvaal Craton, South Africa", *South African Journal of Geology,* vol. 103, no. 1, pp. 38-46.

Holwell, D., Boyce, A. & McDonald, I. 2007, "Sulfur isotope variations within the Platreef Ni-Cu-PGE deposit: Genetic implications for the origin of sulfide mineralization", *Economic Geology,* vol. 102, no. 6, pp. 1091-1110.

Holwell, D. & Jordaan, A. 2006, "Three-dimensional mapping of the Platreef at the Zwartfontein South mine: implications for the timing of magmatic events in the northern limb of the Bushveld Complex, South Africa", *Applied Earth Science: Transactions of the Institutions of Mining and Metallurgy: Section B,* vol. 115, no. 2, pp. 41-48.

Holwell, D.A. & McDonald, I. 2006, "Petrology, geochemistry and the mechanisms determining the distribution of platinum-group element and base metal sulphide mineralisation in the Platreef at Overysel, northern Bushveld Complex, South Africa", *Mineralium Deposita,* vol. 41, no. 6, pp. 575-598.

Howarth, G.H. & Prevec, S.A. 2013, "Trace element, PGE, and Sr–Nd isotope geochemistry of the Panzhihua mafic layered intrusion, SW China: Constraints on ore-forming processes and evolution of parent magma at depth in a plumbing-system", *Geochimica et Cosmochimica Acta,* vol. 120, pp. 459-478.

Huang, F., Chen, J., Xu, J., Wang, B. & Li, J. 2015, "Os–Nd–Sr isotopes in Miocene ultrapotassic rocks of southern Tibet: partial melting of a pyroxenite-bearing lithospheric mantle?", *Geochimica et Cosmochimica Acta,* vol. 163, pp. 279-298.

Hulbert, L. & Von Gruenewaldt, G. 1986, "The structure and petrology of the upper and lower chromitite layers on the farms Grasvally and Zoetveld, south of Potgietersrus", *Mineral Deposits of Southern Africa.Geol Soc South Africa, Johannesburg,* vol. 2, pp. 1237-1249.

Hutchinson, D. & Kinnaird, J.A. 2005, "Complex multistage genesis for the Ni–Cu–PGE mineralisation in the southern region of the Platreef, Bushveld Complex, South Africa", *Applied Earth Science: Transactions of the Institutions of Mining and Metallurgy: Section B,* vol. 114, no. 4, pp. 208-224.

Hutchinson, D. & McDonald, I. 2008, "Laser ablation ICP-MS study of platinum-group elements in sulphides from the Platreef at Turfspruit, northern limb of the Bushveld Complex, South Africa", *Mineralium Deposita,* vol. 43, no. 6, pp. 695-711.

I

Ihlenfeld, C. & Keays, R.R. 2011, "Crustal contamination and PGE mineralization in the Platreef, Bushveld Complex, South Africa: evidence for multiple contamination events and transport of magmatic sulfides", *Mineralium Deposita,* vol. 46, no. 7, pp. 813-832.

J

Jahn, B., Wu, F., Lo, C. & Tsai, C. 1999, "Crust–mantle interaction induced by deep subduction of the continental crust: geochemical and Sr–Nd isotopic evidence from post-collisional mafic–ultramafic intrusions of the northern Dabie complex, central China", *Chemical Geology,* vol. 157, no. 1-2, pp. 119-146.

James, D., Fouch, M., VanDecar, J. & Van Der Lee, S. 2001, "Tectospheric structure beneath southern Africa", *Geophysical Research Letters,* vol. 28, no. 13, pp. 2485-2488.

Janoušek, V., Farrow, C. & Erban, V. 2006, "Interpretation of whole-rock geochemical data in igneous geochemistry: introducing Geochemical Data Toolkit (GCDkit)", *Journal of Petrology,* vol. 47, no. 6, pp. 1255-1259.

Jochum, K.P., Nohl, U., Herwig, K., Lammel, E., Stoll, B. & Hofmann, A.W. 2005, "GeoReM: a new geochemical database for reference materials and isotopic standards", *Geostandards and Geoanalytical Research,* vol. 29, no. 3, pp. 333-338.

Jochum, K.P., Weis, U., Schwager, B., Stoll, B., Wilson, S.A., Haug, G.H., Andreae, M.O. & Enzweiler, J. 2016, "Reference values following ISO guidelines for frequently requested rock reference materials", *Geostandards and Geoanalytical Research,* .

K

Kinnaird, J.A., Hutchinson, D., Schurmann, L., Nex, P. & de Lange, R. 2005, "Petrology and mineralisation of the southern Platreef: northern limb of the Bushveld Complex, South Africa", *Mineralium Deposita,* vol. 40, no. 5, pp. 576-597.

Kinnaird, J.A. & McDonald, I. 2005, "An introduction to mineralisation in the northern limb of the Bushveld Complex", *Applied Earth Science: Transactions of the Institutions of Mining and Metallurgy: Section B,* vol. 114, no. 4, pp. 194-198.

Kinnaird, J.A. 2005, "Geochemical evidence for multiphase emplacement in the southern Platreef", *Applied Earth Science: Transactions of the Institution of Mining & Metallurgy, Section B,* vol. 114, no. 4, pp. 225-242.

Kreissig, K., Nägler, T.F., Kramers, J.D., van Reenen, D.D. & Smit, C.A. 2000, "An isotopic and geochemical study of the northern Kaapvaal Craton and the Southern Marginal Zone of the Limpopo Belt: are they juxtaposed terranes?", *Lithos,* vol. 50, no. 1-3, pp. 1-25.

Kröner, A., Jaeckel, P. & Brandl, G. 2000, "Single zircon ages for felsic to intermediate rocks from the Pietersburg and Giyani greenstone belts and bordering granitoid orthogneisses, northern Kaapvaal Craton, South Africa", *Journal of African Earth Sciences,* vol. 30, no. 4, pp. 773-793.

Kruger, F.J. 2005, "Filling the Bushveld Complex magma chamber: lateral expansion, roof and floor interaction, magmatic unconformities, and the formation of giant chromitite, PGE and Ti-V-magnetitite deposits", *Mineralium Deposita,* vol. 40, no. 5, pp. 451-472.

Kruger, F. 1994, "The Sr-isotopic stratigraphy of the western Bushveld Complex", *South African Journal of Geology,* vol. 97, no. 4, pp. 393-398.

L
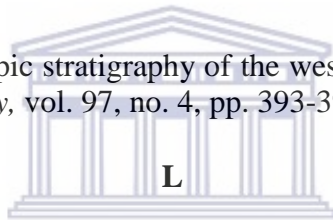
Laurent, O., Paquette, J., Martin, H., Doucelance, R. & Moyen, J. 2013, "LA-ICP-MS dating of zircons from Meso-and Neoarchean granitoids of the Pietersburg block (South Africa): crustal evolution at the northern margin of the Kaapvaal craton", *Precambrian Research,* vol. 230, pp. 209-226.

Laurent, O., Zeh, A., Gerdes, A., Villaros, A., Gros, K. & Słaby, E. 2017, "How do granitoid magmas mix with each other? Insights from textures, trace element and Sr–Nd isotopic composition of apatite and titanite from the Matok pluton (South Africa)", *Contributions to Mineralogy and Petrology,* vol. 172, no. 9, pp. 80.

Li, X. H., Su, L., Chung, S. L., Liu, Y., Song, B., & Liu, D. Y. 2006, "Formation of the Jinchuan ultramafic intrusion and associated world-class Ni--Cu sulfide deposit by the~ 825 Ma South China mantle plume", *Geochemistry, Geophysics and Geosystem G3*, vol. 3, pp. 6.

Liew, T. & Hofmann, A. 1988, "Precambrian crustal components, plutonic associations, plate environment of the Hercynian Fold Belt of central Europe: indications from a Nd and Sr isotopic study", *Contributions to Mineralogy and Petrology,* vol. 98, no. 2, pp. 129-138.

Lugmair, G. & Marti, K. 1978, "Lunar initial 143Nd/144Nd: differential evolution of the lunar crust and mantle", *Earth and Planetary Science Letters,* vol. 39, no. 3, pp. 349-357.

M

Maier W. D., Barnes S.-J., and Karykowski B. T. 2016, "A chilled margin of komatiite and Mg-rich basaltic andesite in the western Bushveld Complex, South Africa", *Contributions to Mineralogy and Petrology*, vol. 171, no. 57.

Maier, W.D., Arndt, N.T. & Curl, E.A. 2000, "Progressive crustal contamination of the Bushveld Complex: evidence from Nd isotopic analyses of the cumulate rocks", *Contributions to Mineralogy and Petrology,* vol. 140, no. 3, pp. 316-327.

Maier, W., De Klerk, L., Blaine, J., Manyeruke, T., Barnes, S., Stevens, M. & Mavrogenes, J. 2008, "Petrogenesis of contact-style PGE mineralization in the northern lobe of the Bushveld Complex: comparison of data from the farms Rooipoort, Townlands, Drenthe and Nonnenwerth", *Mineralium Deposita,* vol. 43, no. 3, pp. 255-280.

Manyeruke, T.D., Maier, W.D. & Barnes, S. 2005, "Major and trace element geochemistry of the Platreef on the farm Townlands, northern Bushveld Complex.", *South African Journal of Geology,* vol. 108, no. 3.

Mao, Y., Qin, K., Tang, D., Feng, H. & Xue, S. 2016, "Crustal contamination and sulfide immiscibility history of the Permian Huangshannan magmatic Ni-Cu sulfide deposit, East Tianshan, NW China", *Journal of Asian Earth Sciences,* vol. 129, pp. 22-37.

McDonald, I. & Holwell, D.A. 2007, "Did lower zone magma conduits store PGE-rich sulphides that were later supplied to the Platreef?", *South African Journal of Geology,* vol. 110, no. 4, pp. 611-616.

McDonald, I., Holwell, D.A. & Armitage, P.E. 2005, "Geochemistry and mineralogy of the Platreef and "Critical Zone" of the northern lobe of the Bushveld Complex, South Africa: implications for Bushveld stratigraphy and the development of PGE mineralisation", *Mineralium Deposita,* vol. 40, no. 5, pp. 526-549.

McDonald, I., Holwell, D.A. & Wesley, B. 2009, "Assessing the potential involvement of an early magma staging chamber in the generation of the Platreef Ni–Cu–PGE deposit in the northern limb of the Bushveld Complex: a pilot study of the Lower Zone Complex at Zwartfontein", *Applied Earth Science: Transactions of the Institution of Mining & Metallurgy, Section B,* vol. 118, no. 1, pp. 5-20.

McDonough, W.F. & Sun, S. 1995, "The composition of the Earth", *Chemical Geology,* vol. 120, no. 3-4, pp. 223-253.

Míková, J. & Denková, P. 2007, "Modified chromatographic separation scheme for Sr and Nd isotope analysis in geological silicate samples", *Journal of Geosciences,* vol. 52, no. 3/4, pp. 221.

Mitchell, A.A. & Scoon, R.N. 2012, "The Platreef of the Bushveld Complex, South Africa: a New Hypothesis of Multiple, Non-Sequential Magma Replenishment Based on Observations at the Akanani Project, North-West of Mokopane", *South African Journal of Geology,* vol. 115, no. 4, pp. 535-550.

N

Nakamura, N. 1974, "Determination of REE, Ba, Fe, Mg, Na and K in carbonaceous and ordinary chondrites", *Geochimica et Cosmochimica Acta,* vol. 38, no. 5, pp. 757-775.

Nex, P.A.M. 2005, "The structural setting of mineralisation on Tweefontein Hill, northern limb of the Bushveld Complex, South Africa", *Applied Earth Science: Transactions of the Institution of Mining & Metallurgy, Section B,* vol. 114, no. 4, pp. 243-251.

Norrish, K. & Hutton, J.T. 1969, "An accurate X-ray spectrographic method for the analysis of a wide range of geological samples", *Geochimica et Cosmochimica Acta,* vol. 33, no. 4, pp. 431-453.

P
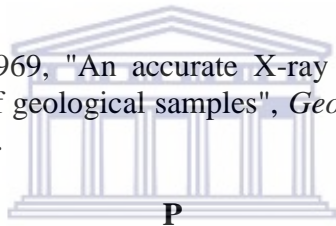
Penniston-Dorland, S.C., Wing, B.A., Nex, P.A., Kinnaird, J.A., Farquhar, J., Brown, M. & Sharman, E.R. 2008, "Multiple sulfur isotopes reveal a magmatic origin for the Platreef platinum group element deposit, Bushveld Complex, South Africa", *Geology,* vol. 36, no. 12, pp. 979-982.

Pin, C., Briot, D., Bassin, C. & Poitrasson, F. 1994, "Concomitant separation of strontium and samarium-neodymium for isotopic analysis in silicate samples, based on specific extraction chromatography", *Analytica Chimica Acta,* vol. 298, no. 2, pp. 209-217.

Pin, C. & Zalduegui, J.S. 1997, "Sequential separation of light rare-earth elements, thorium and uranium by miniaturized extraction chromatography: application to isotopic analyses of silicate rocks", *Analytica Chimica Acta,* vol. 339, no. 1, pp. 79-89.

Potts, P.J. 1987, *A handbook of silicate rock analysis,* Blackie Glasgow; London.

Poujol, M. 2001, "U-Pb isotopic evidence for episodic granitoid emplacement in the Murchison greenstone belt, South Africa", *Journal of African earth sciences (Oxford, England: 1994),* vol. 33, no. 1, pp. 155-163.

Poujol, M. & Robb, L. 1999, "New U-Pb zircon ages on gneisses and pegmatite from south of the the Murchison greenstone belt, South Africa", *South African Journal of Geology,* vol. 102, pp. 93-98.

Poujol, M., Robb, L.J., Respaut, J. & Anhaeusser, C.R. 1996, "3.07-2.97 Ga greenstone belt formation in the northeastern Kaapvaal Craton; implications for the origin of the Witwatersrand Basin", *Economic Geology,* vol. 91, no. 8, pp. 1455-1461.

Pronost, J., Harris, C. & Pin, C. 2008, "Relationship between footwall composition, crustal contamination, and fluid–rock interaction in the Platreef, Bushveld Complex, South Africa", *Mineralium Deposita,* vol. 43, no. 8, pp. 825-848.

R

Reimold, W.U., Hauser, N., Hansen, B.T., Thirlwall, M. & Hoffmann, M. 2017, "The impact pseudotachylitic breccia controversy: Insights from first isotope analysis of Vredefort impact-generated melt rocks", *Geochimica et Cosmochimica Acta,* vol. 214, pp. 266-281.

Reisberg, L., Tredoux, M., Harris, C., Coftier, A. & Chaumba, J. 2011, "Re and Os distribution and Os isotope composition of the Platreef at the Sandsloot–Mogolakwena mine, Bushveld complex, South Africa", *Chemical Geology,* vol. 281, no. 3, pp. 352-363.

Richardson, S.H. & Shirey, S.B. 2008, "Continental mantle signature of Bushveld magmas and coeval diamonds", *Nature,* vol. 453, no. 7197, pp. 910-913.

Roelofse, F. & Ashwal, L.D. 2012, "The Lower Main Zone in the Northern Limb of the Bushveld Complex—a> 1· 3 km thick sequence of intruded and variably contaminated crystal mushes", *Journal of Petrology,* vol. 53, no. 7, pp. 1449-1476.

Rudnick, R., McDonough, W., McCulloch, M. & Taylor, S. 1986, "Lower crustal xenoliths from Queensland, Australia: evidence for deep crustal assimilation and fractionation of continental basalts", *Geochimica et Cosmochimica Acta,* vol. 50, no. 6, pp. 1099-1115.

S

SACS (South African Committee for Stratigraphy), 1980, "Stratigraphy of South Africa. Part 1: Lithostratigraphy of the Republic of South Africa, South West Africa/Namibia and the Republics of Bophuthatswana, Transkei and Venda (L.E. Kent, Compiler)", *Geological Survey South Africa*, Handbook 8, pp. l-690.

SACCRM (South African Committee for Certified Reference Materials), 1984. Certificate of Analysis: NIM-P Pyroxenite SARM 5 - Certified Reference Materials. Pretoria. Available at: http://www.mintek.co.za/wp content/uploads/2011/10/SARM-5.pdf.

Sharman, E., Penniston-Dorland, S., Kinnaird, J., Nex, P., Brown, M. & Wing, B. 2013, "Primary origin of marginal Ni-Cu-(PGE) mineralization in layered intrusions: Δ33S evidence from The Platreef, Bushveld, South Africa", *Economic Geology,* vol. 108, no. 2, pp. 365-377.

Sharman-Harris, E., Kinnaird, J., Harris, C. & Horstmann, U. 2005, "A new look at sulphide mineralisation of the northern limb, Bushveld Complex: a stable isotope study", *Applied Earth Science: Transactions of the Institutions of Mining and Metallurgy: Section B,* vol. 114, no. 4, pp. 252-263.

Sharpe, M. 1981, "The chronology of magma influxes to the eastern compartment of the Bushveld Complex as exemplified by its marginal border groups", *Journal of the Geological Society,* vol. 138, no. 3, pp. 307-326.

Sharpe, M., Evensen, N. & Naldrett, A. 1986, "Sm/Nd and Rb/Sr evidence for liquid mixing, magma generation and contamination in the Eastern Bushveld Complex", *Geological Society of South Africa, Geocongress 1986, abstract volume, Johannesburg,* vol. 6217, pp. 624.

Shibata, T & Yoshikawa, Masako & Tatsumi, Y. (2003). An analytical method for determining precise Sr and Nd isotopic compositions and results for thirteen rock standard materials. *Frontier Research on Earth Evolution,* Vol. 1, pp. 363-367.

Shirey, S.B., Harris, J.W., Richardson, S.H., Fouch, M.J., James, D.E., Cartigny, P., Deines, P. & Viljoen, F. 2002, "Diamond genesis, seismic structure, and evolution of the Kaapvaal-Zimbabwe craton", *Science (New York, N.Y.),* vol. 297, no. 5587, pp. 1683-1686.

Shu, Y., Zeng, Z., Yin, X., Wang, X. & Chen, S. 2018, "Geochemical and Sr─Nd isotopic constraints on the origin of volcanic rocks from the northern Okinawa Trough", *Geological Journal,* .

Smith, J.W., Holwell, D.A., McDonald, I. & Boyce, A.J. 2016, "The application of S isotopes and S/Se ratios in determining ore-forming processes of magmatic Ni–Cu–PGE sulfide deposits: a cautionary case study from the northern Bushveld Complex", *Ore Geology Reviews,* vol. 73, pp. 148-174.

Sproule, R., Lambert, D. & Hoatson, D. 2002, "Decoupling of the Sm–Nd and Re–Os isotopic systems in sulphide-saturated magmas in the Halls Creek Orogen, Western Australia", *Journal of Petrology,* vol. 43, no. 2, pp. 375-402.

121

Steiger, R. & Jäger, E. 1977, "Subcommission on geochronology: convention on the use of decay constants in geo-and cosmochronology", *Earth and Planetary Science Letters,* vol. 36, no. 3, pp. 359-362.

Stewart, B.W. & DePaolo, D.J. 1990, "Isotopic studies of processes in mafic magma chambers: II. The Skaergaard Intrusion, East Greenland", *Contributions to Mineralogy and Petrology,* vol. 104, no. 2, pp. 125-141.

Sun, S.S. & McDonough, W.F., 1989, "Chemical and isotopic systematics of oceanic basalts: implications for mantle composition and processes". In: Saunders, A.D., Norry, M.J. Eds.., Magmatism in the Ocean Basins, *Geological Society Special Publications*, no. 42, pp. 313–345.

Sun, T., Qian, Z., Deng, Y., Li, C., Song, X. & Tang, Q. 2013, "PGE and isotope (Hf-Sr-Nd-Pb) constraints on the origin of the Huangshandong magmatic Ni-Cu sulfide deposit in the Central Asian orogenic belt, northwestern China", *Economic Geology,* vol. 108, no. 8, pp. 1849-1864.

T

Tanaka, T., Togashi, S., Kamioka, H., Amakawa, H., Kagami, H., Hamamoto, T., Yuhara, M., Orihashi, Y., Yoneda, S. & Shimizu, H. 2000, "JNdi-1: a neodymium isotopic reference in consistency with LaJolla neodymium", *Chemical Geology,* vol. 168, no. 3, pp. 279-281.

Taylor, S.R. & McLennan, S.M., 1985, "The Continental Crust: Its Composition and Evolution", Blackwell, 312 pp.

V

Van der Merwe, F., Viljoen, F. & Knoper, M. 2012, "The mineralogy and mineral associations of platinum group elements and gold in the Platreef at Zwartfontein, Akanani Project, Northern Bushveld Complex, South Africa", *Mineralogy and Petrology,* vol. 106, no. 1-2, pp. 25-38.

Van der Merwe, M.J. 2008, "The geology and structure of the Rustenburg Layered Suite in the Potgietersrus/Mokopane area of the Bushveld Complex, South Africa", *Mineralium Deposita,* vol. 43, no. 4, pp. 405-419.

Van der Merwe, M. 1978, *The geology of the basic and ultramafic rocks of the Potgietersrus limb of the Bushveld Complex,* .

Van Tongeren, J., Zirakparvar, N. & Mathez, E. 2016, "Hf isotopic evidence for a cogenetic magma source for the Bushveld Complex and associated felsic magmas", *Lithos,* vol. 248, pp. 469-477.

Vezinet, A., Moyen, J., Stevens, G., Nicoli, G., Laurent, O., Couzinié, S. & Frei, D. 2018, "A record of 0.5 Ga of evolution of the continental crust along the northern edge of the Kaapvaal Craton, South Africa: Consequences for the understanding of Archean geodynamic processes", *Precambrian Research,* vol. 305, pp. 310-326.

W

Walraven, F. 1989, *The Geology of the Pilgrim's Rest Area: Explanation of Sheet 2430, Scale 1: 250 000,* Government Printer= Staatsdrukker.

Walraven, F., Armstrong, R. & Kruger, F. 1990, "A chronostratigraphic framework for the north-central Kaapvaal craton, the Bushveld Complex and the Vredefort structure", *Tectonophysics,* vol. 171, no. 1, pp. 23-48.

Wasserburg, G., Jacobsen, S., DePaolo, D., McCulloch, M. & Wen, T. 1981, "Precise determination of SmNd ratios, Sm and Nd isotopic abundances in standard solutions", *Geochimica et Cosmochimica Acta,* vol. 45, no. 12, pp. 2311-2323.

Wilson A. H. 2015, "The earliest stages of emplacement of the Eastern Bushveld Complex: development of the Lower Zone, Marginal Zone and Basal Ultramafic Sequence", *Journal of Petrololgy*, vol. 56, no. 2, pp. 347–388.

Wilson, A.H. 2012, "A chill sequence to the Bushveld Complex: insight into the first stage of emplacement and implications for the parental magmas", *Journal of Petrology,* vol. 53, no. 6, pp. 1123-1168.

Y

Xu, W., Xu, X., & Zeng, G. 2017, "Crustal contamination versus an enriched mantle source for intracontinental mafic rocks: Insights from early Paleozoic mafic rocks of the South China Block", *Lithos*, vol. 286–287, pp. 388–395.

Y

Yudovskaya, M.A. & Kinnaird, J.A. 2010, "Chromite in the Platreef (Bushveld Complex, South Africa): occurrence and evolution of its chemical composition", *Mineralium Deposita,* vol. 45, no. 4, pp. 369-391.

Yudovskaya, M.A., Kinnaird, J.A., Sobolev, A.V., Kuzmin, D.V., McDonald, I. & Wilson, A.H. 2013a, "Petrogenesis of the Lower Zone olivine-rich cumulates beneath the Platreef and their correlation with recognized occurrences in the Bushveld Complex", *Economic Geology,* vol. 108, no. 8, pp. 1923-1952.

Yudovskaya, M., Kinnaird, J., Naldrett, A.J., Rodionov, N., Antonov, A., Simakin, S. & Kuzmin, D. 2013b, "Trace-element study and age dating of zircon from chromitites of the Bushveld Complex (South Africa)", *Mineralogy and Petrology,* vol. 107, no. 6, pp. 915-942.

Yudovskaya, M.A., Kinnaird, J.A., Grobler, D.F., Costin, G., Abramova, V.D., Dunnett, T., and Barnes, S. -J. 2017a, "Zonation of Merensky -style platinum -group element mineralization in Turfspruit thick reef facies (Northern Limb of the Bushveld Complex)", *Economic Geology*, vol. 112, no.6, pp. 1333-1365.

Yudovskaya, M., Belousova, E., Kinnaird, J., Dubinina, E., Grobler, D.F., Pearson N. 2017b, "Re-Os and S isotope evidence for the origin of Platreef mineralization (Bushveld Complex)", *Geochimica et Cosmochimica Acta,* vol. 214, pp. 282-307.

Z

Zeh, A., Gerdes, A. & Barton Jr, J.M. 2009, "Archean accretion and crustal evolution of the Kalahari Craton—the zircon age and Hf isotope record of granitic rocks from Barberton/Swaziland to the Francistown Arc", *Journal of Petrology,* vol. 50, no. 5, pp. 933-966.

Zeh, A., Jaguin, J., Poujol, M., Boulvais, P., Block, S. & Paquette, J. 2013, "Juvenile crust formation in the northeastern Kaapvaal Craton at 2.97 Ga—Implications for Archean terrane accretion, and the source of the Pietersburg gold", *Precambrian Research,* vol. 233, pp. 20-43.

Zeh, A., Ovtcharova, M., Wilson, A.H. & Schaltegger, U. 2015, "The Bushveld Complex was emplaced and cooled in less than one million years–results of zirconology, and geotectonic implications", *Earth and Planetary Science Letters,* vol. 418, pp. 103-114.

Zhang, C. L., Yang, D. S., Wang, H. Y., Takahashi, Y., & Ye, H. M. 2011, "Neoproterozoic mafic-ultramafic layered intrusion in Quruqtagh of northeastern Tarim Block, NW China: Two phases of mafic igneous activity with different mantle sources", *Gondwana Research*, vol. 19, pp. 177–190.

Zhong, H., Yao, Y., Prevec, S.A., Wilson, A.H., Viljoen, M.J., Viljoen, R.P., Liu, B. & Luo, Y. 2004, "Trace-element and Sr–Nd isotopic geochemistry of the PGE-bearing Xinjie layered intrusion in SW China", *Chemical Geology,* vol. 203, no. 3-4, pp. 237-252.

Zhou, M., Lesher, C.M., Yang, Z., Li, J. & Sun, M. 2004, "Geochemistry and petrogenesis of 270 Ma Ni–Cu–(PGE) sulfide-bearing mafic intrusions in the Huangshan district, Eastern Xinjiang, Northwest China: implications for the tectonic evolution of the Central Asian orogenic belt", *Chemical Geology,* vol. 209, no. 3-4, pp. 233-257.

Zhou, M., Zhao, J., Qi, L., Su, W. & Hu, R. 2006, "Zircon U-Pb geochronology and elemental and Sr–Nd isotope geochemistry of Permian mafic rocks in the Funing area, SW China", *Contributions to Mineralogy and Petrology,* vol. 151, no. 1, pp. 1-19.

Zirakparvar, N. A., Mathez, E. A., Scoates, J. S., & Wall, C. J. 2014, "Zircon Hf isotope evidence for an enriched mantle source for the Bushveld Igneous Complex", *Contributions to Mineralogy and Petrology*, vol. 168, pp. 1–18.

125

9 APPENDIX

9.1 Appendix A: Whole-rock major element data

Sample ID	OY482-01	OY482-02	OY482-03	OY482-04	OY482-05	OY482-06	OY482-07
Depth	277.15	279.3	284.85	291.97	316.16	338.57	350.43
Rock type	GN-II	GN-II	FPyx-II	GN-I	GN-I	GN-I	GN-III
SiO_2	48.45	48.98	49.34	49.68	45.23	49.31	50.77
Al_2O_3	15.96	18.24	8.13	11.08	10.96	13.56	13.87
Fe_2O_3	6.12	5.43	14.07	11.31	11.74	7.70	10.00
MnO	0.11	0.11	0.20	0.17	0.13	0.12	0.15
MgO	9.77	10.22	18.52	16.25	15.18	13.19	9.04
CaO	13.76	12.42	6.93	8.95	7.78	10.87	11.77
Na_2O	1.63	1.89	1.01	1.08	1.89	1.42	2.21
K_2O	0.44	0.37	0.07	0.11	0.52	0.45	0.19
TiO_2	0.16	0.12	0.21	0.16	0.14	0.14	0.24
P_2O_5	0.02	0.02	0.02	0.02	0.02	0.02	0.03
SO_3	0.01	0.01	0.12	0.01	0.81	0.04	0.03
LOI	3.58	2.20	1.38	1.20	5.60	3.19	1.70
TOT	100.00	100.00	100.00	100.00	100.00	100.00	100.00
Mg#	75.96	78.87	72.29	74.00	71.92	77.25	64.17

Sample ID	OY482-08	OY482-09	OY482-10	OY482-11	OY482-12	OY482-13	OY482-14
Depth	351.41	352.52	354.28	358.51	360.31	365.78	371.46
Rock type	GN-I	GN-I	GN-I	GN-I	GN-I	GN-I	GN-III
SiO_2	47.88	48.96	50.06	49.22	50.23	54.13	51.70
Al_2O_3	13.07	15.30	15.51	12.13	13.63	9.97	12.57
Fe_2O_3	8.89	6.68	8.46	8.60	9.04	9.69	10.92
MnO	0.13	0.11	0.14	0.14	0.15	0.17	0.13
MgO	13.73	11.38	9.56	14.97	10.02	11.88	8.02
CaO	10.85	12.94	13.34	10.83	12.18	8.63	10.07
Na_2O	1.35	1.47	1.84	1.08	1.88	2.26	3.58
K_2O	0.31	0.51	0.31	0.48	0.46	0.15	0.30
TiO_2	0.15	0.13	0.16	0.15	0.23	0.17	0.17
P_2O_5	0.02	0.02	0.01	0.02	0.03	0.03	0.02
SO_3	0.01	0.01	0.02	0.00	0.09	0.04	1.02
LOI	3.62	2.51	0.60	2.40	2.09	2.90	1.50
TOT	100.00	100.00	100.00	100.00	100.00	100.00	100.00
Mg#	75.38	77.14	69.12	77.52	68.71	70.84	59.27

Note: All oxides are expressed in weight percent (wt. %). Rock type abbreviations: ALG: Anorthositic leucogabbro; A.Gr: Archaean granite; Dol: Dolomite; FPyx: feldspathic pyroxenite; GN: gabbronorite; HNFL: Hornfelsed BIF/Shale; HZG: harzburgite; LGN: leucogabbronorite; NRT: norite; OB-Pyx: olivine-bearing pyroxenite

Sample ID	OY482-15	OY482-16	OY482-18	OY482-19	OY482-20	OY482-21	OY482-22
Depth	377.64	380.12	390.64	394.02	395.33	398.36	401.26
Rock type	GN-I	GN-I	GN-I	GN-I	GN-III	GN-I	GN-I
SiO_2	49.51	56.02	47.03	49.30	49.07	54.50	49.20
Al_2O_3	13.77	12.48	10.28	17.36	13.43	11.63	14.47
Fe_2O_3	7.64	7.43	12.46	6.38	10.85	7.80	6.77
MnO	0.12	0.17	0.16	0.11	0.16	0.12	0.11
MgO	11.65	10.19	16.52	8.73	10.23	9.45	10.30
CaO	10.88	8.97	8.10	12.06	11.06	11.97	13.53
Na_2O	1.59	2.55	1.87	1.79	2.32	1.75	1.99
K_2O	0.53	0.32	0.27	1.00	0.37	0.06	0.62
TiO_2	0.16	0.14	0.17	0.11	0.20	0.15	0.16
P_2O_5	0.02	0.02	0.02	0.02	0.02	0.03	0.02
SO_3	0.02	0.03	0.63	0.01	0.19	0.03	0.15
LOI	4.12	1.70	2.50	3.15	2.11	2.52	2.69
TOT	100.00	100.00	100.00	100.00	100.00	100.00	100.00
Mg#	75.14	73.09	72.42	73.06	65.12	70.59	75.08

Sample ID	OY482-23	OY482-24	OY482-25	OY482-27	OY482-28	OY482-29	OY482-30
Depth	404.07	405.89	408.13	409.64	412.87	413.23	415.72
Rock type	GN-III	GN-I	GN-I	FPyx-III	GN-I	FPyx-III	FPyx-III
SiO_2	53.86	49.79	48.76	48.51	46.57	50.32	52.44
Al_2O_3	11.11	13.82	15.20	9.79	16.01	7.06	5.90
Fe_2O_3	8.47	9.63	8.84	12.71	7.41	11.11	17.05
MnO	0.13	0.15	0.12	0.17	0.12	0.16	0.23
MgO	9.99	9.77	10.68	15.25	10.06	14.88	16.35
CaO	11.40	12.00	10.65	8.58	10.69	10.61	4.95
Na_2O	1.63	2.15	1.89	1.32	1.75	1.51	1.36
K_2O	0.12	0.39	0.67	0.26	0.98	0.22	0.11
TiO_2	0.15	0.21	0.17	0.22	0.14	0.24	0.27
P_2O_5	0.02	0.02	0.02	0.02	0.02	0.05	0.07
SO_3	0.02	0.19	0.24	0.16	0.17	0.42	0.38
LOI	3.10	1.89	2.76	3.02	6.09	3.41	0.91
TOT	100.00	100.00	100.00	100.00	100.00	100.00	100.00
Mg#	70.02	66.79	70.53	70.39	72.88	72.63	65.51

Sample ID	OY482-31	OY482-32	OY482-33	OY482-34	OY482-35	OY482-36	OY482-37
Depth	419.76	421.12	422.71	424.77	426.95	438.13	446.66
Rock type	GN-III	GN-III	GN-III	FPyx-III	FPyx-III	GN-III	GN-I
SiO_2	43.45	50.67	49.58	44.97	49.02	51.52	49.45
Al_2O_3	10.24	11.45	10.72	8.98	4.30	13.76	14.31
Fe_2O_3	11.78	12.12	12.68	12.83	15.24	9.05	9.75
MnO	0.17	0.18	0.16	0.16	0.18	0.16	0.15
MgO	14.16	11.95	11.94	19.03	17.17	8.10	11.36
CaO	11.32	9.76	9.46	7.82	7.97	11.25	9.57
Na_2O	1.27	1.82	2.22	0.85	1.81	2.77	1.84
K_2O	0.04	0.37	0.38	0.13	0.16	0.54	0.99
TiO_2	0.20	0.18	0.19	0.18	0.23	0.20	0.16
P_2O_5	0.03	0.02	0.02	0.02	0.03	0.03	0.03
SO_3	0.13	0.10	0.66	0.03	0.51	0.03	0.20
LOI	7.22	1.40	2.00	5.00	3.39	2.62	2.21
TOT	100.00	100.00	100.00	100.00	100.00	100.00	100.00
Mg#	70.42	66.15	65.10	74.61	69.06	63.93	69.77

Sample ID	OY482-38	OY482-39	OY482-40	OY482-42	OY482-44	SS339-03	SS339-04
Depth	452.65	455.77	459.81	469.05	475.13	52.4	38.76
Rock type	GN-I	FPyx-IV	FPyx-IV	FPyx-IV	A.Gr	FPyx-I	GN-II
SiO_2	49.14	53.94	49.17	53.02	81.55	50.08	47.94
Al_2O_3	12.27	9.41	3.94	15.02	8.89	9.89	18.66
Fe_2O_3	10.06	11.35	15.15	7.33	0.58	13.17	5.70
MnO	0.15	0.16	0.20	0.12	0.02	0.19	0.10
MgO	14.93	13.13	19.26	11.21	0.16	18.75	8.63
CaO	8.18	6.58	4.15	6.60	1.39	6.13	12.69
Na_2O	1.55	2.55	1.22	2.87	5.60	0.97	2.29
K_2O	0.50	0.24	0.08	0.44	0.08	0.08	0.75
TiO_2	0.20	0.27	0.21	0.26	0.07	0.17	0.16
P_2O_5	0.02	0.06	0.04	0.06	0.05	0.01	0.02
SO_3	0.11	0.51	0.46	0.11	0.01	0.01	0.01
LOI	2.87	1.80	6.13	2.97	1.60	0.55	3.04
TOT	100.00	100.00	100.00	100.00	100.00	100.00	100.00
Mg#	74.62	69.63	71.58	75.19	n.c	73.83	75.00

129

Sample ID	SS339-05	SS339-07	SS339-08	SS339-09	SS339-10	SS339-11	SS339-12
Depth	12.36	50.22	60.72	61.93	65	70	73.15
Rock type	GN-II	ALG	OB-Pyx	Pyx	HZG	OB-Pyx	OB-Pyx
SiO_2	50.62	49.75	47.77	50.42	36.87	48.08	48.89
Al_2O_3	14.13	22.99	2.42	3.72	0.81	2.96	4.52
Fe_2O_3	8.67	3.69	15.24	15.15	14.00	15.09	14.86
MnO	0.12	0.05	0.19	0.21	0.09	0.20	0.20
MgO	11.69	2.74	28.23	24.58	37.39	25.66	24.46
CaO	11.16	14.60	2.39	3.85	0.93	3.24	4.12
Na_2O	1.32	2.62	0.95	1.00	0.54	1.46	1.16
K_2O	0.34	1.02	0.01	0.05	0.03	0.17	0.09
TiO_2	0.21	0.07	0.14	0.18	0.06	0.21	0.16
P_2O_5	0.02	0.01	0.02	0.03	0.01	0.02	0.02
SO_3	0.01	0.26	1.04	0.41	0.51	0.82	0.62
LOI	1.70	2.20	1.60	0.40	8.75	2.10	0.90
TOT	100.00	100.00	100.00	100.00	100.00	100.00	100.00
Mg#	72.76	59.54	78.59	76.27	84.10	77.11	76.53

Sample ID	SS339-13	SS339-15	SS339-16	SS339-18	SS339-19	SS339-29	SS339-40
Depth	82.24	99.36	110.56	120.66	131.07	179.22	181.39
Rock type	Pyx	OB-Pyx	GN-II	GN-II	OB-Pyx	Dol	Dol
SiO_2	48.57	45.92	45.09	47.12	47.73	0.01	1.65
Al_2O_3	5.50	2.93	13.23	11.82	4.60	0.01	0.76
Fe_2O_3	14.61	16.82	12.24	11.12	14.51	3.71	0.18
MnO	0.21	0.22	0.15	0.17	0.20	0.79	1.29
MgO	24.35	26.17	8.80	12.59	25.04	23.07	20.10
CaO	4.39	3.51	13.46	12.05	4.40	39.39	41.43
Na_2O	0.58	0.75	2.96	1.70	1.13	0.72	0.77
K_2O	0.03	0.01	0.21	0.27	0.02	0.01	0.01
TiO_2	0.14	0.16	0.31	0.22	0.15	0.01	0.20
P_2O_5	0.02	0.02	0.05	0.02	0.02	0.01	0.01
SO_3	0.11	0.71	1.03	0.24	0.43	0.23	0.17
LOI	1.49	2.78	2.47	2.68	1.78	32.04	33.43
TOT	100.00	100.00	100.00	100.00	100.00	100.00	100.00
Mg#	76.75	75.50	58.75	69.16	77.37	n.c	n.c

Sample ID	TN200-01	TN200-02	TN200-03	TN200-04	TN200-05	TN200-06	TN200-07
Depth	196.06	225.78	230.77	235.2	235.95	238.33	243.23
Rock type	LGN	FPyx-I	FPyx-I	FPyx-I	FPyx-I	GN-II	FPyx-I
SiO_2	53.45	46.95	47.38	48.89	49.10	49.18	46.19
Al_2O_3	19.88	6.20	7.10	5.43	6.80	13.66	8.90
Fe_2O_3	6.47	15.41	14.26	13.73	13.61	8.28	13.57
MnO	0.09	0.20	0.19	0.21	0.22	0.14	0.18
MgO	4.39	21.60	20.77	23.70	23.63	12.25	19.31
CaO	10.86	5.11	6.02	4.84	4.39	11.70	5.93
Na_2O	2.87	1.12	1.07	0.79	0.79	1.77	2.04
K_2O	0.79	0.11	0.12	0.12	0.12	0.39	0.23
TiO_2	0.48	0.20	0.18	0.18	0.16	0.15	0.15
P_2O_5	0.02	0.02	0.02	0.02	0.02	0.02	0.03
SO_3	0.01	1.18	1.01	0.49	0.58	0.47	1.00
LOI	0.70	1.89	1.89	1.60	0.60	1.99	2.48
TOT	100.00	100.00	100.00	100.00	100.00	100.00	100.00
Mg#	57.33	73.52	74.27	77.37	77.48	74.57	73.81

Sample ID	TN200-08	TN200-09	TN200-10	TN200-11	TN200-12	TN200-13	TN200-14
Depth	249.17	254.87	255.42	260.65	262.88	268.37	274.03
Rock type	FPyx-I	FPyx-I	NRT-II	NRT-II	NRT-II	NRT-II	NRT-I
SiO_2	48.24	49.27	49.36	47.18	47.67	47.46	48.03
Al_2O_3	10.97	8.63	15.51	14.71	15.74	18.39	17.91
Fe_2O_3	14.42	13.68	10.64	12.59	10.45	10.62	9.49
MnO	0.19	0.22	0.17	0.17	0.13	0.14	0.15
MgO	16.65	20.97	13.24	12.69	10.70	8.90	9.99
CaO	6.33	5.53	8.18	8.51	9.49	10.43	9.89
Na_2O	1.09	0.77	1.37	1.65	2.24	1.94	1.92
K_2O	0.21	0.13	0.36	0.20	0.63	0.24	0.37
TiO_2	0.17	0.17	0.18	0.16	0.19	0.16	0.09
P_2O_5	0.02	0.02	0.03	0.03	0.04	0.03	0.01
SO_3	0.93	0.51	0.36	0.93	0.74	0.69	0.36
LOI	0.79	0.10	0.60	1.19	1.99	1.00	1.80
TOT	100.00	100.00	100.00	100.00	100.00	100.00	100.00
Mg#	69.58	75.22	71.14	66.63	66.97	62.40	67.59

131

Sample ID	TN200-16	TN200-17	TN200-18	TN200-21	TN200-22	TN200-24	TN200-26
Depth	278.02	286.78	287.73	296.21	301.6	303.8	304.53
Rock type	FPyx-V	NRT-I	NRT-I	NRT-II	NRT-I	FPyx-III	NRT-II
SiO_2	43.10	40.52	45.30	45.38	44.40	43.61	45.41
Al_2O_3	6.00	17.01	17.05	10.65	15.43	3.15	9.84
Fe_2O_3	23.87	21.80	12.83	14.55	16.19	18.62	19.30
MnO	0.27	0.19	0.18	0.26	0.21	0.20	0.30
MgO	18.89	9.90	10.25	14.52	10.96	20.68	14.86
CaO	2.92	6.22	8.61	10.01	7.75	4.39	5.62
Na_2O	0.97	1.26	1.20	0.90	0.97	0.37	1.33
K_2O	0.27	0.48	1.92	0.73	1.12	0.15	0.48
TiO_2	0.32	1.15	0.18	0.25	0.13	0.26	0.22
P_2O_5	0.02	0.02	0.02	0.02	0.02	0.03	0.03
SO_3	1.19	0.46	0.25	0.44	1.04	0.50	1.33
LOI	2.18	1.00	2.20	2.29	1.80	8.05	1.29
TOT	100.00	100.00	100.00	100.00	100.00	100.00	100.00
Mg#	61.06	47.36	61.28	66.40	57.28	68.76	60.39

Sample ID	TN200-29	TN200-38	TN200-39	TN200-40	TN754-01	TN754-02	TN754-03
Depth	317.14	321.45	323.14	325.55	211.83	223.34	231.17
Rock type	NRT-I	HNFL	HNFL	HNFL	LGN	FPyx-III	FPyx-II
SiO_2	42.36	54.16	65.85	58.72	52.82	48.00	52.07
Al_2O_3	15.97	0.01	0.01	0.70	17.76	4.83	6.69
Fe_2O_3	18.58	36.84	26.85	28.72	8.38	16.68	12.11
MnO	0.30	0.06	0.22	0.33	0.11	0.19	0.18
MgO	7.80	3.10	4.46	5.53	4.77	20.79	21.66
CaO	9.13	2.85	1.51	3.45	11.03	3.72	4.51
Na_2O	0.38	0.14	0.12	0.30	2.30	1.72	0.88
K_2O	2.51	0.00	0.00	0.28	0.96	0.33	0.44
TiO_2	0.05	0.01	0.05	0.08	0.35	0.34	0.24
P_2O_5	0.01	0.12	0.02	0.02	0.10	0.06	0.03
SO_3	0.41	0.12	0.21	0.28	0.02	1.23	0.08
LOI	2.49	2.60	0.70	1.59	1.40	2.11	1.10
TOT	100.00	100.00	100.00	100.00	100.00	100.00	100.00
Mg#	45.41	n.c	n.c	n.c	53.00	71.18	77.99

Sample ID	TN754-04	TN754-05	TN754-06	TN754-08	TN754-09	TN754-10	TN754-11
Depth	250.87	260.65	264	279.85	306.62	316.77	321.74
Rock type	FPyx-II	GN-III	FPyx-III	FPyx-II	HZG	OB-Pyx	OB-Pyx
SiO_2	49.05	48.41	49.98	48.99	38.00	38.24	36.73
Al_2O_3	10.08	13.61	6.37	8.87	1.27	4.01	3.93
Fe_2O_3	11.04	9.65	14.56	13.69	17.66	23.34	26.25
MnO	0.13	0.14	0.25	0.21	0.13	0.20	0.38
MgO	17.70	9.23	18.10	17.63	32.85	21.03	26.18
CaO	7.22	13.86	6.15	7.30	0.56	3.78	1.38
Na_2O	1.28	2.02	1.77	1.06	0.11	0.95	0.20
K_2O	0.66	0.56	0.42	0.50	0.53	1.10	0.05
TiO_2	0.15	0.27	0.59	0.21	0.07	0.19	0.27
P_2O_5	0.02	0.04	0.08	0.03	0.02	0.03	0.03
SO_3	0.55	0.60	0.53	0.31	0.11	2.89	1.27
LOI	2.12	1.61	1.20	1.20	8.70	4.24	3.34
TOT	100.00	100.00	100.00	100.00	100.00	100.00	100.00
Mg#	76.06	65.46	71.12	71.84	78.66	64.09	66.40

Sample ID	TN754-12	TN754-41	TN754-42
Depth	326.31	334.18	345.64
Rock type	OB-Pyx	HNFL	HNFL
SiO_2	31.76	51.25	37.08
Al_2O_3	2.18	0.37	0.20
Fe_2O_3	28.85	36.20	51.32
MnO	0.22	0.40	0.27
MgO	26.88	3.03	1.14
CaO	1.21	7.46	8.93
Na_2O	0.59	0.24	0.31
K_2O	0.08	0.14	0.03
TiO_2	0.14	0.07	0.02
P_2O_5	0.02	0.07	0.22
SO_3	3.32	0.57	0.29
LOI	4.75	0.20	0.20
TOT	100.00	100.00	100.00
Mg#	64.87	n.c	n.c

Note: All oxides are expressed in weight percent (wt. %). n.c: not calculated. Rock type abbreviations: ALG: Anorthositic leucogabbro; A.Gr: Archaean granite; Dol: Dolomite; FPyx: feldspathic pyroxenite; GN: gabbronorite; HNFL: Hornfelsed BIF/Shale; HZG: harzburgite; LGN: leucogabbronorite; NRT: norite; OB-Pyx: olivine-bearing pyroxenite

133

9.2   Appendix B: Whole-rock trace element data

Sample ID	OY482-01	OY482-03	OY482-14	OY482-18	OY482-20	OY482-22	OY482-25
Depth	277.15	284.85	371.46	390.64	395.33	401.26	408.13
Rock type	GN-II	FPyx-II	GN-III	GN-I	GN-III	GN-I	GN-I
Ba	111.93	27.95	73.00	78.00	108.54	161.00	169.00
Co	24.45	89.85	145.00	138.00	61.12	78.00	68.10
Cs	1.04	0.36	0.70	1.50	0.73	1.50	1.20
Hf	0.28	0.50	0.60	0.70	0.49	0.30	0.40
Nb	0.66	8.93	2.50	0.90	0.86	0.60	0.30
Rb	15.57	2.99	10.70	14.20	11.45	34.20	30.50
Sr	235.70	88.10	208.90	202.30	211.44	300.00	264.30
Th	0.38	0.57	0.90	0.60	0.45	0.50	0.50
U	0.11	0.16	1.20	0.30	0.22	0.20	0.20
V	81.56	147.70	165.00	126.00	150.65	98.00	112.00
Y	3.86	4.94	10.70	4.20	7.04	4.60	5.30
Zr	10.48	23.00	20.10	19.10	13.42	10.10	14.60
Cu	15.40	394.40	2859.80	2211.10	529.01	753.20	731.90
Mo	2.25	3.72	3.60	2.80	3.22	2.40	2.50
Ni	195.22	780.00	2801.90	4304.20	872.21	1169.50	1196.50
Pb	49.25	2.19	4.40	5.50	18.37	2.80	4.50
Zn	34.82	94.40	20.00	31.00	77.29	40.00	47.00
La	2.76	2.45	5.30	2.80	3.50	3.00	3.40
Ce	4.87	4.90	11.30	5.10	6.98	5.70	6.80
Pr	0.61	0.61	1.46	0.63	0.87	0.69	0.79
Nd	2.63	2.34	6.70	2.80	4.21	3.10	3.40
Sm	0.46	0.53	1.51	0.55	1.02	0.64	0.76
Eu	0.37	0.22	0.47	0.28	0.37	0.41	0.39
Gd	0.71	0.77	1.68	0.66	1.28	0.69	0.80
Tb	0.10	0.14	0.31	0.12	0.19	0.12	0.15
Dy	0.72	0.84	1.78	0.71	1.11	0.78	1.02
Ho	0.12	0.19	0.38	0.15	0.27	0.16	0.19
Er	0.45	0.52	1.04	0.48	0.79	0.44	0.52
Tm	0.05	0.09	0.17	0.08	0.14	0.06	0.09
Yb	0.35	0.85	1.11	0.51	0.71	0.47	0.50
Lu	0.08	0.10	0.18	0.07	0.12	0.07	0.10

Note: All trace elements are expressed in ppm. Rock type abbreviations: ALG: Anorthositic leucogabbro; A.Gr: Archaean granite; Dol: Dolomite; FPyx: feldspathic pyroxenite; GN: gabbronorite; HNFL: Hornfelsed BIF/Shale; HZG: harzburgite; LGN: leucogabbronorite; NRT: norite; OB-Pyx: olivine-bearing pyroxenite.

Sample ID	OY482-28	OY482-29	OY482-30	OY482-31	OY482-33	OY482-35	OY482-36
Depth	412.87	413.23	415.72	419.76	422.71	426.95	438.13
Rock type	GN-I	FPyx-III	FPyx-III	GN-III	GN-III	FPyx-III	GN-III
Ba	246.00	72.00	21.65	27.00	113.00	40.35	190.00
Co	57.00	109.80	104.95	98.50	145.20	129.51	48.10
Cs	1.80	1.10	1.14	1.20	0.80	1.02	0.70
Hf	0.40	0.60	0.65	0.60	0.30	0.96	0.50
Nb	0.70	2.80	4.74	1.10	1.00	2.66	0.40
Rb	51.90	13.80	9.71	2.30	15.70	6.61	20.70
Sr	388.40	128.50	61.80	94.10	208.60	54.96	352.00
Th	0.60	1.40	1.89	0.50	0.60	0.80	0.30
U	0.10	0.90	1.61	0.40	0.50	0.67	0.20
V	72.00	218.00	167.20	142.00	170.00	218.36	171.00
Y	3.60	11.40	9.45	10.00	9.20	10.81	9.70
Zr	11.50	22.90	18.66	17.40	17.30	33.33	13.60
Cu	720.80	1390.70	966.50	1041.40	1356.40	2768.56	207.50
Mo	2.40	3.40	5.62	2.90	2.00	3.00	2.80
Ni	1144.20	1520.00	1205.50	1649.30	2658.10	2246.44	92.10
Pb	4.20	4.20	12.99	16.60	6.60	18.91	3.20
Zn	49.00	45.00	159.00	96.00	52.00	130.05	22.00
La	3.30	4.60	5.09	4.60	4.00	3.93	4.90
Ce	6.00	11.10	10.64	9.60	8.70	9.61	10.40
Pr	0.66	1.48	1.27	1.29	1.14	1.24	1.35
Nd	2.70	6.50	5.36	6.00	5.70	5.59	6.30
Sm	0.53	1.58	1.27	1.42	1.27	1.49	1.49
Eu	0.37	0.39	0.24	0.43	0.46	0.28	0.61
Gd	0.53	1.81	1.36	1.56	1.41	1.58	1.61
Tb	0.09	0.33	0.21	0.28	0.25	0.29	0.30
Dy	0.60	2.08	1.56	1.70	1.51	1.78	1.97
Ho	0.11	0.38	0.35	0.37	0.33	0.43	0.38
Er	0.39	1.18	1.07	1.10	0.91	1.27	1.03
Tm	0.05	0.19	0.18	0.18	0.16	0.18	0.16
Yb	0.40	1.12	1.28	1.15	0.95	1.39	0.94
Lu	0.05	0.19	0.21	0.18	0.15	0.22	0.15

135

Sample ID	OY482-37	OY482-38	OY482-39	OY482-40	SS339-04	SS339-05	SS339-07
Depth	446.66	452.65	455.77	459.81	38.76	12.36	50.22
Rock type	GN-I	GN-I	FPyx-IV	FPyx-IV	GN-II	GN-II	ALG
Ba	306.00	195.00	74.00	17.25	175.00	112.00	211.00
Co	79.20	80.40	112.00	185.85	18.40	41.70	34.50
Cs	2.20	3.00	1.90	1.70	2.90	0.70	1.40
Hf	0.30	0.60	1.70	0.84	0.30	0.30	0.05
Nb	0.40	0.60	5.30	5.30	0.30	0.60	0.05
Rb	42.60	25.60	19.30	11.66	34.90	15.20	41.20
Sr	369.20	280.00	178.30	71.40	327.40	248.80	340.80
Th	0.40	0.70	1.50	0.85	0.40	0.70	0.05
U	0.20	0.20	2.00	0.79	0.20	0.20	0.05
V	96.00	114.00	147.00	122.95	61.00	105.00	36.00
Y	4.20	5.40	12.20	6.08	3.20	4.60	1.30
Zr	9.50	14.80	61.40	32.71	6.50	10.10	1.20
Cu	882.40	691.60	1839.20	2102.00	26.20	37.00	757.70
Mo	3.00	2.70	3.10	4.21	1.50	1.10	2.70
Ni	1485.60	942.60	1717.10	4136.00	60.00	53.70	1411.40
Pb	3.80	4.80	8.80	7.32	1.90	1.30	5.00
Zn	21.00	61.00	62.00	149.55	36.00	23.00	36.00
La	2.90	3.30	9.40	2.96	3.20	3.70	2.20
Ce	5.90	6.60	20.30	6.61	6.50	7.30	4.00
Pr	0.66	0.78	2.48	0.75	0.76	0.82	0.43
Nd	2.70	3.30	11.20	3.36	2.80	3.20	1.50
Sm	0.57	0.68	2.30	0.89	0.61	0.65	0.30
Eu	0.31	0.32	0.46	0.11	0.59	0.45	0.49
Gd	0.56	0.71	2.30	0.80	0.56	0.71	0.25
Tb	0.10	0.13	0.37	0.13	0.10	0.13	0.04
Dy	0.74	0.95	2.30	1.17	0.52	0.76	0.27
Ho	0.18	0.20	0.47	0.19	0.11	0.19	0.04
Er	0.37	0.63	1.29	0.69	0.39	0.55	0.11
Tm	0.08	0.09	0.19	0.15	0.06	0.09	0.02
Yb	0.47	0.59	1.17	0.84	0.31	0.57	0.15
Lu	0.08	0.10	0.19	0.14	0.05	0.08	0.02

Sample ID	SS339-08	SS339-09	SS339-10	SS339-12	SS339-13	SS339-15	SS339-18
Depth	60.72	61.93	65	73.15	82.24	99.36	120.66
Rock type	OB-Pyx	Pyx	HZG	OB-Pyx	Pyx	OB-Pyx	GN-II
Ba	16.77	20.85	29.85	25.50	19.00	32.33	98.00
Co	156.81	108.03	137.12	176.45	88.60	126.73	71.40
Cs	0.45	0.30	0.61	1.25	0.42	0.86	0.40
Hf	0.29	0.26	0.12	0.14	0.11	0.18	0.30
Nb	0.43	0.97	0.30	1.34	1.51	0.52	0.20
Rb	1.17	3.63	2.58	3.86	1.80	2.01	10.40
Sr	13.41	27.17	24.46	33.90	33.95	45.75	258.80
Th	0.29	0.98	0.10	0.19	0.19	0.23	0.05
U	0.08	0.35	0.03	0.05	0.04	0.08	0.05
V	86.86	115.87	56.51	117.10	111.45	111.47	150.00
Y	2.62	4.23	1.97	3.41	2.78	4.45	7.70
Zr	8.82	9.52	4.41	5.20	6.20	6.72	7.40
Cu	3380.44	942.41	1190.42	2664.00	421.60	1256.32	555.90
Mo	1.69	3.06	2.05	4.22	4.18	2.96	2.10
Ni	4858.81	2539.71	2259.57	6033.50	1065.50	2069.72	918.10
Pb	23.88	77.76	22.87	18.77	3.72	55.24	5.30
Zn	97.11	96.99	57.87	135.30	88.80	89.12	34.00
La	1.03	2.12	0.73	1.15	1.03	1.36	3.00
Ce	2.04	4.54	1.17	1.93	1.85	2.22	6.70
Pr	0.26	0.52	0.14	0.20	0.18	0.27	0.86
Nd	1.07	2.39	0.66	1.07	0.92	1.24	4.50
Sm	0.29	0.51	0.11	0.32	0.21	0.47	1.08
Eu	0.10	0.10	0.07	0.11	0.07	0.12	0.54
Gd	0.29	0.53	0.22	0.36	0.27	0.44	1.24
Tb	0.04	0.09	0.05	0.06	0.06	0.09	0.22
Dy	0.46	0.62	0.27	0.57	0.44	0.69	1.39
Ho	0.07	0.16	0.06	0.12	0.10	0.15	0.33
Er	0.37	0.44	0.24	0.35	0.25	0.69	0.98
Tm	0.06	0.09	0.03	0.07	0.05	0.11	0.14
Yb	0.34	0.46	0.26	0.47	0.33	0.76	0.82
Lu	0.07	0.10	0.05	0.09	0.06	0.13	0.14

137

Sample ID	SS339-19	TN200-03	TN200-04	TN200-05	TN200-08	TN200-09	TN200-11
Depth	131.07	230.77	235.2	235.95	249.17	254.87	260.65
Rock type	OB-Pyx	FPyx-I	FPyx-I	FPyx-I	FPyx-I	FPyx-I	NRT-II
Ba	113.43	25.40	34.95	29.50	41.00	43.55	59.00
Co	49.51	163.35	119.70	118.55	138.90	140.95	132.00
Cs	0.36	1.56	2.30	0.50	1.40	1.11	0.80
Hf	0.36	0.30	0.36	0.27	0.30	0.33	0.50
Nb	0.58	1.81	2.18	1.16	0.50	2.70	0.80
Rb	10.95	5.55	9.26	4.37	6.30	7.77	7.40
Sr	206.87	58.85	39.45	49.38	79.40	98.75	173.90
Th	0.23	0.83	0.55	0.34	0.50	1.01	0.90
U	0.09	0.20	0.14	0.08	0.10	0.18	0.20
V	159.71	83.00	94.95	81.40	77.00	81.85	75.00
Y	8.84	4.29	3.33	2.67	3.50	3.22	4.20
Zr	9.98	11.61	15.76	8.34	11.80	10.83	16.60
Cu	497.23	1143.45	694.85	580.90	299.50	344.60	840.00
Mo	2.26	4.43	2.82	5.75	3.50	3.56	3.30
Ni	870.60	2941.50	1784.50	1443.00	986.40	1599.00	1770.20
Pb	59.16	6.85	15.53	5.69	10.30	11.30	9.60
Zn	55.37	91.45	96.10	97.65	15.00	90.40	13.00
La	3.02	2.80	2.19	1.44	2.00	2.64	3.00
Ce	6.62	5.63	5.10	2.95	4.20	5.15	6.10
Pr	0.92	0.64	0.54	0.33	0.46	0.55	0.76
Nd	4.08	2.74	2.15	1.28	2.40	2.19	3.00
Sm	1.22	0.71	0.50	0.32	0.38	0.53	0.57
Eu	0.57	0.14	0.15	0.12	0.15	0.16	0.26
Gd	1.50	0.79	0.44	0.32	0.43	0.41	0.63
Tb	0.28	0.10	0.07	0.06	0.07	0.08	0.11
Dy	1.61	0.78	0.47	0.60	0.52	0.49	0.66
Ho	0.32	0.18	0.12	0.13	0.13	0.11	0.15
Er	1.09	0.47	0.44	0.33	0.39	0.40	0.46
Tm	0.14	0.08	0.05	0.05	0.06	0.07	0.08
Yb	1.00	0.45	0.44	0.37	0.50	0.37	0.46
Lu	0.16	0.07	0.07	0.06	0.08	0.07	0.09

Sample ID	TN200-12	TN200-13	TN200-14	TN200-16	TN200-22	TN200-24	TN754-01
Depth	262.88	268.37	274.03	278.02	301.6	303.8	211.83
Rock type	NRT-II	NRT-II	NRT-I	FPyx-V	NRT-I	FPyx-III	LGN
Ba	155.00	68.00	63.00	20.00	190.00	14.70	239.34
Co	156.80	105.00	93.60	175.65	127.00	87.90	31.23
Cs	2.10	0.90	1.30	1.51	1.20	0.97	1.97
Hf	0.60	0.50	0.05	0.34	0.10	1.99	1.36
Nb	1.30	0.60	0.10	2.24	0.30	6.44	2.11
Rb	24.20	8.60	15.80	14.17	36.00	9.71	29.09
Sr	215.80	257.00	316.50	28.07	174.60	9.24	253.95
Th	0.80	0.80	0.05	0.65	0.05	7.96	2.47
U	0.30	0.20	0.05	0.15	0.05	2.12	0.54
V	72.00	60.00	37.00	161.50	61.00	63.50	122.28
Y	4.80	3.80	1.20	3.20	1.90	12.07	13.83
Zr	22.30	12.70	2.60	10.21	4.20	77.48	44.76
Cu	1314.90	611.10	474.60	875.00	446.60	374.60	36.88
Mo	2.90	3.00	3.10	3.68	2.90	5.60	4.42
Ni	1529.20	1379.60	979.00	1942.50	667.10	1029.50	97.12
Pb	7.80	9.50	5.10	4.99	9.60	1.79	88.30
Zn	22.00	12.00	23.00	127.60	13.00	66.45	60.30
La	4.60	3.50	0.80	1.81	1.20	15.88	13.60
Ce	9.00	6.40	1.60	3.26	2.50	34.27	24.97
Pr	1.01	0.78	0.18	0.33	0.27	3.74	2.96
Nd	4.00	3.00	0.50	1.16	0.90	14.40	11.91
Sm	0.83	0.58	0.15	0.25	0.23	2.74	2.47
Eu	0.30	0.28	0.14	0.09	0.16	0.20	0.69
Gd	0.76	0.54	0.14	0.29	0.25	2.30	2.59
Tb	0.14	0.11	0.03	0.06	0.05	0.32	0.43
Dy	0.89	0.63	0.22	0.45	0.39	2.20	2.40
Ho	0.16	0.14	0.04	0.13	0.08	0.44	0.49
Er	0.51	0.38	0.14	0.45	0.24	1.42	1.52
Tm	0.08	0.07	0.02	0.08	0.04	0.25	0.18
Yb	0.46	0.46	0.13	0.71	0.30	1.93	1.42
Lu	0.08	0.06	0.02	0.14	0.06	0.35	0.22

Sample ID	TN754-02	TN754-03	TN754-05	TN754-06	TN754-08	TN754-09	TN754-11
Depth	223.34	231.17	260.65	264	279.85	306.62	321.74
Rock type	FPyx-III	FPyx-II	GN-III	FPyx-III	FPyx-II	HZG	OB-Pyx
Ba	118.80	74.35	130.00	90.90	54.45	53.76	15.11
Co	178.15	80.85	94.30	99.90	103.80	107.86	97.05
Cs	2.04	1.51	1.60	0.91	0.81	17.86	0.80
Hf	1.64	0.69	0.90	1.35	0.33	0.16	0.78
Nb	4.15	1.92	1.20	11.05	2.13	1.10	0.96
Rb	22.76	21.05	29.60	14.89	11.77	136.80	3.62
Sr	50.70	61.55	196.90	57.18	88.65	6.27	5.48
Th	3.41	2.58	1.20	2.20	0.54	0.37	0.60
U	1.95	0.53	0.20	0.40	0.18	0.52	0.22
V	146.55	120.30	140.00	152.60	127.45	35.67	96.04
Y	10.42	5.96	9.70	13.00	4.67	2.85	3.64
Zr	62.70	28.65	36.00	57.39	14.48	6.28	27.68
Cu	1870.00	213.15	977.00	1195.00	620.00	212.21	275.48
Mo	3.96	3.66	4.70	5.78	6.19	1.28	1.89
Ni	6649.50	737.50	2318.70	2117.00	942.00	1286.59	1665.71
Pb	4.88	2.55	8.00	6.45	16.03	41.06	10.03
Zn	97.10	100.95	18.00	106.50	96.25	104.72	137.71
La	13.28	6.52	6.80	10.98	2.50	0.34	1.61
Ce	23.28	12.45	13.70	22.11	4.71	0.83	3.46
Pr	2.18	1.38	1.64	2.42	0.57	0.13	0.36
Nd	7.67	5.50	7.10	10.36	2.41	0.65	1.32
Sm	1.56	1.01	1.58	2.21	0.55	0.19	0.31
Eu	0.25	0.28	0.53	0.41	0.22	0.06	0.07
Gd	1.52	0.90	1.77	2.15	0.66	0.31	0.37
Tb	0.24	0.17	0.29	0.33	0.11	0.08	0.07
Dy	1.72	1.01	1.70	2.41	0.78	0.39	0.44
Ho	0.39	0.21	0.37	0.45	0.15	0.06	0.14
Er	1.14	0.73	0.95	1.44	0.53	0.27	0.39
Tm	0.17	0.09	0.15	0.21	0.09	0.06	0.08
Yb	1.17	0.73	1.10	1.57	0.65	0.62	0.65
Lu	0.18	0.10	0.14	0.20	0.09	0.13	0.09

9.3 Appendix C: PGE (Pt, Pd & Au) data

Sample ID	Rock type	Au	Pd	Pt
OY482-03	FPyx-II	0.08	0.93	0.46
OY482-13	GN-I	0.03	0.03	0.05
OY482-15	GN-I	0.03	0.05	0.03
OY482-18	GN-I	0.96	10.00	8.50
OY482-19	GN-I	0.06	0.03	0.05
OY482-21	GN-III	0.24	0.03	0.03
OY482-23	GN-III	0.03	0.03	0.03
OY482-25	GN-I	0.17	1.86	1.24
OY482-27	GN-III	0.09	1.57	1.06
OY482-28	GN-I	0.20	0.94	0.53
OY482-32	GN-III	0.07	0.60	0.52
OY482-36	GN-III	0.14	0.03	0.03
OY482-40	FPyx-IV	0.05	0.03	0.03
OY482-42	FPyx-IV	0.19	2.13	1.85
SS339-07	ALG	0.09	0.35	0.28
SS339-08	OB-Pyx	0.24	1.93	1.62
SS339-10	HZG	0.05	0.28	0.22
SS339-11	OB-Pyx	0.12	1.13	0.90
SS339-15	OB-Pyx	0.07	0.95	0.81
SS339-16	GN-II	0.15	1.63	1.43
SS339-19	OB-Pyx	0.20	1.53	1.30
TN200-01	LGN	0.05	0.05	0.05
TN200-02	FPyx-I	0.05	0.60	0.42
TN200-07	FPyx-I	0.09	0.16	0.14
TN200-10	NRT-II	0.05	0.05	0.05
TN200-17	NRT-I	0.05	0.07	0.07
TN200-18	NRT-I	0.05	0.07	0.05
TN200-24	FPyx-III	0.05	0.20	0.12
TN200-26	NRT-II	0.05	0.25	0.17
TN754-03	FPyx-II	0.05	0.03	0.08
TN754-08	FPyx-II	0.05	0.35	0.43
TN754-09	HZG	0.05	0.28	0.24

Note: Au, Pd and Pt are expressed in ppm. Rock type abbreviations: ALG: Anorthositic leucogabbro; FPyx: feldspathic pyroxenite; GN: gabbronorite; HZG: harzburgite; LGN: leucogabbronorite; NRT: norite; OB-Pyx: olivine-bearing pyroxenite.

141

9.4   Appendix D: Whole-rock Sr–Nd isotope data

Sample ID	Rock type	$^{87}Sr/^{86}Sr$	±2σ Sr	$^{143}Nd/^{144}Nd$	±2σ Nd
OY482-01	GN-II	0.717427	±14	0.511437	±9
OY482-03	FPyx-II	0.713963	±13	0.511583	±10
OY482-20	GN-III	0.719679	±13	0.511659	±9
OY482-30	FPyx-III	0.735492	±13	0.511562	±8
OY482-35	FPyx-III	0.730117	±15	0.511705	±12
OY482-40	FPyx-IV	0.756343	±11	0.511595	±10
SS339-08	OB-Pyx	0.717545	±11	0.511562	±17
SS339-09	Pyx	0.721987	±12	0.511528	±12
SS339-12	OB-Pyx	0.718186	±13	0.511777	±15
SS339-13	Pyx	0.713722	±10	0.511693	±14
SS339-15	OB-Pyx	0.713270	±22	0.511911	±15
SS339-19	OB-Pyx	0.713723	±10	0.511870	±9
TN200-03	FPyx-I	0.716483	±15	0.511435	±10
TN200-04	FPyx-I	0.728767	±15	0.511272	±10
TN200-05	FPyx-I	0.715145	±11	0.511443	±11
TN200-09	FPyx-I	0.715503	±20	0.511228	±11
TN200-16	FPyx-V	0.755665	±12	0.511351	±10
TN200-24	FPyx-III	0.803079	±18	0.511240	±8
TN754-01	LGN	0.719175	±11	0.511303	±12
TN754-02	FPyx-III	0.748539	±20	0.511204	±8
TN754-03	FPyx-II	0.736747	±20	0.511201	±12
TN754-06	FPyx-III	0.733946	±12	0.511311	±8
TN754-08	FPyx-II	0.722454	±12	0.511586	±16
TN754-11	OB-Pyx	0.818253	±41	0.511424	±12

Note: The listed 2σ refers to the last digit. Rock type abbreviations: FPyx: feldspathic pyroxenite; GN: gabbronorite; LGN: leucogabbronorite; OB-Pyx: olivine-bearing pyroxenite; Pyx: Pyroxenite. Errors (2σ) correspond to the last two digits of the Sr and Nd isotope values.

9.5   Appendix E: Plots of εNd versus selected major and trace elements
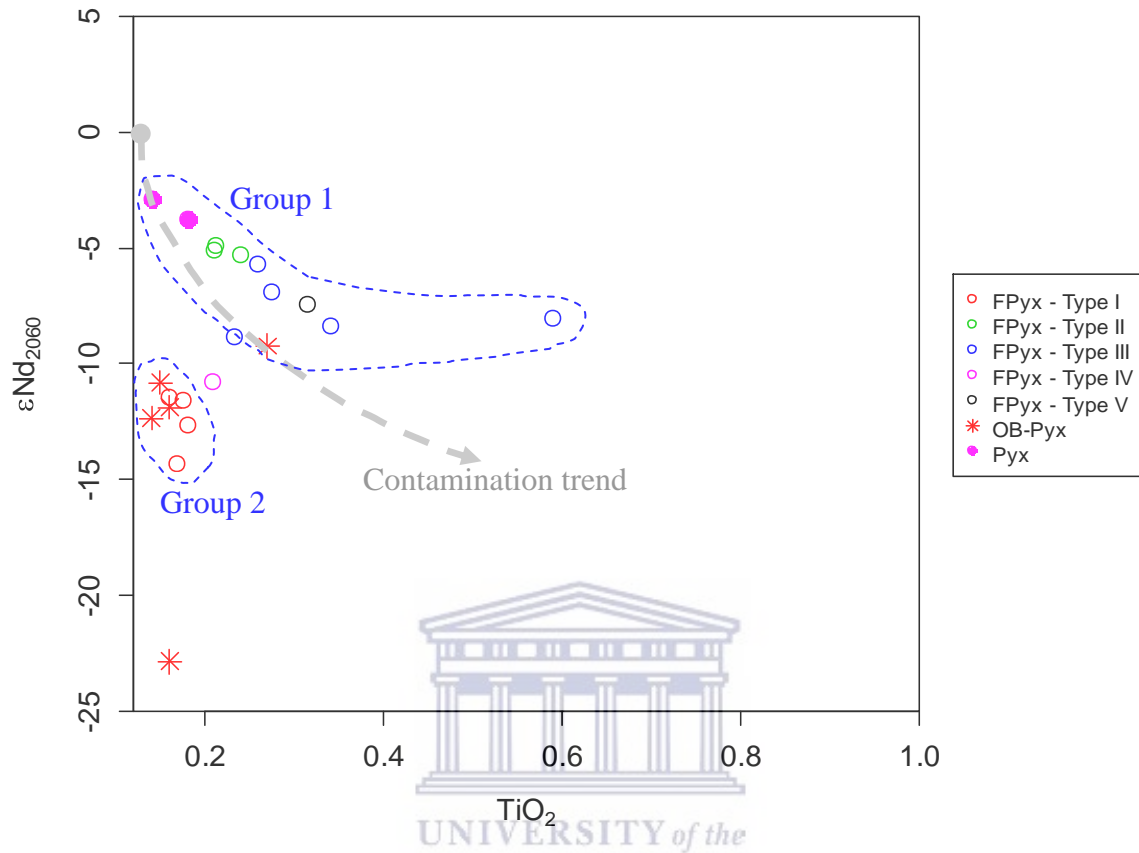

Figure 22: Plot of εNd$_{2060}$ versus TiO$_2$ (wt. %) for the Platreef rocks in this study. The εNd are calculated at the nearest round-off age of 2060 Ma for the BIC (Buick et al., 2001; Yudovskaya et al., 2013b; Zeh et al., 2015). The isotopic groups (1 and 2) for the Platreef rocks are the same as in Figure 14. Legend abbreviation: FPyx: Feldspathic pyroxenite; OB-Pyx: Olivine pyroxenite; Pyx: Pyroxenite.
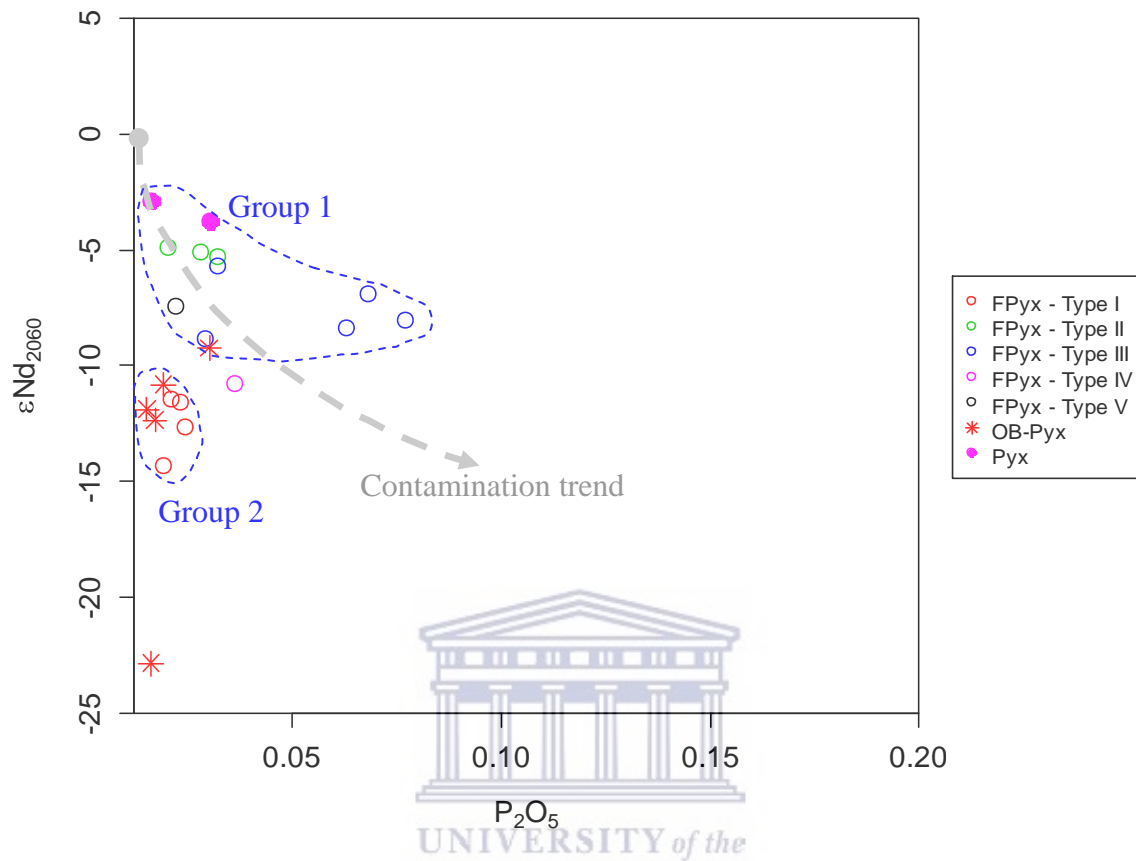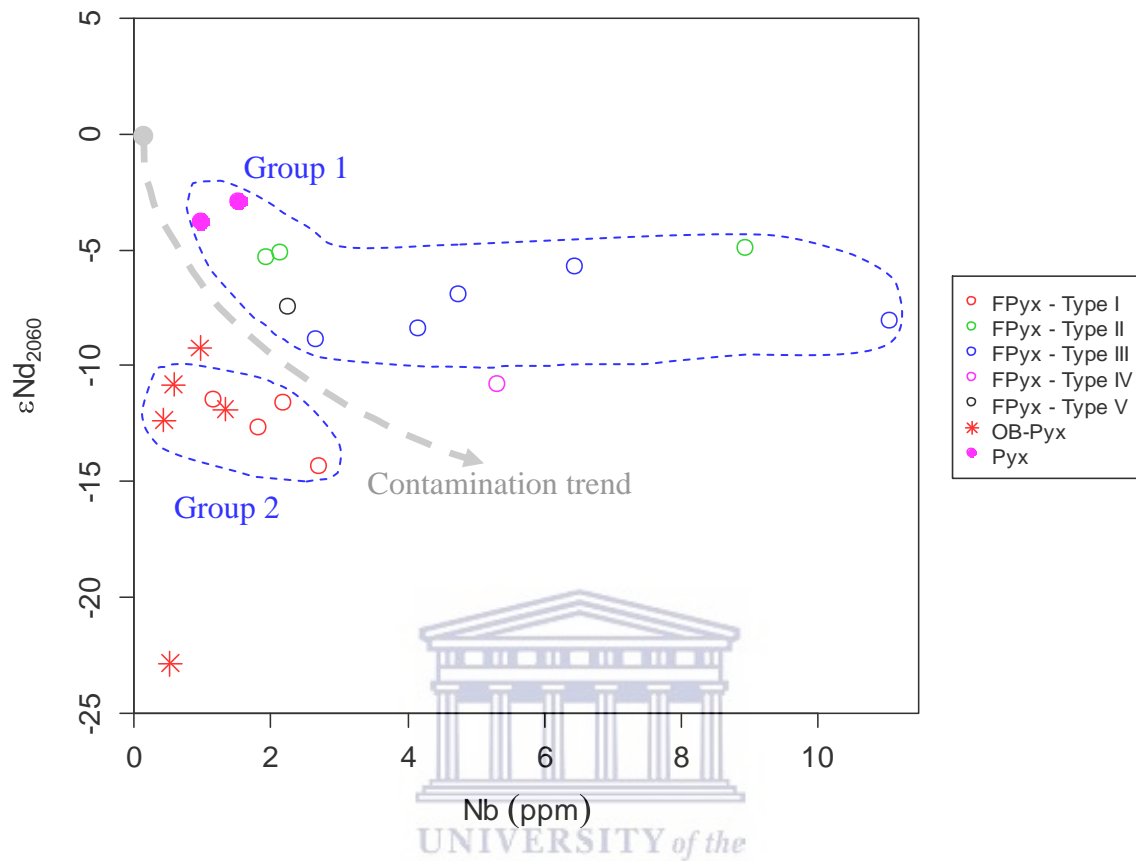
Figure 23: Plot of εNd$_{2060}$ versus P$_2$O$_5$ (wt. %) for the Platreef rocks in this study.The εNd are calculated at the nearest round-off age of 2060 Ma for the BIC (Buick et al., 2001; Yudovskaya et al., 2013b; Zeh et al., 2015). The isotopic groups (1 and 2) for the Platreef rocks are the same as in Figure 14. Legend abbreviation: FPyx: Feldspathic pyroxenite; OB-Pyx: Olivine pyroxenite; Pyx: Pyroxenite.
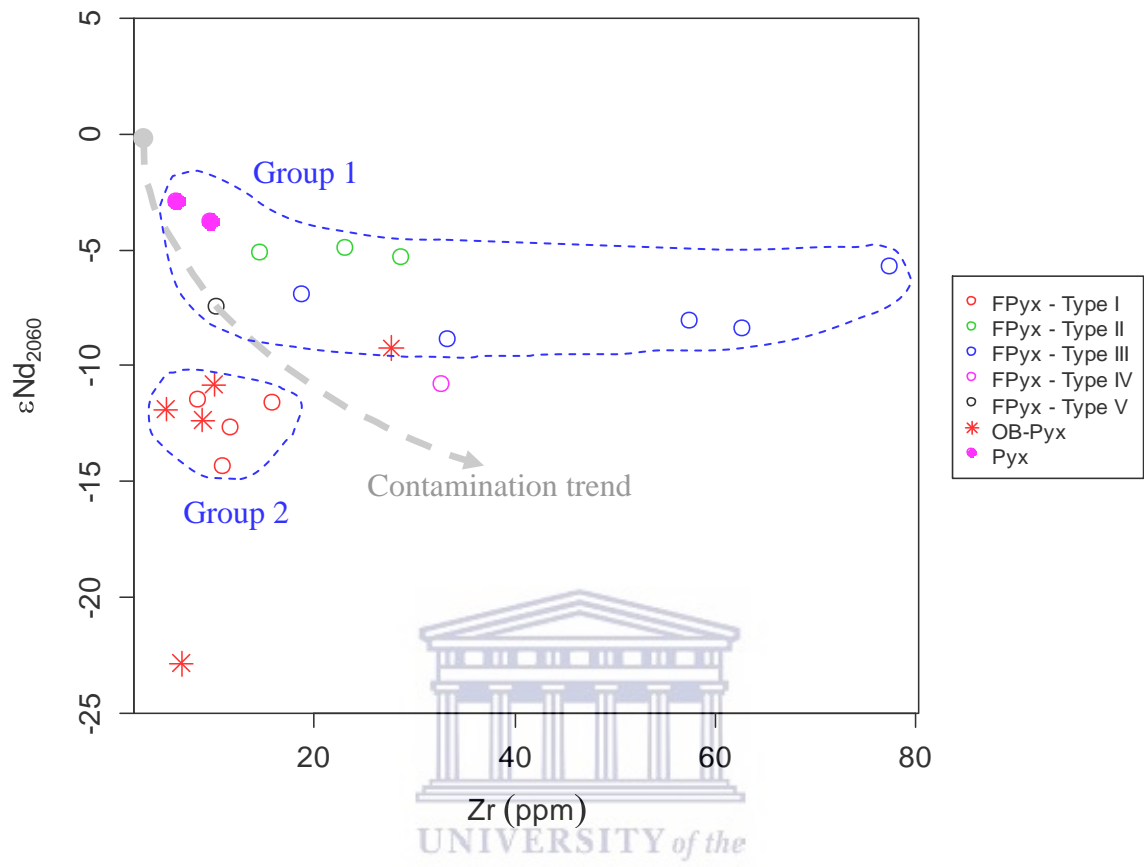
Figure 24: Plot of εNd$_{2060}$ versus Nb for the Platreef rocks in this study.The εNd are calculated at the nearest round-off age of 2060 Ma for the BIC (Buick et al., 2001; Yudovskaya et al., 2013b; Zeh et al., 2015). The isotopic groups (1 and 2) for the Platreef rocks are the same as in Figure 14. Legend abbreviation: FPyx: Feldspathic pyroxenite; OB-Pyx: Olivine pyroxenite; Pyx: Pyroxenite.

145

Figure 25: Plot of εNd$_{2060}$ versus Zr for the Platreef rocks in this study. The εNd are calculated at the nearest round-off age of 2060 Ma for the BIC (Buick et al., 2001; Yudovskaya et al., 2013b; Zeh et al., 2015). The isotopic groups (1 and 2) for the Platreef rocks are the same as in Figure 14. Legend abbreviation: FPyx: Feldspathic pyroxenite; OB-Pyx: Olivine pyroxenite; Pyx: Pyroxenite.
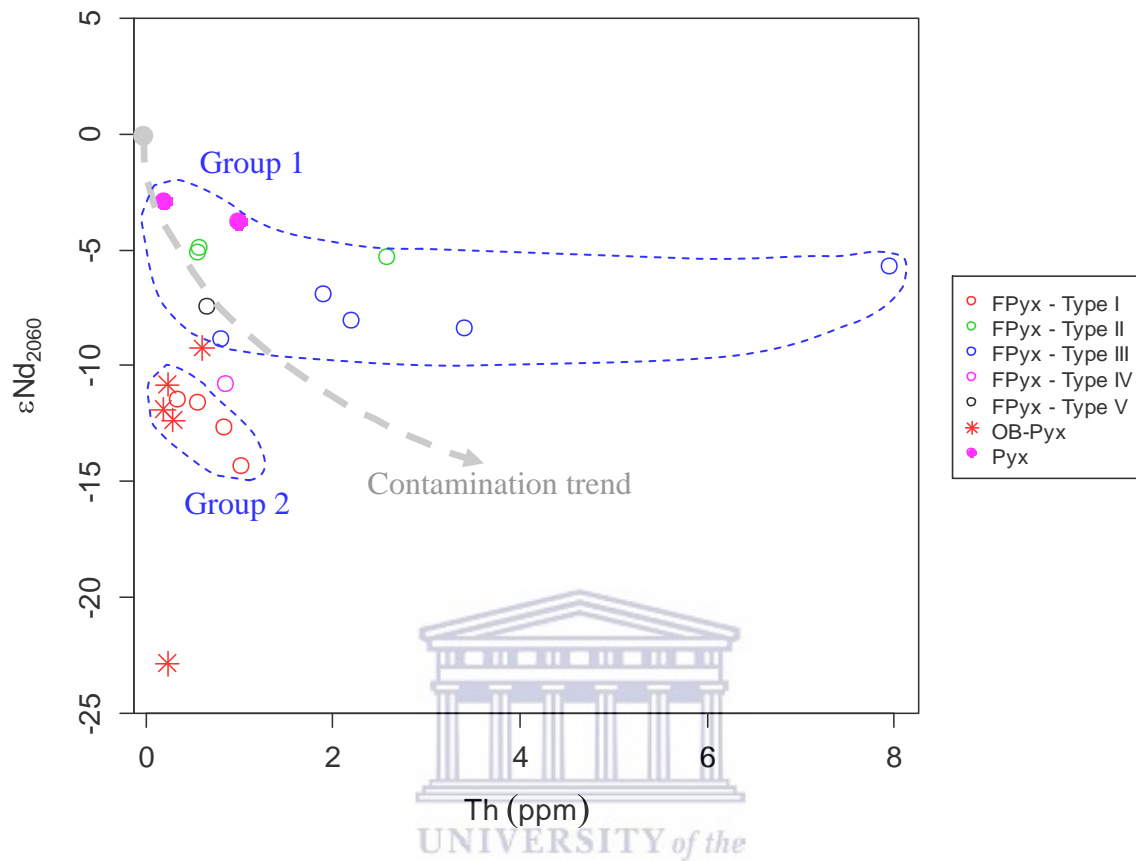
Figure 26: Plot of εNd$_{2060}$ versus Th for the Platreef rocks in this study. The εNd are calculated at the nearest round-off age of 2060 Ma for the BIC (Buick et al., 2001; Yudovskaya et al., 2013b; Zeh et al., 2015). The isotopic groups (1 and 2) for the Platreef rocks are the same as in Figure 14. Legend abbreviation: FPyx: Feldspathic pyroxenite; OB-Pyx: Olivine pyroxenite; Pyx: Pyroxenite.
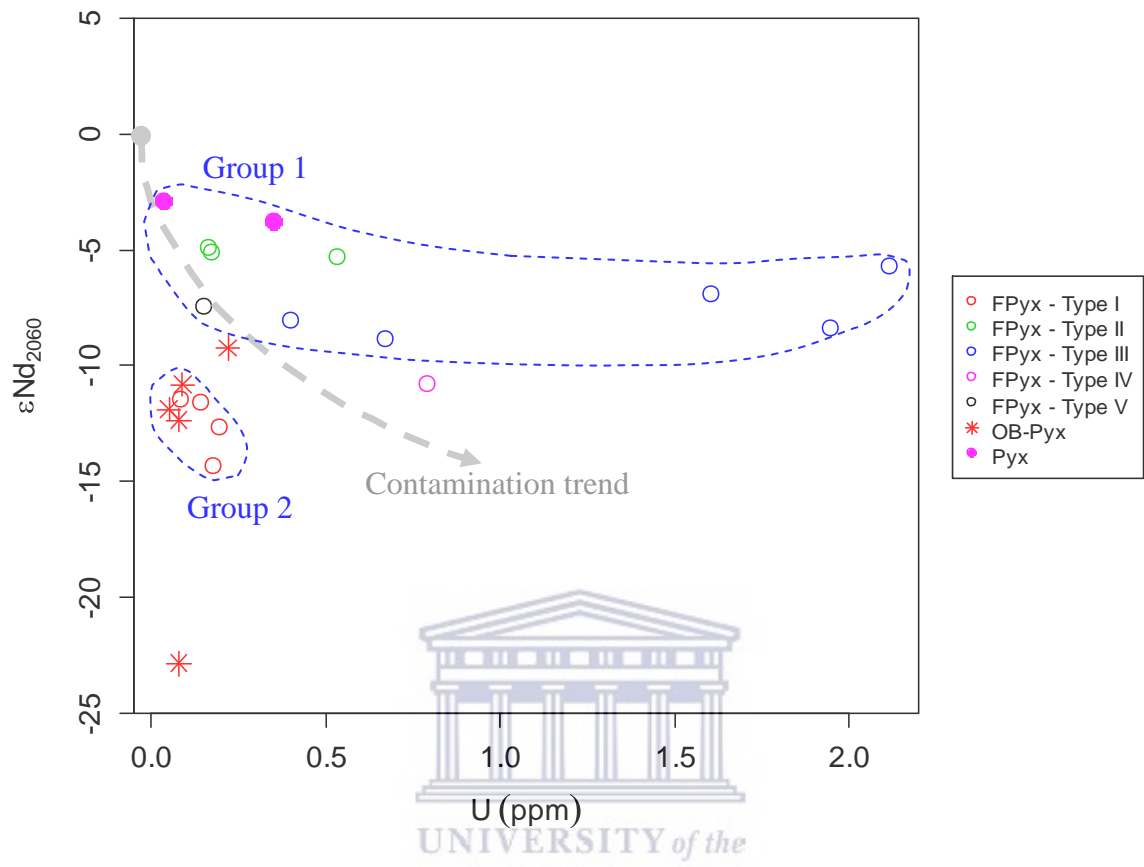
147

Figure 27: Plot of εNd$_{2060}$ versus U for the Platreef rocks in this study. The εNd are calculated at the nearest round-off age of 2060 Ma for the BIC (Buick et al., 2001; Yudovskaya et al., 2013b; Zeh et al., 2015). The isotopic groups (1 and 2) for the Platreef rocks are the same as in Figure 14. Legend abbreviation: FPyx: Feldspathic pyroxenite; OB-Pyx: Olivine pyroxenite; Pyx: Pyroxenite.